Optimisation of rhadinoviral vectors

Dissertation
zur Erlangung des Doktorgrades
der Mathematisch-Naturwissenschaftlichen Fakultät
der Christian-Albrechts-Universität zu Kiel

vorgelegt durch
Ines Heyn

Kiel, 2022

Erste/r Gutachter:	Prof. Dr. Helmut Fickenscher
Zweite/r Gutachter:	Prof. Dr. Axel Scheidig
Tag der mündlichen Prüfung:	17.08.2022

In biology, nothing is clear, everything is too complicated, everything is a mess, and just when you think you understand something, you peel off a layer and find deeper complications beneath. Nature is anything but simple."

Richard Preston, The Hot Zone (1995)

Table of contents

Abstract

Viral vectors have long been in the focus of research as a tool for gene therapy as they allow the transfer of foreign genes into host cells. However, different advantages are linked with the different viral vectors. Herpesviruses in general offer a large insert capacity and persist episomally. In addition, herpesvirus saimiri was shown to establish a persistent, non-productive infection in human T cells without altering the expression of the T-cell surface markers. Therefore, a special interest arose for its development into a viral vector for application in human T cells and ultimate use in individualised gene therapy.

One conceivable application was the redirection of T cells against specific surface antigens. For this project, the genes for human Vγ9- and Vδ2-chains were inserted into a herpesvirus saimiri vector. Two different virus variants were used with the Vγ9-chain inserted at different positions within the viral genome. Transcription of both chains in mature human donor T cells transformed with these vector variants was detectable for at least eight months post-transduction. However, the expression of either protein chain was not detected and the redirection of antigen specificity of mature T cells of different donors could not be achieved.

Self-reparing vectors were used for generating deletion variants. Under the same conditions, promoter, and genomic locus, the general ability for long-term transcription and expression was demonstrated by the use of fluorophores as transgenes. In addition, further promoters were studied including the newly identified *ORF75* promoter. The murine leukemia retrovirus *SL3* promoter was identified as another candidate for long-term transgene expression in human T cells. With an *ORF9*-specific real-time PCR, the rhadinoviral DNA was shown to persist at high copy numbers within these transformed T cells. The deletion of the individual ORFs *3, 12-14, 16, 21, 71, 72, 73,* and *75* was achieved without or with only minor impairments to virus replication in permissive cells. Other single deletions of the *ORFs 45, 49, 52, 69*, and *70-72,* or double deletion of the *ORF16* and *ORF71* or *ORF3* and *ORF75* deletions were identified to lead to the loss of productive infection in permissive cells. The single deletions of *ORF16* or *ORF71* did not relevantly influence apoptosis of transformed human T cells.

In summary, the successful transformation and transgene expression in mature human T cells for up to four years can be achieved with promising, self-repairing deletion variants. Potentially up to 50 kb insert capacity constitutes a considerable potential for the further development of herpesvirus saimiri, *e.g.,* into a therapeutic vector for adoptive T cell therapy.

Zusammenfassung

Virale Vektoren stehen seit langem im Mittelpunkt der Gentherapie-Forschung, da sie den Fremdgen-Transfer in Wirtszellen ermöglichen. Die unterschiedlichen viralen Vektoren bieten dabei unterschiedliche Vorteile. Herpesviren bieten generell eine große Insertionskapazität und persistieren episomal. Darüberhinaus wurde für Herpesvirus saimiri eine persistente, nicht-produktive Infektion in humanen T-Zellen demonstriert,die die Expression der Oberflächenmarker nicht verändert. Aus diesem Grund entstand ein besonderes Interesse an der Entwicklung zu einem viralen Vektor für die Anwendung in humanen T-Zellen und schließlich für die individualisierte Gentherapie.

Eine mögliche Anwendung war die Umlenkung von T-Zellen gegen spezifische Oberflächenantigene. Für dieses Projekt wurden die Gene für humane Vγ9- und Vδ2-Ketten in einen Herpesvirus-saimiri-Vektor eingefügt. Zwei verschiedene Virusvarianten wurden verwendet, bei denen die Vγ9-Kette an unterschiedlichen Positionen im viralen Genom eingefügt wurde. Die Transkription beider Ketten in reifen humanen Spender-T-Zellen, die mit diesen Vektorvarianten transformiert wurden, war mindestens acht Monate nach der Transduktion nachweisbar. Die Expression der beiden Proteinketten konnte jedoch nicht nachgewiesen werden und die Neuausrichtung der Antigenspezifität reifer T-Zellen verschiedener Spender wurde nicht erreicht.

Selbstreparierende Vektoren wurden für die Erzeugung von Deletionsvarianten verwendet. Unter den gleichen Bedingungen, mit dem gleichen Promotor und genomischen Locus wurde die allgemeine Fähigkeit zur Langzeittranskription und -expression durch die Verwendung von Fluorophoren als Transgene nachgewiesen. Außerdem wurden weitere Promotoren untersucht, darunter der neu identifizierte *ORF75*-Promotor. Der *SL3*-Promotor des murinen Leukämie-Retrovirus wurde als weiterer Kandidat für eine langfristige Transgenexpression in humanen T-Zellen identifiziert. Mit einer *ORF9*-spezifischen Echtzeit-PCR wurde gezeigt, dass die rhadinovirale DNA in diesen transformierten T-Zellen in hoher Kopienzahl persistiert. Die Deletion der einzelnen *ORFs 3, 12-14, 16, 21, 71, 72, 73* und *75* wurde ohne oder mit nur geringen Einschränkungen der Virusreplikation in permissiven Zellen erreicht. Andere Einzeldeletionen der *ORFs 45, 49, 52, 69* und *70-72* oder Doppeldeletionen von *ORF16* und *ORF71* oder *ORF3* und *ORF75* führten zum Verlust der produktiven Infektion in permissiven Zellen. Die Einzeldeletionen von *ORF16* oder *ORF71* hatten keinen relevanten Einfluss auf die Apoptose der transformierten humanen T-Zellen.

Zusammenfassend kann mit aussichtsreichen, selbstreparierenden Deletionsvarianten die erfolgreiche Transformation und Transgenexpression in reifen humanen T-Zellen für bis zu vier Jahre erreicht werden. Die potentielle Insertionskapazität von bis zu 50 kb stellt ein erhebliches Potential für die Weiterentwicklung des Herpesvirus saimiri dar, z. B. zu einem therapeutischen Vektor für die adoptive T-Zelltherapie.

Abbreviations

0716, 0117, 0717, ...	abbreviated time point of transduction, month and year
aphA1	aminoglycoside phosphotransferase type 1
BAC	bacterial artificial chromosome
bGH	bovine growth hormone
bp	base pairs
CAM	chloramphenicol
cat	chloramphenicol acetyl transferase
CPE	cytopathogenic effect
CPT	camptothecin
DMSO	dimethylsulfoxide
DNA	deoxyribonucleic acid
dNTPs	deoxynucleotide triphosphates
dpi	days post-infection
E. coli	*Escherichia coli*
EDTA	2-[2-[bis(carboxymethyl)amino]ethyl-(carboxymethyl)amino]acetic acid
eGFP	enhanced green fluorescent protein
FADD	Fas-associating protein with death domain
FGARAT	formyl-glycinamide phosphoribosyl-amidotransferase
FLICE	FADD-like interleukin-1β-converting enzyme
FLIP	FLICE-interacting protein
for	forward
FBS	fetal bovine serum
FITC	fluorescein isothiocyanate
GAPDH	glyceraldehyde 3-phosphate dehydrognease
gD, gB, gH	glycoproteins D/B/H
hpi	hours post-infection
HSV	herpes simplex virus
HVS	herpesvirus saimiri
HTLV-1	human T cell leukemia virus type-1
HTLV promoter	HTLV-EF1α promoter of HTLV-1
IE	immediate early
IL	interleukin
IRES	internal ribosomal entry site (derived from poliovirus or encephalomyocarditis virus)
K38, K39, K40, K41	T cell donors
KAN	kanamycin
kb	kilobase pair(s)
KSHV	Kaposi's sarcoma-associated herpesvirus
LB	Luria Bertani
MHC	major histocompatibility complex
MHV-68	murine herpesvirus type 68
MOI	multiplicity of infection
mpt	months post-transduction
mRFP	monomeric red fluorescent protein 1
NCBI	National Center for Biotechnology Information
NGS	next-generation sequencing
OMK	owl monkey kidney
ORF	open reading frame
PBS	phosphate buffered saline
PCR	polymerase chain reaction
PE	phycoerythrin
PerCP Cy5.5	peridinin chlorophyll protein-cyanine 5.5
pfu	plaque forming unit(s)

PI	propidium iodide
psm	positive selection marker
RACE	rapid amplification of cDNA ends
rev	reverse
RFLP	restriction fragment length polymorphism
RNA	ribonucleic acid
RT	reverse transcriptase
SDS	sodium dodecyl sulfate
SL3	murine leukemia retrovirus SL3-3 (LTR)
StpC	Saimiri transformation-associated protein of subgroup C viruses
S.O.C.	super optimal broth with glucose medium
TBE	TRIS-borate-EDTA buffer
TCR	T-cell receptor
Tip	tyrosine-kinase interacting protein
TRAIL	tumour necrosis factor-related apoptosis-inducing ligand
TRIS	2-Amino-2-(hydroxymethyl)propane-1,3-diol
U	unit
WT	wild-type
WTf	wild-type with miniF sequence

1. Introduction

1.1 The order *Herpesvirales* and the rhadinovirus herpesvirus saimiri

The herpesviral taxonomy was updated in 2009 and the newly founded order *Herpesvirales* now consists of the families *Malacoherpesviridae*, *Alloherpesviridae*, and *Herpesviridae* (fig. 1; Davison, 2002; Davison et al., 2009; Lefkowitz et al., 2018). The *Herpesviridae* were classified into the three subfamilies *Alpha*-, *Beta*-, and *Gammaherpesvirinae*. All herpesviruses show an amazing adaptation to their specific host. So far, over 90 herpesvirus species have been identified but hosts rarely show severe adverse reactions upon infection with their species-specific herpesvirus, indicating a long-lasting co-evolution (McGeoch & Cook, 1994; Davison et al., 2009). The virus of concern for this dissertation is often quoted as the prototype of the γ_2-subclass herpesviruses, the rhadinoviruses. Its designation is herpesvirus saimiri (HVS), also known as Saimiriine Herpesvirus type 2 in the formal systematics.

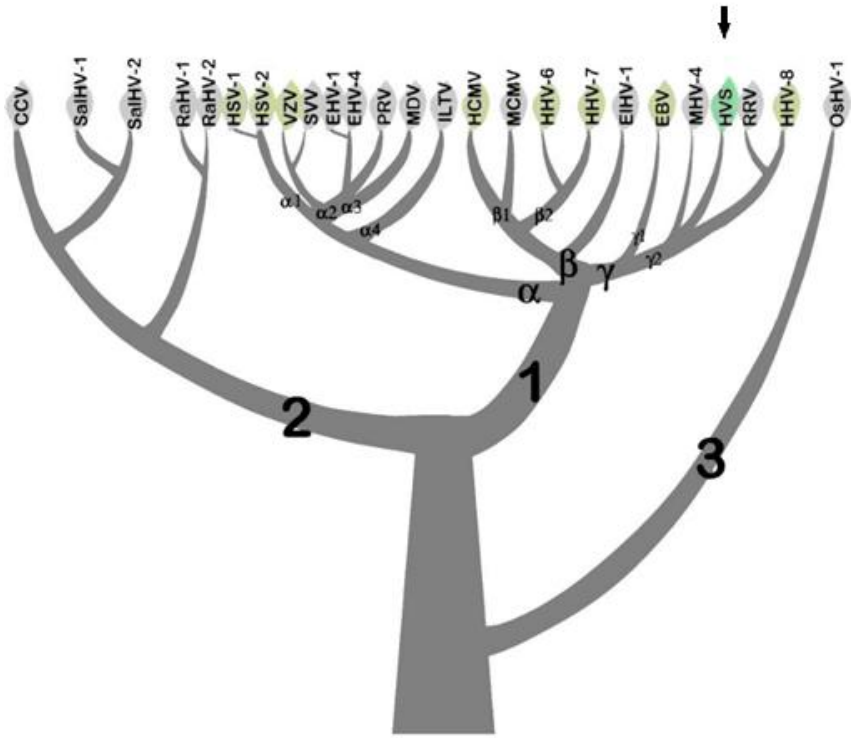

Fig. 1: The herpesviral evolutionary tree. This figure shows the phylogenetic tree of some major herpesvirus species, based on estimated evolutionary rates for the hosts and applying their timescales to the viruses. The three big branches symbolise the three families, *Malacoherpesviridae* (3), *Alloherpesviridae* (2), and *Herpesviridae* (1) and further deviding into subfamilies, genera, and finally selected species, indicated as leaves. The length and distance of the branches also visualise the evolutionary distance between the species. Human pathogenic viruses are coloured in light green, Herpesvirus saimiri (HVS) is indicated in dark green and via black arrow. Abbreviations: CCV, channel catfish virus; SalHV, salmonid herpesvirus; RaHV, ranid herpesvirus; HVS, herpes simplex virus; VZV, Varicella-zoster virus; SVV, simian varicella virus; EHV, equine herpesvirus; PRV, pseudorabies virus; MDV, Marek's disease virus; ILTV, infectious laryngotracheitis virus; HCMV, Human cytomegalovirus; MCMV, murine cytomegalovirus; HHV, human herpesvirus; EIHV, elephant endotheliotropic herpesvirus; EBV, Epstein-Barr virus; MHV, murid herpesvirus; RRV, rhesus rhadinovirus; OsHV, oyster herpesvirus. Modified from Davison, 2002.

Infection with HVS does not affect the well-being of its natural host, the squirrel monkey *Saimiri sciureus* but induces lymphoproliferative diseases and even death upon experimental infection in other species, such as New World monkeys or New Zealand white rabbits (Meléndez et al., 1969; Hunt & Meléndez, 1969; Meléndez et al., 1971; Medveczky et al., 1989). In the squirrel monkey, the infection with different HVS strains does not result in any observable disease (Biesinger et al., 1990; Ensser et al., 2003). Viral replication was reported in permissive epithelial cells of various tissues and in lymphocytes of infected animals (Simmer et al., 1991). Because of its persistence in lymphocytes it was classified as a lymphotropic virus. The animals are lifelong latently infected and carry the viral episomes within their nuclei at copy numbers ranging from 50 to 200 per cell (Biesinger et al., 1992).

The organisation of the HVS virion is similar to that of all other herpesviruses (fig. 2). The envelope of HVS carries the glycoproteins, of which gB (ORF8), gH (ORF22), and gL (ORF47) are the most important ones for herpesviral entry. Four more glycoproteins (gM, ORF39; gN, ORF53; putative glycoprotein, ORF51; major glycoprotein, ORF68) may further influence the host cell range. Beneath the envelope, a protein layer termed tegument is located. It consists of proteins needed for the immediate take-over of the host-cell biosynthesis, such as transcription factors. The ikosaedric capsid is situated within the tegument and confers additional protection for the double-stranded deoxyribonucleic acid (DNA) genome which is coiled around a protein core (fig. 2).

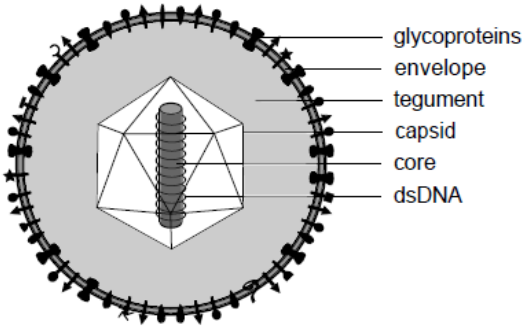

Fig. 2: Organisation of a herpesviral virion. Herpesviruses are enveloped viruses. The envelope is interspersed by glycoproteins. Beneath the double lipid layer, the tegument is situated, containing proteins initiating the viral take-over of the host-cell biosynthesis. The ikosaedric capsid is located within the tegument and carries the double-stranded DNA convoluted around the core.

When the virus was first discovered, the HVS DNA was found to be easily separated by equilibrium density centrifugation into a low GC-containing DNA (L-DNA) and high GC-containing DNA (H-DNA) (Fickenscher & Fleckenstein, 2001). The complete genome consisting of both parts was termed M-DNA. H-DNA was later found to be crucial for the persistence in dividing cells, while the L-DNA carries the 75 open-reading frames (ORFs), which code for the HVS proteins (Collins et al., 2002; Verma & Robertson, 2003; White et al., 2003). Depending on

the virus strain and the varying number of the 1.4 kb tandem repeats within the H-DNA, the HVS genome size can amount from 130-160 kb (Albrecht et al., 1992).

In addition to the transforming qualities of HVS for T cells of New and Old World monkeys, HVS C488 was discovered to transform human T cells as well (Biesinger et al., 1992). HVS has furthermore been serving as a model for the understanding of pathogenesis of its closest human pathogenic relative, the T-lymphotropic Kaposi's sarcoma-associated herpesvirus (KSHV, also HHV8), for which permissive cell lines are lacking for *in vitro* studies (Chang et al., 2009; Jung et al., 1999).

The leftmost region of the genome carries ORF1 coding for the Saimiri transformation-associated protein (Stp) which is responsible for the transforming capacity of HVS (Biesinger et al., 1990; Albrecht et al., 1992). The three different subgroups of HVS were classified into A, B, and C, according to their oncogenicity mediated by Stp expression (Medveczky et al., 1984, 1989; Szomolanyi et al., 1987). Only members of subgroup C are able to transform human T cells to stable proliferation and additionally encode the tyrosine-kinase interacting protein (Tip) at this genome locus. For these projects, all generated virus variants were derived from the wild-type strain HVS C488 (Bremer, 2014; Ensser et al., 2003).

Monkeys infected with strain C488 were reported to show a broad variety of infected cell types with productive infection with a broad spectrum of virus gene expression. Transformed human T cells, however, were found to show a strictly limited HVS gene expression and the release of infectious virions was not detectable (Biesinger et al., 1992; Fickenscher et al., 1996, 1997). These qualities, amongst others, marked HVS as a candidate for development into a gene therapy vector (Desrosiers et al., 1985; Fickenscher & Fleckenstein, 2001; Smith et al., 2005; Turrel et al., 2012). The fact that HVS-transformed T cells retained their phenotype including the major histocompatibility complex (MHC) dependent antigen specificity made them an important tool to study T-cell biology and T-cell gene defects (Allende et al., 2000; Altare et al., 1998; Bröker et al., 1993; De Carli et al., 1993; Gallego et al., 1997; Mittrücker et al., 1993; Weber et al., 1993).

1.2 Viral vectors in gene therapy

Since 1990, viral vector systems have been introduced into the treatment of various diseases such as cardiovascular, metabolic, muscular, hematologic, ophthalmologic, infectious, or malignant disorders (Lundstrom, 2018). The viral entry machinery opens a safe and specific way for transgenes or suicide genes into target cells. However, different viral vector systems offer different advantages and disadvantages. Adenoviral vectors are frequently used vectors nowadays. They provide a broad host range and insert capacity of up to 7.5 kb but induce strong immunogenicity and allow transient expression only. Retroviral systems, as used for the therapy of severe combined immunodeficiencies, have the advantage of insert capacities

of up to 8 kb and long-term transgene expression but pose the risk of insertional mutagenesis by integration into the host cell genome with their preference to integrate within the proximity of promoter regions or introns (Laufs et al., 2004; Hacein-Bey-Abina et al., 2003a and 2003b). Herpesviral vectors instead offer the benefits of a broad host range and large insert capacities of more than 30 kb, paired with a low toxicity and latent infection with long-term expression. So far, only the best studied herpesvirus, herpes simplex virus (HSV), was used in clinical trials (Andtbacka et al., 2015; Markert et al., 2000; Senzer et al., 2009; Geevarghese et al., 2010).

Similar to HSV, the γ_2-herpesvirus or rhadinovirus HVS offers large insert capacity and long-term expression, while persisting episomally within the karyoplasm at high copy numbers. Thus, the risk of insertional genomic mutagenesis is eliminated and the chance of gene silencing by epigenetic mechanisms reduced (Grassmann & Fleckenstein, 1989; Simmer et al., 1991). Although HVS-infected cells of various tissues including cancer cells were reported to shed infectious virus, human HVS-transformed T cells do not release infectious virions into the supernatant (Biesinger et al., 1992; Bröker et al., 1993; Calderwood et al., 2004b; Fickenscher et al., 1996; Meinl & Hohlfeld, 2000; Weber et al.,1993).

1.3 Herpesvirus saimiri as a vector candidate for gene therapy

As early as 1985, the first step was taken towards the establishment of a HVS gene therapy vector. The bovine growth hormone (bGH) was successfully expressed from a HVS vector after infection in New World primates (Desrosiers et al., 1985). Fifteen years later, autologous reinfusion of HVS-transformed T cells in macaques was well tolerated by the animals and did not result in adverse events, such as lymphoproliferative disease or death (Knappe et al., 2000). Thus, HVS became attractive as a vector candidate for gene therapy in human T cells, either for the redirection of antigen specificity against tumour markers or for transgene introduction and stable, long-term transgene expression.

Over the years, different set-ups and reporter genes were successfully used to monitor and regulate transgene expression, such as β-galactosidase, luciferase, or enhanced green-fluorescent protein (eGFP; Frolova-Jones et al., 2000; Smith, et al., 2005; Stevenson, et al., 1999; Toptan, 2010). Several different promoters have been evaluated for transgene expression in different cell lines. This includes human promoters for elongation factor 1α, phosphoglycerate kinase 1, α-survivin, and CD2, as well as several viral promoters such as promoters of human cytomegalovirus, simian virus 40, HSV-1 thymidine kinase, mouse mammary tumour virus, human T-cell lymphotropic virus type 1 (HTLV-1) and HVS promoters of *ORF1*, *ORF14*, and *ORF71-73* (Desrosiers et al., 1985; Giles et al., 2003; Hall et al., 2000; Hüske, 2010; Toptan, 2010; Turrel et al., 2011; Wieser, 2004). The transgene expression of reporter genes could be proven as well as the functional expression of mammalian

genes such as bovine growth hormone (bGH) or human tumour-necrosis factor-related apoptosis-inducing ligand (TRAIL). Insert sizes in those experiments ranged from 1-8 kb. The expression time was monitored in confluent epithelial cells usually for days up to a maximum of six months, in tumour-like spheroids for ten weeks, in infected mice for three months, and in transformed T cells up to twelve months. Many obstacles were reported such as silencing of transgenes over time within transformed cells (Stevenson et al., 2000; Toptan, 2010; Wieser, 2004) and problems with leakiness of the HVS tetracycline-on system (Hüske, 2010). In this project, the expression cassettes were inserted into the well-established transition area between *ORF75* and the terminal H-DNA (Grassmann et al., 1989).

1.4 Bacterial artificial chromosomes and *en passant* mutagenesis

Historically, the manipulation of herpesviral genomes was laborious, inefficient, and time consuming. The establishment of bacterial artificial chromosomes (BACs) for entire herpesvirus genomes in 1997 enabled easy alterations of viral genomes with already well established molecular methods (Messerle et al., 1997). The miniF vector allowed for inserts of up to 300 kb while preventing more than two copies per cell, minimising the risk of recombination events between BACs in a single cell (Shizuya et al., 1992). The first one to be generated was the murine cytomegalovirus BAC, soon to be followed by BACs for other herpesviral genomes (Tischer & Kaufer, 2012; Wussow et al., 2011). The first BAC of HVS was generated by Armin Ensser by co-transfection of five overlapping genomic cosmids containing the complete C488 genome (Toptan, 2010). A further improvement of the manipulation procedures of viral genomes was achieved in 2006, when the two-step red-mediated recombination, or *en passant* mutagenesis, was introduced into herpesvirology (Tischer et al., 2006). The method offers the seamless alteration of BAC DNA, carried within the specific *E. coli* strain GS1783. Three types of alterations can be introduced by *en passant* mutagenesis: single point-mutations, insertions, and deletions of large sequences (fig. 3). The *en passant* mutagenesis depends on the careful design of the required oligonucleotides and on an appropriate transfer vector plasmid.

The three methods presented in fig. 3 differ in the preparing steps but share the same procedure starting with the PCR amplification using the specifically designed oligonucleotides. The PCR fragment is isolated by purification after gel electrophoresis. Subsequently, the purified product is electroporated into competent bacterial cells, carrying the genome which is to be manipulated. In a first homologous recombination, mediated by the heat-induced *red*-recombination genes, the PCR product is inserted specifically at the site of interest into the genome. In a second recombination event, the monosaccharide arabinose is used to induce expression of the restriction enzyme I-SceI to generate a double-strand break within the BAC

genome. Finally, heat treatment at 42 °C induces expression of *red* genes, initiating the second recombination which releases the positive selection marker from the genome.

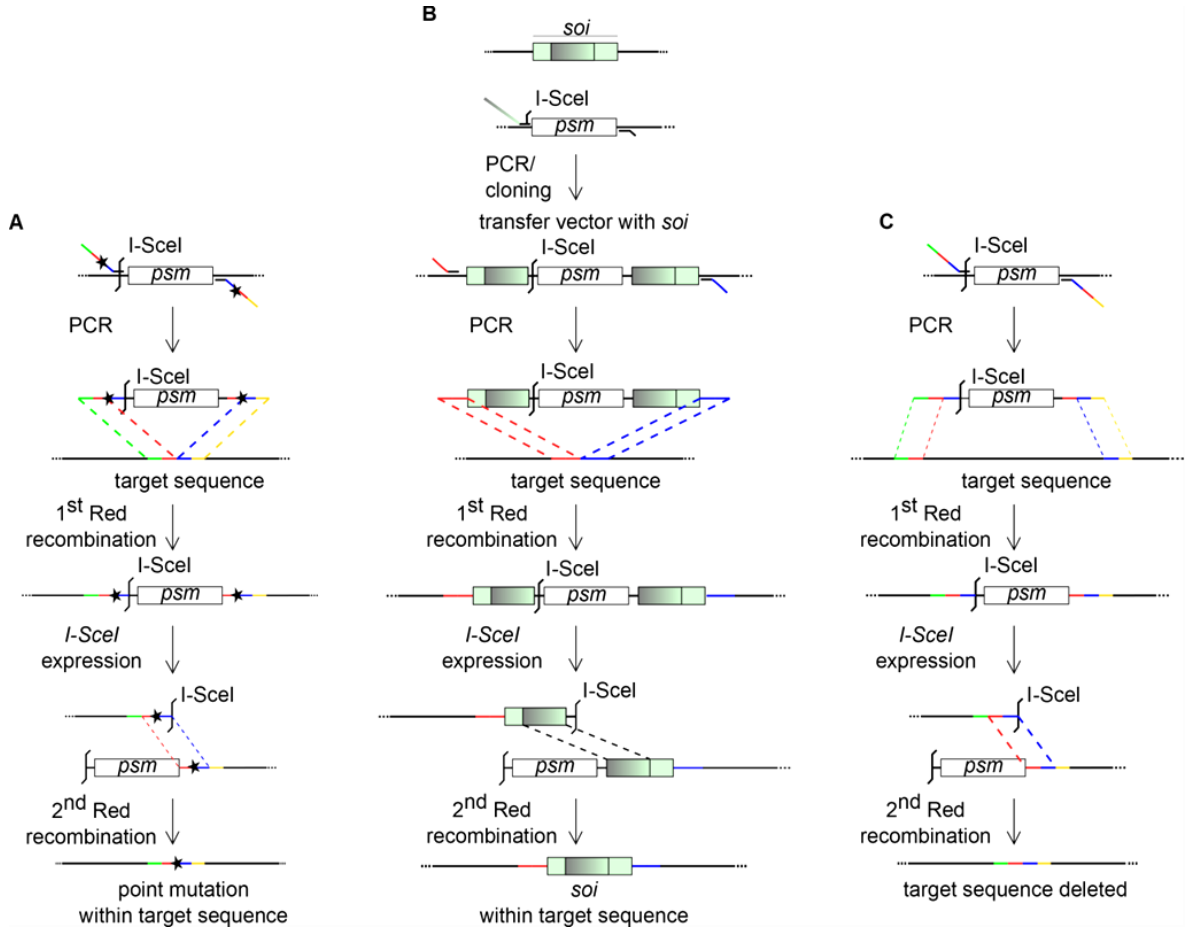

Fig. 3: Three manipulation strategies for BACs via *en passant* mutagenesis. The two-step red recombination allows for introduction of single point-mutations (**A**, star), of a sequence of interest (*soi,* light green) into a target sequence (**B**), or the deletion of a target sequence (**C**). Specifically designed oligonucleotides determine the exact position of the desired alteration (green, yellow, red, and blue lines) within the BAC in a first red recombination event. A positive selection marker (*psm*), the kanamycin resistance gene *aphA1,* is introduced along with the alteration in order to positively select recombinant bacteria only. The release of the *psm* is mediated by forcing a double-strand break via expression of the endonuclease I-SceI and inducing a second red recombination event. Duplications, either introduced by oligonucleotide-design (red and blue lines in **A** and **C**), or by cloning of the transfer vector (colour-gradient box in **B**), upstream and downstream of the *psm*, cause the desired, subsequent removal of the *psm* from the seamlessly modified DNA (modified after Tischer et al., 2006).

To generate a single point mutation (fig. 3A), the oligonucleotides already carried the desired point mutation within their homologous sequences. Furthermore, the oligonucleotides contained a binding site for the positive selection marker (psm) *aphA1* which was amplified in a polymerase chain reaction (PCR) from the transfer vector plasmid pepKanS2 (Tischer et al., 2006). The PCR product was purified and electroporated into recombination- and electrocompetent bacteria carrying the HVS C488 BAC. Once inserted, a sequence duplication stemming from careful oligonucleotide design, allowed for the removal of the psm *aphA1* by a second homologous recombination.

The deletion of a viral gene was even simpler, as far as oligonucleotide design was concerned. The sequence to be deleted was simply replaced by the psm *aphA1* (fig. 3C). To achieve that, 50 base pairs (bp) of homologous region flanking the sequence to be deleted were taken, followed by 25 bp of the other end of the deletion, to create a duplication of 50 bp, and lastly, 25 bp binding to the pepKanS2 vector concluded the oligonucleotide sequence.

To insert genes of interest (fig. 3B) into a BAC, first a transfer vector had to be generated, including the psm *aphA1.* The vector had to be designed to allow for the second recombination by already inserted homologous recombination regions flanking the *aphA1*. Otherwise, the oligonucleotides had to consist of 50 bp homologous to the site of insertion and a binding sequence of approximately 20-25 bp to the transfer vector.

The end product of the *en passant* mutagenesis was always a seamlessly manipulated genome without any residual restriction enzyme sites and only with the intended sequence alteration.

1.5 Human T-cell receptors

Human T cells reliably recognise their specific antigens to ensure the elimination of pathogens and malignant cells. For this purpose, they express two types of antigen-specific receptors, the T-cell receptors (TCRs). Two basic types of TCRs exist, termed according to the two heterologous chains they consist of: the alpha and beta chain form the αβ TCR, while the gamma and delta chain are part of the γδ TCR. During T-cell maturation in the thymus, an uncommitted progenitor cell develops into a CD2-positive T-cell progenitor and passes through two gene rearrangements (Murphy & Weaver, 2018). Similar to the rearrangement of immunoglobulins, the TCR-chains are formed from genes for constant, varying, joining, and diversity regions. Usually, the genomic organisation of the human TCR chain loci makes it unlikely to impossible for a human T cell to express more than one receptor, since after successful rearrangement of the α-chain locus, the complete δ-chain locus is lost due to recombination, due to its location between the varying and joining segments (fig. 4B, Parham, 2009). The T cells committed to the γδ lineage during the first or second rearrangement leave the thymus without undergoing further selection, while αβ TCR-positive cells undergo positive and negative selection within the thymus and commit to either CD4 or CD8 types (fig. 4A; Holländer et al., 2006; Parham, 2009). Mature human T cells were originally reported to exclusively carry one type of receptor on lipid rafts, however recent investigations established that the expression of both receptors on a single cell is possible (Edwards et al., 2020).

The distribution of the different receptors is highly uneven on cells in the blood stream, with 95-99 % of CD3-positive peripheral blood lymphocytes expressing the αβ TCR and a minority

of only 1-5 % carrying the γδ TCR. However, γδ-positive T lymphocytes make up 20-50 % of the lymphoid cells in tissues (Holländer et al., 2006; Murphy & Weaver, 2018; Silva-Santos et al., 2015). While human αβ-positive T cells can generally be found within the lymphatic system and show MHC-dependent restriction, γδ-positive cells can also be found in epithelial tissues with the predominating subtypes Vγ1 and Vδ3. Their main function apparently is not the MHC-mediated recognition of pathogen antigens but rather the recognition of proteins expressed or altered due to an infection or damage and elimination of the corresponding cell (Murphy & Weaver, 2018; Silva-Santos et al., 2015).

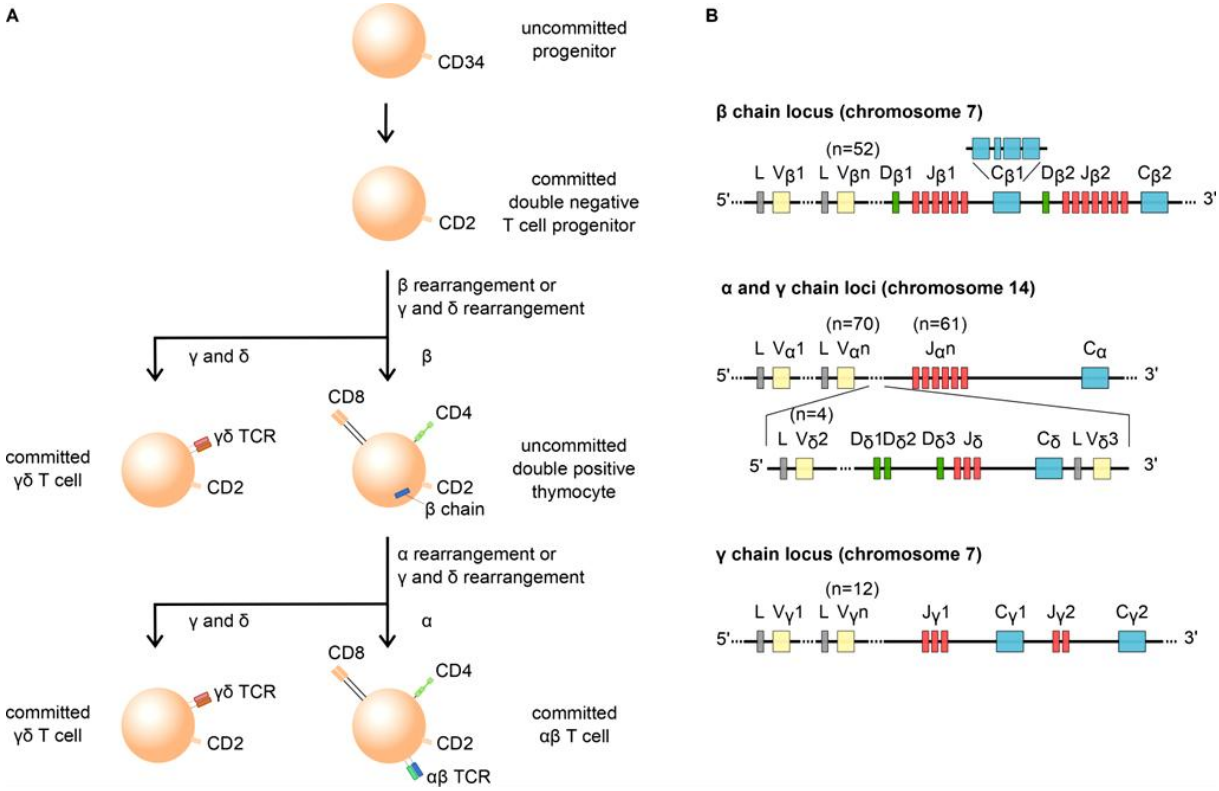

Fig. 4: T-cell maturation and T-cell receptor-gene rearrangement: A The current consensus of T-cell maturation from uncommitted progenitor cells in the thymus to committed αβ- or γδ-positive T cells is shown. T cells pass two checkpoints during gene rearrangement, first for the β-chain and later for the α-chain. During both rearrangements, the commitment to the γδ lineage is possible. The γδ-committed cells leave the thymus, while αβ-positive cells undergo further selection. When T cells are committed to the α-chain rearrangement, the γ-chain locus is eliminated from the genome, due to somatic recombination. **B** The somatic rearrangement of the different gene segments (L, leader sequence; V, variable; D, diversity; J, joining; C, constant) leads to the high antigen diversity of the human TCRs. (images modified according to Parham, 2009 (**A**) and Holländer et al., 2006 (**B**))

In comparison to αβ-positive T cells, which recognise pathogen-associated molecular patterns presented by antigen-presenting cells, γδ T-cells have a limited chain-diversity, mostly lack the CD4 and CD8 co-receptors, and are able to recognise stressed cells. Thus, γδ T-cells can be classified as part of an interface between the adaptive and innate immune systems, termed transitional immunity (Kabelitz et al., 1991; Murphy & Weaver, 2018). The specific Vγ9Vδ2-positive subclass was reported to comprise 50-90 % of the γδ T-cell population in the blood of healthy humans. Cells of this subclass were found to directly recognise phos-

phoantigens (Eberl et al., 2003; Tanaka et al., 1995). Their recognition and lysis of a broad range of tumour cells, independently of MHC presentation and co-stimulation, was demonstrated *in vitro* and *in vivo,* which makes them attractive in anti-tumour immunotherapy (Corvaisier et al., 2005; D'Asaro et al., 2010; Kabelitz et al., 2004; Lo Presti et al., 2014; Liu et al., 2005).

1.6 Cell death and apoptosis

The three major mechanisms of cell death have been identified as necrosis, apoptosis, and autophagy. Autophagy does not necessarily result in cell death but is rather a strategic process to recycle energy by self-digesting cellular proteins, organelles, or even whole cells (Holländer et al., 2006). During necrosis cells start to swell, until the cell membrane is ruptured and the cell contents is released, potentially damaging the surrounding cells. Apoptotic cells, by contrast, start to shrink due to chromatin condensation and nuclear fragmentation. The cell membrane stays intact but starts to bleb and the cell contents is divided into apoptotic bodies and, hence, do not damage the surrounding cells (Khalil, 2021). Thus, apoptosis was defined as the programmed cell death and is highly regulated. Cells signalling infection or irreparable damage usually are convinced to undergo apoptosis, while necrosis is often found with general inflammatory responses, although more recently many interactions between the two have been reported (Khalil, 2021). Apoptosis can be induced generally via the extrinsical, intrinsical, and perforin/granzyme pathways (Elmore, 2007).

Extrinsic activation is usually mediated by death-receptor ligand binding, for example by binding of Fas receptor CD95/FasR to its ligand CD95L/FasL, or by binding of death receptor 5/TRAIL-R2 to its ligand TRAIL. Expression of FasL is usually limited to natural killer and T cells, with T cells needing additional stimuli such as interleukin 2 to express FasL. Usually, binding of more than one receptor to its ligand (cross-linking) is required for a successful initiation of the apoptotic pathway, leading to the intracellular binding of the death domains of the cytoplasmic receptors. Subsequently, adaptor proteins such as Fas-associated death domain (FADD) or tumour-necrosis factor receptor-associated death domain can bind to the death domains with their death effector domain and subsequently activate caspase 8 (FADD-like interleukin-1β-converting enzyme, FLICE) (Elmore, 2007, Holländer et al., 2006).

Intrinsic activation is normally achieved by DNA damage but also a plethora of exogenous or endogenous signals can lead to its activation, including oxidative stress, pathological protein folding, irradiation, cytostatics, as well as the withdrawal of growth hormones or differentiation stimuli. Intrinsic pathway activation leads to the activation of caspase 9.

Lastly, the perforin/granzyme pathway is activated by the release of perforin and granzymes from natural killer cells or cytotoxic T cells, resulting in the formation of a pore complex within the cell membrane through which granzymes A and B enter the cell, finally leading to the

activation of caspase 10. All three mechanisms have the activation of a specific initiator caspase (8, 9, 10) in common, that in turn will activate the execution phase of apoptosis, involving caspases 3, 6, 7, and potentially 12, finally leading to the aforementioned structural degradation steps by further caspases (Elmore, 2007, Holländer et al., 2006).

Cellular inhibitory signal proteins to counter the triggering of apoptotic pathways are, amongst others, Bcl-2, Bcl-x_L, and survivin which regulate caspases, as well as cellular FLICE inhibitory protein (cFLIP). All these pathways are highly interconnected (Elmore, 2007; Holländer, 2006; Khalil, 2021). The role of apoptosis and autophagy in viral infections is crucial, since both processes have the potential to clear the infection, which is the reason, why viruses developed evasion strategies. Autophagy for example is often reported to be hijacked by viruses, in fact, going as far as that inhibition of autophagy impairs the viral replication while its stimulation is beneficial for it (Lussignol & Esclatine, 2017). Other strategies to evade the host immune system are the take-over of cellular anti-apoptotic genes, such as Bcl-2 and FLIP, or the expression of immunoglobulin G binding proteins inhibiting the opsonisation of virus-infected cells by binding to the constant part of immunoglobulin G instead of the variable part (Lubinski et al., 1998).

1.7 Aims of the projects

The projects aimed for the generation of improved rhadinoviral vectors. Several possible applications of rhadinoviral vectors have been proposed and were investigated.

The primary goal was to generate a vector for the antigen redirection of human T cells for adoptive T cell therapy. Previous studies demonstrated that the redirection of transformed human T cells expressing a chimeric TCR was feasible. The Vγ9Vδ2-TCR was reported to recognise and target autologous cancer cells efficiently and independently from MHC restriction. Therefore, these two chains were chosen as transgenes in a rhadinoviral vector in order to enable mature human T cells to express the Vγ9Vδ2-TCR and, thus, take a step into the development of another therapeutic tool for individualised cancer treatment.

Furthermore, the duration and the stability of transgene expression under different promoters were of interest. Fluorophores were intended to be used to visualise the activity of different promoters over time in transformed human T cells.

In order to increase insert capacity for potential transgenes, the generation of self-repairing minimal variants of HVS C488 was aimed at for use in T cells but also for other purposes. The goal far ahead is to create minimised vector variants with a reduced viral genome and, thereby, increased insert capacity for transgenes, without affecting the replication and production of high-titre virus stocks in permissive culture cells.

2. Materials and methods

2.1 Materials

2.1.1 Plasmids, bacterial artificial chromosomes, and bacteria

Table 1: Plasmids used for cloning and amplification

Designation	Description	Reference
topoCD2	CD2 enhancer and promoter in topoTA	Hüske, 2010
topoBGH	BGH- polyA signal sequence in topoTA	Toptan, 2010
topoHTLV	HTLV-1 promoter in topoTA	Hüske, 2010
topo hr1Vγ9PolioIRESKandupVδ2	human *Vγ9* and PolioIRES, divided by duplication and *aphA1* from human *Vδ2* and IRES	Bremer, 2014
pep-mRFP-in	mRFP1, divided by kanamycin resistance gene *aphA1* and I-SceI restriction enzyme site	Tischer et al., 2006
pepKanS2	kanamycin resistance gene *aphA1* and I-SceI restriction enzyme site	Tischer et al., 2006

Table 2: Bacterial artificial chromosomes

BAC	Description	Reference
WTf	wild-type HVS C488 with miniF-sequence within *ORF14*	Toptan et al., 2010
WTfΔ62	wild-type HVS C488 with miniF-sequence within *ORF14* and deleted *ORF62*	Werny, 2017
WTfΔ63	wild-type HVS C488 with miniF-sequence within *ORF14* and deleted *ORF63*	Propp, 2015
WTfΔ64	wild-type HVS C488 with miniF-sequence within *ORF14* and deleted *ORF64*	Werny, 2017
WT22fDR	wild-type HVS C488 with miniF-sequence within *ORF22* and additional directly orientated repeat (DR) for self-repair	Heyn, 2014
WT29fDX	wild-type HVS C488 with miniF-sequence within *ORF29b*^{R} and additional inversely orientated repeat (DX) for self-repair	Heyn, 2015
WT22fDRΔ71	WT22fDR with deleted *ORF71*	Zingler, 2015
WT29fDXΔ16	WT29fDX with deleted *ORF16*	Zingler, 2015
WT29fDXΔ71	WT29fDX with deleted *ORF71*	Zingler, 2015
eGFP	wild-type HVS C488 with miniF sequence within *ORF14* and *eGFP* and IRES under control of StpC/Tip promoter	Toptan, 2010

Table 3: Bacteria used for plasmids and bacterial artificial chromosomes

Bacteria	Description	Reference
E. coli DH5α	chemically competent	New England Biolabs, Frankfurt/Main
E. coli GS1783	electrocompetent, *red* genes under heat-inducible promoter, I-SceI gene under arabinose inducible promoter	Tischer et al., 2006
E. coli Stellar competent cells	part of SMARTer® RACE 5'/3' kit	Takara

2.1.2 Cell lines and viruses

Table 4: Cell lines

Cell line	Description	Source
OMK	Owl monkey kidney cells, permissive for HVS (ATCC CRL 1556)	Daniel et al., 1976
T-lymphocyte lines of donors K38-41	T-cell lines derived from different blood-donors	Department of Immunology, Kiel

Table 5: Viruses

Virus designation	Description	Source
WT	wild-type HVS C488	Biesinger et al., 1990
WTf	wild-type HVS C488 with miniF sequence disrupting ORF14	Toptan, 2010
WT22fDR	wild-type HVS C488 with self-repair ability (insertion of miniF sequence depends on virus passage)	Heyn, 2014
WT29fDX	wild-type HVS C488 with self-repair ability (insertion of miniF sequence depends on virus passage)	Heyn, 2014
WT22fDRΔ71	self-repair enabled HVS C488 with deleted *ORF71*	Zingler, 2015
WT29fDXΔ16	self-repair enabled HVS C488 with deleted *ORF16*	Zingler, 2015
WT29fDXΔ71	self-repair enabled HVS C488 with deleted *ORF71*	Zingler, 2015

2.1.3 Buffer, kits, reagents and media

Table 6: Buffer

Buffer	Composition
DNA Isolation from bacterial cells (mini preparation)	
P1	10 mM 2-[2-[bis(carboxymethyl)amino]ethyl-(carboxymethyl)amino]acetic acid (EDTA) pH 8; 25 mM 2-amino-2-(hydroxymethyl)propane-1,3-diol (TRIS) HCl pH 8; 100 µg/ml RNase A
P2	0.2 M NaOH; 1 % sodium dodecyl sulfate (SDS)
P3	3 M potassium acetate pH 5.5; glacial acetic acid for pH adjustment
Agarose gel electrophoresis	
TRIS-borate-EDTA buffer (TBE) 10x	TRIS base 1 M; Boric acid 1 M; EDTA 0.02 M
agarose gels	0.6-1.5 % agarose; 1x TBE; 0.5 µg/ml ethidium bromide
DNA loading dye (6x)	50 % (v/v) glycerol; 10 mM EDTA; 0.25 % (w/v) bromphenol blue
Flow cytometry and immune staining	
flow cytometry buffer	1x phosphate buffered saline (PBS); 5 % FBS
PBS	136 mM NaCl; 1.5 mM KCl; 64 mM Na_2HPO_4; 0.5 mM KH_2PO_4; pH 7.3

Table 7: Reagents

Reagent	Supplier
Gel electrophoresis	
agarose	ThermoFisher Scientific, Waltham, USA
ethidium bromide	Carl Roth, Karlsruhe, Germany
GeneRuler™ DNA 100 bp ladder	ThermoFisher Scientific
GeneRuler™ DNA ladder mix	ThermoFisher Scientific
GeneRuler™ DNA 1 kb ladder	ThermoFisher Scientific
Bacteria	
ampicillin sodium salt	Merck, Darmstadt, Germany
agar	Difco, Augsburg
arabinose	Carl Roth
chloramphenicol	Carl Roth
glycerol	Gerbu Biochemicals, Gailberg, Germany
kanamycin sulfate	Carl Roth
SDS	BioRad, München
Cell culture	
camptothecin (CPT)	Merck
concanavalin A (ConA)	Merck
dimethylsulfoxide (DMSO)	Biomol, Hamburg, Germany
Dulbecco's Modified Eagles Medium (DMEM) with phenol red; with 3.7 g/l $NaHCO_3$ and 4.5 g/l D-glucose	Bio&Sell, Feucht/Nürnberg
BD FACS™ Clean	Becton Dickinson, Franklin Lakes, USA
BD FACSFlow™	Becton Dickinson
BD FACS™ Shutdown Solution	Becton Dickinson
Proleukin® (interleukin 2)	Clinigen Healthcare B.V., Schiphol, Netherlands
Lipofectamine™ reagent, Lipofectamine™ 2000	ThermoFisher Scientific
L-glutamine (Gln)	PAN-Biotech, Aidenbach
Fetal bovine serum (FBS); charge A10107-1169	ThermoFisher Scientific
Hydrogen peroxide	Carl Roth
Opti-MEM™	ThermoFisher Scientific
Panserin™ 401	PAN™-Biotech
PBS	Bio&Sell
penicillin/streptomycin	PAN-Biotech
RPMI 1640 (with phenolred; with 2 g/l $NaHCO_3$)	Bio&Sell
trypan blue	Biochrom
trypsin-EDTA	PAN-Biotech
water, sterile (Ampuwa®)	Fresenius Kabi, Homburg, Germany
Molecular biological methods	
BigDye™ terminator v1.1	ThermoFisher Scientific
DNase I	Roche, Basel, Switzerland
deoxynucleotide triphosphates (dNTPs)	ThermoFisher Scientific
HotStarTaq® DNA polymerase	Quiagen, Hilden, Germany
oligonucleotides	Biomers GmbH, Ulm, Germany
Phusion® high-fidelity DNA polymerase	ThermoFisher Scientific
proteinase k	Qiagen
restriction enzymes	ThermoFisher Scientific
RNase A	ThermoFisher Scientific
T4 DNA ligase	ThermoFisher Scientific
T4 DNA polymerase	ThermoFisher Scientific
Taq DNA polymerase	ThermoFisher Scientific
water, nuclease- and DNA-free for PCR	Genaxxon, Ulm

Table 8: Oligonucleotides for *en passant* mutagenesis

Designation	location/ function	orientation	oligonucleotide sequence 5' → 3'
Project: promoter testing			
HF2947	BGH L/HDNA	for	AGT ATC ACG CGA AGT TCA CAA GGT GCG CAA AAC GCC CCT TCC CCC TCT TCA TTA AAT TTA AAT CCA TAG AGC CC
HF2948	HTLV prom. L/HDNA	rev	GCT CTA TGC AGC CCC CAC TGA TTT TCC CCC CGG GGG ATA ACT TGG TAG GCC GAT GGC GCG CCG CTC CGG TGC CCG
HF2949	SL3 prom. L/HDNA	rev	GCT CTA TGC AGC CCC CAC TGA TTT TCC CCC CGG GGG ATA ACT TGG TAG GCC TCG AGT AAC GCC ATT TTG CAA GGC
HF3449	CD2 prom. L/HDNA	rev	GCT CTA TGC AGC CCC CAC TGA TTT TCC CCC CGG GGG ATA ACT TGG TAG GCA ATC AAA TCT TAA GTG TCT TAA AT
HF3127	BGH left	for	CAA ATA TAG TGT TTT CAC TAA AAA ATT AAA AAG TAT CAC GCG AAG TTC ACA AAT TAA ATT TAA ATC CAT AGA GCC C
HF3125	HTLV prom. L/HDNA left	rev	TTC CCC CCG GGG GAT AAC TTG GTA GGC GAA GAG GGG AAG GGG CGT TTT GCG CAC CCG ATG GCG CGC CGC TCC GGT GCC CG
HF3126	SL3 prom. L/HDNA left	rev	TTC CCC CCG GGG GAT AAC TTG GTA GGC GAA GAG GGG GAA GGG GCG TTT TGC GCA CCC TCG AGT AAC GCC ATT TTG CAA GGC
HF3127	BGH left	for	CAA ATA TAG TGT TTT CAC TAA AAA ATT AAA AAG TAT CAC GCG AAG TTC ACA AAT TAA ATT TAA ATC CAT AGA GCC C
HF3128	replace *ORF75* by mRFP	for	GTT ATA TTC TCG TAT CTT AGT GTC AGA GTT TTT ATT ACT GTT ACT TAG TAC AAG GCT TAG ATG CTG AAT TTA GAA GAT ATT AAA TTT AAA TCC ATA GAG CCC
HF3129		rev	GCA AGC ACA GAA CTT CAG TTG ACT CAT CTT CTA AAT TCA GCA TCT AAG CCT TGT ACT AAG TAA CAG TAA TAA AAA CTC TAT GGC CTC CTC CGA GGA CGT CAT CA
Project: minimised vectors			
HF2988	Δ*71*	for	AGT ACA GAC ATT TCA AAT AAC TTA TTA TAA ACC ACA TTC ATG CTA GAC TAT TAC AGA ATT TCG AGG TCA TAT AAA TAG GGA TAA CAG GGT AAT CGA TTT
HF2989		rev	AAG ATC AAG TGT CTG AAG CAT TTT CTT TAT ATG ACC TCG AAA TTC TGT AAT AGT CTA GCA TGA ATG TGG TTT ATA GAA AAA CTC ATC GAG CAT CA
HF2986	Δ*16*	for	TGT TTA ACA AGC ATA TTC ATA ACA GCA GCT GAG TTA CCA CAT CTA AGA AAA ACT CCT CAA CTA TTA TTA ATT TTT TAG GGA TAA CAG GGT AAT CGA TTT
HF2987		rev	GAT GAA TTG TTG AAT AAA TAG ACA TAA AAA TTA ATA ATA GTT GAG GAG TTT TTC TTA GAT GTG GTA ACT CAG CTG GAA AAA CTC ATC GAG CAT CA
HF3119	Stopp*63*	for	CGT ACT AGG ATT TTC TGC TAA AGA GCT CAC AGA TGC CAC ACC ATA ACT GTT TTT TTT ATA TGA CTT TAT TAT AGA AGC ATT GTA TAG GGA TAA CAG GGT AAT CGA TTT A
HF3120		rev	GGA ACA TTG TAT GAA TGT TCA TGA TAC AAT GCT TCT ATA ATA AAG TCA TAT AAA AAA AAC AGT TAT GGT GTG GCA TCT GTG AGC GAA AAA CTC ATC GAG CAT CA
HF3121	Δ*M63*	for	CCA GAT CAA ATG TCC CCG TAC TAG GAT TTT CTG CTA AAG AGC TCA CAG ATG CCA CAC CAT AAA GTA TAA ACC CCA GTC AAC TGA ACT ATT AGG GAT AAC AGG GTA ATC GAT TTA
HF3122		rev	CGG TTT CAG TAA TAA ACT TTT GGA TAG ATT TTG ATA GTT CAG TTG ACT GGG GTT TAT ACT TTA TGG TGT GGC ATC TGT GAG CTC TTT AGC AGA GAA AAA CTC ATC GAG CAT CA
HF3215	Δ*3*	for	GCT GTA TTT AAA AAC TAT TGT TTA ATT ATT AAA GTC AAT TGC TGA ACA AGA CTT TTG TGG CAG AAA CTT ATG TAA CTT TAA GTG CAT TAA TTT AGG GAT AAC AGG GTA ATC GAT TTA
HF3216		rev	GCA CAA GAT ATG CTA TAT AAG TGA ATT TAG TAT AAT TAA TGC ACT TAA AGT TAC ATA AGT TTC TGC CAC AAA AGT CTT GTT CAC AAC CAA TTA ACC AAT TCT GAT TA

Designation	location/ function	orientation	oligonucleotide sequence 5' → 3'
HF3220	Δ*69*	for	AAT ATC CCA ACC GTC AAA GCT TTT CAG ACA TCA CAG ATT TAC GTA TAG AAA ATT TAT ATG ATT GTT GTC TTT CTT TAG GGA TAA CAG GGT AAT CGA TTT A
HF3221		rev	ACA ATA ACA CTG TCT AAA ATC TTA AAA GAA AGA CAA CAA TCA TAT AAA TTT TCT ATA CGT AAA TCT GTG ATG TCT CAA CCA ATT AAC CAA TTC TGA TTA
HF3222	Δ*52*	for	AAT GAA TAT TTT GAG TAA GTG TAA ACA ATT TTA TTT AAA ATG TAA AAA TTG ATG GCT ACA ACA ACA AAA CTT TAT TAG GGA TAA CAG GGT AAT CGA TTT A
HF3223		rev	ACT AAA TAA AGA ATA TTA AAG CTT TAT AAA GTT TTG TTG TTG TAG CCA TCA ATT TTT ACA TTT TAA ATA AAA TTG CAA CCA ATT AAC CAA TTC TGA TTA
HF3224	Δ*49*	for	ACA ATG ACA CAC AAG CCT GTT AAG GTA TGT AC TTA TTT TAT TAC ATA TAA TGT TTA ATC TTG TTT TTC TAG GAG GTA GGG ATA ACA GGG TAA TCG ATT TA
HF3225		rev	AGG CAA GAT TTT CTG ATC TGG ATA TCC TCC TAG AAA AAC AAG ATT AAA CAT TAT ATG TAA TAA AAT AAG TAC ATA CAA CCA ATT AAC CAA TTC TGA TTA
HF3226	Δ*45*	for	ATT AGT CTA TTA ATA AAA ACA AAT AAA CGT AAA ATT AGT TAC AAT GAT GTG TTT TTA GTA TTA AGG CAA TGC CCA TAG GGA TAA CAG GGT AAT CGA TTT A
HF3227		rev	AGA GCA TCA GAA GAA GCC TAT TTC TTG GGC ATT GCC TTA ATA CTA AAA ACA CAT CAT TGT AAC TAA TTT TAC GTT CAA CCA ATT AAC CAA TTC TGA TTA
HF3264	Δ*12-14*	for	TGA CTT ATC AAC ATA CAA ATA AAA AAT TTT CAG AAA CAC TAA GTC TAG TTT TAA AGT TAG AAT GAC TTT ACA TTG TAG GGA TAA CAG GGT AAT CGA TTT A
HF3265		rev	ATT TAC ATT GTA AAC TAT ATA TAG GCA ATG TAA AGT CAT TCT AAC TTT AAA ACT AGA CTT AGT GTT TCT GAA AAT CAA CCA ATT AAC CAA TTC TGA TTA
HF3266	Δ*M21*	for	TTC CTA TAA CTG CTT CTA ATA GTG TGT CCG AGC TTT TAA GTC TAC ATG ATC CTG AAG AAA TTG TAG AAG TAT GTT TAG GGA TAA CAG GGT AAT CGA TTT A
HF3267		rev	AGA TCT GTT ATG TGC TTT GCA TTG AAA CAT ACT TCT ACA ATT TCT TCA GGA TCA TGT AGA CTT AAA AGC TCG GAC CAA CCA ATT AAC CAA TTC TGA TTA
HF3268	Δ*70*	for	GTT ACA ATG TAA GTT TTT TAG TTT ATA GCA CGT TTT ACA TGT TAT TTC TCC TTA ATA ATT GTC AAG TTC TAC TTA TAG GGA TAA CAG GGT AAT CGA TTT A
HF3269		rev	ATT ATG GAC ACT TTA TAC AGT ATC TTA AGT AGA ACT TGA CAA TTA TTA AGG AGA AAT AAC ATG TAA AAC GTG CTA CAA CCA ATT AAC CAA TTC TGA TTA
HF3270	Δ*72*	for	TCC TCT GTA AAT GAG TCT GTT ATG TGT AAC ACT GTT GTT TTT AAG TCC ATT TTA GCA TAT AGC TAA AAA TTG GTT TAG GGA TAA CAG GGT AAT CGA TTT A
HF3271		rev	TCA AAC ATT TTA AAA ACC AGT CTG CAA CCA ATT TTT AGC TAT ATG CTA AAA TGG ACT TAA AAA CAA CAG TGT TAC CAA CCA ATT AAC CAA TTC TGA TTA
HF3272	Δ*73*	for	CAT ATA GCT AAA AAT TGG TTG CAG ACT GGT TTT TAA AAT GTT TGA TGA TGC TAT AAT TGC AAC AAA CAC GTT ATA TAG GGA TAA CAG GGT AAT CGA TTT A
HF3273		rev	AAA GAA CGT ATA TCG CCA TCT AGT GTA TAA CGT GTT TGT TGC AAT TAT AGC ATC ATC AAA CAT TTT AAA AAC CAG CAA CCA ATT AAC CAA TTC TGA TTA
HF3296	Δ*70-72*	for	GTT ACA ATG TAA GTT TTT TAG TTT ATA GCA CGT TTT ACA TGT TAT TTC TCT TTA GCA TAT AGC TAA AAA TTG GTT TAG GGA TAA CAG GGT AAT CGA TTT A
HF3297		rev	TCA AAC ATT TTA AAA ACC AGT CTG CAA CCA ATT TTT AGC TAT ATG CTA AAG AGA AAT AAC ATG TAA AAC GTG CTA CAA CCA ATT AAC CAA TTC TGA TTA

Designation	location/ function	orientation	oligonucleotide sequence 5' → 3'
HF3354	Δ*62*	for	AGA AAC TTT CAG CAT GTC AAT AAG ATT ACT GAT AAT TGT TTC TTG ACT CAT GTA AAA TGT CAG TAA AAC TAC TTA TAG GGA TAA CAG GGT AAT CG
HF3355		rev	GCT TCA AGA TTT TTT GTT AGT TCA GTA AGT AGT TTT ACT GAC ATT TTA CAT GAG TCA AGA AAC AAT TAT CAG TAA TTA GAA AAA CTC ATC GAG CAT CAT C
HF3356	Δ*64*	for	TTT ACA CAT TTA ACT AGC GAT ATT CTA GAT GCA GAA TTA AGC AAA TAA CAA ACT TAT TTT GCT TTT GAT TTT TTT TAG GGA TAA CAG GGT AAT CG
HF3357		rev	CAG CAG CAG ATA CTA ATG ACT CTA AAA AAA AAT CAA AAG CAA AAT AAG TTT GTT ATT TGC TTA ATT CTG CAT CTA TTA GAA AAA CTC ATC GAG CAT CAT C
HF3454	Δ*71-73*	for	AGT ACA GAC ATT TCA AAT AAC TTA TTA TAA ACC ACA TTC ATG CTA GAC TAC TAT AAT TGC AAC AAA CAC GTT ATA TAG GGA TAA CAG GGT AAT CGA TTT A
HF3455		rev	AAA GAA CGT ATA TCG CCA TCT AGT GTA TAA CGT GTT TGT TGC AAT TAT AGT AGT CTA GCA TGA ATG TGG TTT ATA CAA CCA ATT AAC CAA TTC TGA TTA
HF3458	Δ*StpC/Tip*	for	GCA TTT CTT TTA ATC ACC ATG CAC ACA CAT TTG TTA ACA GTT TTG TTA CAT TTT TTC AAG ACT GTT TGT GTT GCT TAG GGA TAA CAG GGT AAT CGA TTT A
HF3459		rev	AGT AAC ACA AGA AAC AGC TAA CAA GAG CAA CAC AAA CAG TCT TGA AAA AAT GTA ACA AAA CTG TTA ACA AAT GTG CAA CCA ATT AAC CAA TTC TGA TTA
Project: human γδ TCR expression			
HF3046	ΔVg9-Polio-IRES from γδTCR- BAC	for	GAG ATC CTC TGC ATG GCT CAC TCC CCT CGA GCG GCC GCT AGC ATT TAA ATG TCT GCC CGG GCG GCC GCC AGT GTG TAG GGA TAA CAG GGT AAT CGA TTT
HF3047		rev	CTA ACA AGA GCA ACA CGA TAT CCA TCA CAC TGG CGG CCG CCC GGG CAG ACA TTT AAA TGC TAG CGG CCG CTC GAG GAA AAA CTC ATC GAG CAT CAA ATG A
HF3065	SL3Vγ9 L/HDNA	for	AGT ATC ACG CGA AGT TCA CAA GGT GCG CAA AAC GCC CCT TCC CCC TCT TCA ATC CAA TTC GCT TTA TGA TAA CAA TCT GTG ATT GTC ACC ATA AGC AGC CTA GGG ATA ACA GGG TAA TGC CAG TG
HF3066		rev	CTC TAT GCA GCC CCC ACT GAT TTT CCC CCC GGG GGA TAA CTT GGT AGG CTA ACG CCA TTT TGC AAG GCA TGG GAA
HF3069	HTLVVγ9 L/HDNA	for	AGT ATC ACG CGA AGT TCA CAA GGT GCG CAA AAC GCC CCT TCC CCC TCT TCA ATC CAA TTC GCT TTA TGA TAA CAA TCT GTG ATT GTC ACC ATA AGC AGC CTA GGG ATA ACA GGG TAA TGC CAG TG
HF3070		rev	CTC TAT GCA GCC CCC ACT GAT TTT CCC CCC GGG GGA TAA CTT GGT AGG CGC TCC GGT GCC CGT CAG TGG GCA GAG CGC
HF3131	Vδ2 under *StpC* prom.	for	CCT GTT TCT TCA ATT GGA TAT CTT AGG TTC GGT TCG CTT GCC ATG GTG GCA GAA AGA TCC CGG GGG CGC GCC TGT GGC CA
HF3132		rev	AGT AAC ACA AGA AAC AGC TAA CAA GAG CAA CAC AAA CAG TCT TGA AAA AAG CTT ATG GTG ACA ATC ACA GAT TGT TAT CAT AAA GCG AAT TGG ATT ATT TAT GAG CCA TAT TCA ACG GGA AAC GTC TTG C

Table 9: List of all oligonucleotides used for confirming insertions, cloning, and sequencing

Designation	location/function	orientation	oligonucleotidesequence 5' → 3'
Kanamycin-resistence gene *aphA1* specific (orientation relative to *aphA1* orientation)			
HF1681	*aphA1*	rev	GCA AGA CGT TTC CCG TTG AAT ATG G
HF1690		for	GCA AAG GTA GCG TTG CCA ATG
HF1699		rev	GTA AGC AGA CAG TTT TAT TG
HF1718		rev	TTA TCG CGA GCC CAT TTA TAC C
HF2774		rev	ATA CAA TCG ATA GAT TGT CGC
HF2790		for	TTT CTC CTT CAT TAC AGA AAC GGC
HF3211	GAPDH	for	GCA GGG GGG AGC CAA AAG GG
HF3212		rev	TGC CAG CCC CAG CGT CAA AG
HVS C488 and insert specific (orientation related to location within the BAC)			
HF114	upstream *ORF14*	rev	GAA ACT GAC ACA TAT TAT GAG CC
HF173	*ORF21*, start	for	CAA ACG CCA AAG AAT AGC AG
HF180	*ORF50*, start	rev	CTG CAA TTT GTA GGC ACT C
HF208	*ORF48*, start	for	CTT AGT AAG CCT AGT GTC C
HF234	*ORF5*, central	for	CAC TTA AAG CCC CCA TAA C
HF245	*ORF22*	for	GTA AGG GCA AGC GTC ACT C
HF339	HTLV prom., central	for	TGA AGG AGA GAT GCG AG
HF340	HTLV prom., terminal	rev	TGC TTG CTC AAC TCT AC
HF375	*ORF2*, start	for	ATG ACC GGA AGA GGA CAG CCT C
HF376	*ORF21*, terminal	rev	TCA TTG AGA ATT AAA CGT CCT CGC
HF445	downstream *ORF3*	for	TGC CTA AGT ACC TAG TGC C
HF481	downstream *ORF12*	for	TCT GCT ATC TGT TTG CCT G
HF511	*ORF46*, start	rev	CTT ATG AGC ATC CGA TTC C
HF561	*ORF44*, terminal	for	TTC TCC TCC ACC AAC TGC C
HF557	*ORF29*	rev	AAC GAG TAG GAG GAA AGT C
HF667	*ORF53*, central	rev	CAT CTG TTT GGG CTA TTG TAA ATC
HF713	*ORF53*, start	rev	CTG ATA ACG AAG ATG AGT TGG
HF727	downstream *ORF13*	for	GTG TAT CTC AAA CTC AAC
HF742	*ORF75*	for	TGG CTG CTA ACA GGC ATG G
HF743	*ORF75*	rev	AGC ACG TTG CCC GAG ATT G
HF759	between *ORF75* and right-end H-DNA	for	TCA TCA GCA CTG TTT GAG G
HF768	H-DNA repeat	for	GCC TCA GAA TTT TAG CAC C
HF1109	*ORF75*	for	ATG CTT TTA GTA GTT TGA GG
HF1110	*ORF75*	rev	AGG CAC AGT TGA CAA TGT
HF1505	*RFP*, terminal	for (inserted)	TGT ACA AGG CGC CGG TGG AGT GGC
HF1533	*ORF74*, terminal	for	CAG CGC ATG GCT GCA TGG TGT AA
HF1578	*RFP*, terminal	rev (inserted)	CGA CAT CAA GCT GGA CAT C
HF1729	*sopA*	for	TGG GGT TTC TTC TCA GGC TAT C
HF1730	*sopA*	rev	TAG TCA AAC AAC TCA GCA GGC G
HF1821	*cat*	for	TGC CAC TCA TCG CAG TAC TG
HF1822	*cat*	rev	AGG CAT TTC AGT CAG TTG CTC
HF1836	*GFP*	for	AGC AAG GGC GAG GAG CTG TTC
HF1837	*GFP*	rev	TCA CGA ACT CCA GCA GGA CC
HF1842	downstream *Tip*	for	AGC GCC TAG CCA ATG CTA TGA AG
HF1847	StpC/Tip prom., terminal	rev	GAG TTT CCA AAA TGT ACT AAG CTA AC
HF1850	*ORF1* prom., upstream *StpC*	rev	TCA GAC AAG AAG TGG GCA ATG
HF2324	between *ORF75* and right-end H-DNA	rev	GCA CCT TGT GAA CTT CGC GT

Designation	location/function	orientation	oligonucleotidesequence 5' → 3'
HF2357	*BGH polyA*, start	rev (inserted in eGFPΔ75mRFPbGH)	TTA ATT AAC CTA GGC TGT GCC TTC TAG TTG CCA G
HF2556	CD2 enhancer, central	rev (inserted)	CCT GCC AGA GTG TAA CAA GGT T
HF2557	CD2 enhancer, central	rev (inserted)	GCT CAC TGA GGA TTG AAC TAC TT
HF2558	CD2 prom., start	for (inserted)	GCC AAA GCA GAT GTG TTT AT
HF2729	*Tip*	for	TTC ACC TAG GTT CGC TGG CC
HF2730	*Tip*	rev	AAG ACG CAA GGG CAC AAG G
HF2731	end *StpC*	for	TTT ACT ACT AAT TTA GAC ACG
HF2804	*ORF22*	rev	ATG AAT TAG TTG AGC TAT GGC
HF2815	*ORF29*	for	TTG AAA ATG TGT TTG TTT GAG G
HF2933	upstream *ORF63*	for	ATA TTT AGA TAA TGC TTG CC
HF2991	HTLV prom., start	rev	GCA GTA GTC GCC GTG AAC GTT
HF2992	*mRfP*, start	for	CGT CCT CGG AGG AGG CCA T
HF2993	SL3 promoter, central	for	GCT TAA CCA CAG ATA TCC TGT CGT T
HF2995	SL3 prom., terminal	rev (inserted)	CGC TTA TTG CTG CCC AGC TCT ATA A
HF3048	human *Vδ2* , central	for	CCA AGG TGT CAC AGG CAC AGT AGT A
HF3051	SL3 prom., start	for	GCG GTG AGT GGG AGC TGC TAG CCC TT
HF3060	upstream *ORF16*	for	GCC AAA CTT GCC AGT TAA TTA CAT
HF3061	downstream *ORF71*	for	GCT TCA TTG CTT TTC TAC TAC TCT
HF3062	upstream *ORF71,* terminus *ORF72*	rev	TTG GAC TTG TTA CCT AGA AGA CC
HF3219	upstream *ORF3*	rev	CCC TTT ATA CAA GAC TAA AA
HF3228	*ORF68*, terminus	for	CCT TAG ACA CAT TAC AAA CAC TAA A
HF3229	*ORF70*, terminus	rev	GGA GTG CCA TTT AAC ATT GCT AGC TA
HF3230	*ORF44*, terminus	for	GCT AGA AAA TTT AGA TGA TGG AAA A
HF3242	downstream *ORF16*	rev	CCT ACT GAA AGT GCA TCC AAT GAA
HF3298	*mRFP*	for	TAC TGT TCC ACG ATG GTG TAG TCC
HF3299	*mRFP*, central	rev (inserted)	AAC TTC GAG GAC GGC GGC GTG G
HF3304	downstream *ORF70*	for	TTT GTT TAC AAG TCC CCA TGG
HF3305	upstream *ORF70*	rev	ATA ATT CAT TTT TGA TGT GC
HF3306	*ORF71*, central	for	AAA CAC TGC GTT AGA CAA ATA TCC C
HF3307	*ORF73*, terminus	rev	ATT TCC AAA AGG GCC TAG AGC
HF3308	*ORF72*, start	for	TTT GTA TTT CCC ATA GAC TGG T
HF3309	upstream *ORF73*	rev	TTT CGA TTT TCA ATG TGA GTA GC
HF3466	human *Vδ2*	for	ATG GCT TTG GGT TTA TGG CA
HF3467	human *Vδ2*	rev	ATG TCG CTT GTC TGG TGA AGG
HF3468	human *Vγ9*	for	CTC CAT TGC AGC AGA AAG CC
HF3469	human *Vγ9*	rev	GAG CAA CAC GAT TCT GGG AT
HF3470	*GFP*	for	CTGGGTGCTCAGGTAGTGGTTG
HF3471	*GFP*	rev	GGACGACGGCAACTACAAGA

Table 10: Oligonucleotides used for PCRs after virus passages

Designa-tion	demonstration of	orientation	oligonucleotide (5' - 3')
HF1109	*Orf75*	for	ATG CTT TTA GTA GTT TGA GG
HF1110		rev	AGG CAC AGT TGA CAA TGT
HF1729	*sopA*	rev	TGG GGT TTC TTC TCA GGC TAT C
HF1730		for	TAG TCA AAC AAC TCA GCA GGC G
HF1821	*cat*	rev	TGC CAC TCA TCG CAG TAC TG
HF1822		for	AGG CAT TTC AGT CAG TTG CTC
HF245	*ORF22*	rev	GTA AGG GCA AGC GTC ACT C
HF2804		for	ATG AAT TAG TTG AGC TAT GGC

Designation	demonstration of	orientation	oligonucleotide (5' - 3')
HF557	*ORF29*	rev	AAC GAG TAG GAG GAA AGT C
HF2815		for	TTG AAA ATG TGT TTG TTT GAG G
HF375	Δ*M21*	for	ATG ACC GGA AGA GGA CAG CCT C
HF376		rev	TCA TTG AGA ATT AAA CGT CCT CGC
HF445	Δ*3*	for	TGC CTA AGT ACC TAG TGC C
HF3219		rev	CCC TTT ATA CAA GAC TAA AA
HF481	Δ*12-14*	for	TCT GCT ATC TGT TTG CCT G
HF114		rev	GAA ACT GAC ACA TAT TAT GAG CC
HF3060	Δ*16*	for	GCC AAA CTT GCC AGT TAA TTA CAT
HF3242		rev	CCT ACT GAA AGT GCA TCC AAT GAA
HF3061	Δ*71*	for	GCT TCA TTG CTT TTC TAC TAC TCT
HF3062		rev	TTG GAC TTG TTA CCT AGA AGA CC

Table 11: Culture media for bacterial and eukaryotic cells

Reagent	Composition
Bacterial culture media	
Luria Bertani (LB) agar	10 g/l tryptone; 5 g/l yeast extract; 10 g/l NaCl; pH 7; 15 g/l agar
LB medium	10 g/l tryptone; 5 g/l yeast extract; 10 g/l NaCl; pH 7
freezing medium	50 % LB medium; 50 % glycerol
Super optimal broth with glucose (S.O.C.) medium	20 g/l tryptone; 5 g/l yeast extract; 0.5 g/l NaCl; 2.5 mM KCl; pH 7; 10 mM $MgCl_2$; 20 mM glucose
Cell culture	
D10	DMEM; 10 % FBS; 1 % penicillin/streptomycin; 1 % Gln
R10	RPMI 1640; 10 % FBS; 1 % penicillin/streptomycin; 1 % Gln
TC50	44 % Panserin^{TM} 401, 44 % RPMI 1640; 10 % FBS; 1 % penicillin/streptomycin; 1 % Gln; 50 U/ml interleukin 2

Table 12: Commercial Kits

Kit	Supplier
PCR clean-up gel extraction: NucleoSpin^{TM} Extract II	Macherey-Nagel, Düren
Topo^{TM} TA Cloning^{TM} kit	ThermoFisher Scientific
FITC annexin V apoptosis detection kit I	Becton Dickinson Biosciences, Franklin Lakes, USA
SMARTer® RACE 5'/3' kit	Takara Bio, Kusatsu, Japan
plasmid maxi kit	Quiagen
DNeasy® Blood and Tissue Kit	Quiagen

Table 13: Antibodies and staining

Antibody	concentration	supplier
anti-CD3 (PE)	5 µl/100 µl	Becton Dickinson Biosciences
anti-αβ TCR (PE)	5 µl/100 µl	Becton Dickinson Biosciences
anti-γδ TCR (FITC)	5 µl/100 µl	Becton Dickinson Biosciences
anti-Vδ2	5 µl/100 µl	ThermoFisher Scientific
anti-Vγ9	5 µl/100 µl	ThermoFisher Scientific
anti-mouse Alexa488	2 µl/100 µl	ThermoFisher Scientific

Table 14: Software used for analysis and documentation

Software	Application	Company
BD FACSDiva™ v5.0.3	flow cytometer and application setup and data acquisition	Becton Dickinson
BD spectrum viewer	evaluation of excitation/ emission curves of fluorochromes in common flow cytometers	https://www.bdbiosciences.com/en-us/resources/bd-spectrum-viewer; Becton Dickinson
cellSens Dimension	acquisition of fluorescence images, live-cell imaging	Olympus, Tokyo, Japan
dsDNA calculator	dsDNA copy number calculator	http://cels.uri.edu/gsc/cdna.html; University of Rhode Island, Genomics and Sequencing Center
FCS Express™ 6	analysis of flow cytometry data	De Novo Software, Pasadena, USA
Inkscape	graphic design software	open source
Intas GD	agarose gel documentation	Intas Science Imaging Instruments
Microsoft Excel®	data analysis	Microsoft
NanoDrop™ 2000	DNA concentration	ThermoFisher Scientific
Prism® 5	statistical analysis and graph design	GraphPad Software, Inc., San Diego, USA
Vector NTI® 11	virtual cloning	ThermoFisher Scientific

Table 15: Laboratory equipment

Device type	Device name	Company, location
aspirator	vacuum pump BVC 21 NT	Vacuubrand, Wertheim, Germany
centrifuges	Thermo Scientific™ Biofuge fresco 17	ThermoFisher Scientific
	Heraeus Multifuge® 4KR	ThermoFisher Scientific
electroporator	Gene pulser Xcell™	Bio-Rad Laboratories, Hercules, USA
flow cytometer	FACSCanto™ I	Becton Dickinson Biosciences
gel electrophoresis power supplies	power Supplies 202	VWR
gel electrophoresis chambers	PerfectBlue™ maxi	ExW Peqlab Biotechnology
gel documentation	UV system	Intas Science Imaging, Göttingen, Germany
incubators	CO_2 incubator CB series	Binder , Tuttlingen, Germany
	HT Multitron®	Infors HT, Bottmingen, Switzerland
	Heraeus BBD6220	ThermoFisher Scientific
laminar flow cabinet	HeraSafe® KS	ThermoFisher Scientific
magnetic stirrer	Combimag REO	IKA, Staufen, Germany
microwave	Samsung ME76V	Samsung, Suwon-si, South Korea
microscopes	DM IL	Leica Microsystems, Wetzlar, Germany
	IX81	Olympus
	BZ9000	Keyence, Osaka, Japan
spectrophotometer	NanoDrop™ 2000	ThermoFisher Scientific
orbital shaker	Duomax 1030	Heidolph Instruments, Schwabach, Germany
PCR cycler	Thermocycler T3000	Biometra
	Thermocycler T3	
pipetboys	acu2	INTEGRA Biosciences, Biebertal, Germany
pH meter	SevenEasy™ S20	Mettler Toledo, Columbus, USA
photometer	Biophotometer	Eppendorf, Hamburg, Germany
quantitative PCR instrument	7500 real-time PCR system	ThermoFisher Scientific
scales	BP210 S	Sartorius, Göttingen, Germany
thermal incubator	Thermomixer compact	Eppendorf
vortexer	Vortex genius 3	IKA
water baths	GLS400	Grant Instruments, Shepreth, UK
	WNE 10	Memmert, Schwabach, Germany

2.2 Molecular biological methods

2.2.1 Transfer vectors for *en passant* mutagenesis and their cloning strategy

Different promoters were prepared for the activity analysis within HVS-transformed T cells. The human T-cell leukemia virus (HTLV) long terminal repeat promoter was derived from the plasmid topoHTLV (Linda Hüske), cloned into the commercial vector topoTA (ThermoFisher). The T-cell specific CD2 promoter and enhancer (NCBI reference numbers: NG_046701.1, NG_046633.1) were derived from the plasmid topoCD2 (Linda Hüske). The SL3 promoter was amplified using the oligonucleotides HF2252 and HF2253 from the plasmid pIC19RSL3 (Grassmann et. al, 1989) and ligated subsequently into topoTA. The newly generated topoSL3 was used to transform *E. coli* DH5α. The plasmid topoBGH (Tuna Toptan) was used to isolate the bovine growth hormone (bGH) polyadenylation signal (polyA) sequence.

The chosen vector backbone, pep-mRFP-in (Tischer et al., 2006), was linearised with NotI (20 U, buffer orange 1x, approximately 1 µg DNA, ad 20 µl water). The SL3 promoter was released from the plasmid using the restriction enzymes HindIII and XhoI (20 U each, buffer red 1x, approximately 6 µg DNA, ad 30 µl), while HTLV was digested with AfeI (20 U, buffer orange 1x, approximately 6 µg DNA, ad 30 µl), and CD2 enhancer and promoter were digested with ClaI and AvrII (20 U each, buffer Tango 1x, ad 30 µl). Lastly, PacI was applied to separate the bGH polyA sequence from its vector (2 U, cut smart buffer 1x, approximately 6 µg DNA, ad 30 µl). After incubation at 37 °C for at least 1 h, the enzymes were heat inactivated at 65 °C or 80 °C for 30 min and overhangs generated by restriction enzymes were filled in by T4 polymerase (1.5 U, 0.1 mM dNTPs) for 30 min at room temperature. All samples were separated by gel electrophoresis and purified from the agarose using the NucleoSpin® Extract II kit (Macherey-Nagel). The concentration was estimated by running another agarose gel and comparing the sample intensity with the marker bands. The subsequent ligation of pepmRFP-in with BGH-polyA was performed applying the following formula.

$$\text{ng insert} = \frac{\text{ng vector x kb insert}}{\text{kb vector}} \text{ x } \frac{\text{insert}}{\text{vector}}$$

The insert to vector ratio amounted to 5 for blunt-end ligation, and to 3 for sticky-end ligation, respectively. The ligation mix was used to transform DH5α. After 24 h incubation on agar plates containing the appropriate antibiotic, colony PCR was performed using HF519 and HF2790. The clones positive for insertion were tested for insertion by digestion with NheI. The plasmid was then linearised again using AgeI (20 U, buffer orange 1x, ad 30 µl), blunted again, and ligated with SL3-, CD2-, and HTLV-promoter, respectively. All generated plasmids were proven correct via colony PCR, restriction enzyme digestion, and sequencing. As a

transfer vector for BACs carrying Vδ2 and Vγ9 with a respective IRES for antigen-specificity redirection, the plasmid hr1Vγ9PolioIRESKandupVδ2 (Linda Bremer) was used.

2.2.2 Two-step *red*-mediated *en passant* mutagenesis

Preparation of recombination- and electro-competent *E. coli* GS1783 with a viral BAC: The chosen strain carrying the respective BAC was grown in an over-night culture and used on the next day to inoculate a larger volume of LB medium containing chloramphenicol (CAM). The culture was grown at 32 °C shaking, until the optical density at 600 nm reached 0.5-0.7 and, subsequently, placed in a shaking water bath at 42 °C for 15 min to induce *red*-gene expression. The culture was transferred into an ice-bath for 20 min to allow the cells to cool down. At 4,500 x g, the culture was centrifuged for the following 5 min at 0 °C. The medium was removed and the cells were washed in the same amount of ice-cold 10 % v/v glycerol three times (4,500 x g, 5 min, 0 °C). Subsequently, the bacterial cell pellet was resuspended in a hundredth of the original culture volume of 10 % v/v ice-cold glycerol, and sampled into portions of 50 µl per reaction tube. The samples were either used directly for electroporation, or frozen in a dry ice-ethanol bath.

Electroporation of competent cells and first Red-recombination: Approximately 100 ng of the purified DNA was added to the prepared sample of recombination- and electro-competent bacterial cells carrying the BAC to be manipulated. The mixture was kept on ice until it was transferred into a cold cuvette (1 mm, Sarstedt) and subjected to an electric pulse of 1.5 kV per cm, 25 µF, and 200 Ω. The mixture was transferred into LB broth without antibiotics and grown gently shaking at 32 °C for further 2 h. The culture was plated on LB agar plates containing CAM and KAN and the plates were incubated for 2 d at 32 °C and 5 % CO_2.

Second Red-recombination: An over-night culture of 5 ml was grown at 32 °C in LB (CAM, KAN) and the following day a volume of 100 µl was used to inoculate 2 ml of LB (CAM). The culture was grown for 2-4 h and 2 ml ob LB (CAM) containing 1 % m/v of arabinose were added to induce the expression of I-SceI. After an incubation of 1 h, the culture was placed in a shaking water bath at 42 °C and incubated for further 30 min. Lastly, the culture was transferred back to 32 °C and incubated 2-4 h gently shaking. An appropriate dilution of the culture was plated on LB agar (CAM, 1 % m/v arabinose). Alternatively, an inoculation loop was used to achieve single colonies on the agar. The plates were grown for 2 d at 32 °C and 5 % CO_2.

2.2.3 Isolation of DNA of bacterial artificial chromosomes

BACs were isolated from *E. coli* strain GS1783 after alkaline denaturation (Birnboim & Doly, 1979). The bacteria with the desired BAC were grown gently shaking at 32 °C over night in 3-

10 ml of LB with the required antibiotic/s (30 µg/ml chloramphenicol (CAM); 35 µg/ml kanamycin (KAN)). The following day, 2 ml of the cell culture were centrifuged for 5 min at 17,000 x g. The supernatant was discarded and the cells resuspended in 300 µl of buffer P1. Once the bacterial pellet was completely resuspended, the alkaline lysis was induced by addition of 300 µl of buffer P2 and was stopped after 3-5 min with neutralising buffer P3. After adding P2 and P3, the tube was inverted vigorously several times. The mixture was placed on ice for 10 min to allow precipitation of proteins and lipids and was subsequently centrifuged for 10 min at 17,000 x g. The supernatant was transferred carefully into 600 µl isopropanol in a prepared tube which was gently inverted three to five times. To precipitate the DNA, the tube was centrifuged for 15 min at 17,000 x g. Subsequently, the DNA pellet was washed with 1 ml ethanol (70 % v/v) and 5-10 min at 17,000 x g. The ethanol was removed completely and the DNA pellet was dried at room temperature for 10 min followed by resuspension in 35 µl of DNAse-free water.

For large-scale plasmid or BAC DNA isolations, 500 ml of bacterial culture was grown over night at 37 and 32 °C, respectively, and the DNA isolated after alkaline denaturation with the Plasmid Maxi kit (Quiagen) which results in higher purity and concentrations due to the purification over an anion-exchange column.

2.2.4 Isolation of viral DNA from virus-containing supernatants

To isolate viral DNA 6 ml of the high-titre supernatant were centrifuged in three 2 ml tubes at maximum speed for 2 h at 4 °C. The supernatant was discarded and the pellets were pooled in 200 µl of DNAse mix and incubated at 37 °C for 30 min to digest all remaining cellular DNA. The DNAse was subsequently inactivated for 15 min at 75 °C and cooled down on ice until it reached room temperature. Next, 100 µl of sterile PBS were added, followed by 20 µl of proteinase K and vortexing, and another 20 µl of RNAse A and vortexing. For the following steps, the DNeasy kit (Quiagen) was used. The amount of 200 µl AL buffer was added followed by vortexing and incubation at 56 °C for 10 min. Afterwards 200 µl of pure ethanol (100 % v/v) were added and the mixture vortexed again. The suspension was transferred onto the column and centrifuged at 6,000 x g for 1 min and the flow through was discarded. Washing was performed twice with 500 µl of AW1 (6,000 x g; 1 min) and AW2 (21,100 x g; 3 min). The flow through was discarded and the column was dried at 21,100 x g for 1 min. With 200 µl of AE buffer the DNA was eluated from the column during 5 min of incubation at room temperature and centrifuged into new, clean tubes at 6,200 x g for 1 min. A volume of 20 µl 3M sodium acetate was added to the DNA solution and the tube inverted. After adding 400 ml of ethanol (100 % v/v) the tube was inverted again and incubated at -80 °C for 30 min in a precooled holder. Afterwards the sample was centrifuged again at 21,100 x g for 1 h at

4 °C and the supernatant was discarded. The pellet was air-dried and resuspended in 17 µl of DNAse-free water.

2.2.5 Polymerase chain reaction

The polymerase chain reaction (PCR) is based on thermostable versions of the enzyme DNA polymerase. It amplifies DNA sequences based on oligonucleotide binding (table 16). Three different polymerases were used in these projects, Taq polymerase and HotStarTaq® polymerase, and Phusion® polymerase.

Table 16: Oligonucleotide-combinations for each recombination to confirm insertions and for sequencing

Insert/Deletion	first recombination	second recombination	sequencing
HTLV-mRFP-BGH polyA between *ORF75* and H-DNA	HF439 + HF1578	HF1505 + HF340	HF759, HF1505, HF2992, HF2991, HF1578, HF340, HF2324, HF339
SL3-mRFP-BGH between *ORF75* and H-DNA	HF3051 + HF1578	HF759 + HF3063	HF2324, HF1578, HF2992, HF2993, HF1505, HF2995
CD2-mRFP-BGH between *ORF75* and H-DNA	HF3051 + HF1578	HF1505 + HF2995	HF1576, HF2556, HF2557, HF2558, HF2992, HF3299, HF1699
replace *ORF75* with *mRFP*-BGH	HF1533 + HF1578	HF1505 + HF1846	HF2324, HF2992, HF1533, HF2357
ΔStpC/Tip	HF1718 + HF1842	HF768 + HF1850	HF768, HF1850
Δ3	HF3219 + HF1681 HF445 + HF1699	HF445 + HF3219	HF445, HF3219
Δ12-14	HF481 + HF1699	HF481 + HF114	HF481, HF114
Δ13-14	HF727 + HF1681		
Δ16	HF3060 + HF1699	HF3060 + HF3242	HF3060, HF3242
ΔM21	HF375 + HF1699	HF173 + HF376	HF173, HF375, HF376
Δ45	HF511 + HF2790	HF511 + HF561	HF511, HF3230
Δ49	HF208 + HF2774	HF208 + HF180	HF180, HF208
Δ52	HF234 + HF2774	HF234 + HF713	HF667, HF3061, HF234
Stop63	HF2933 + HF1699		
ΔM63	HF2933 + HF1699		
Δ69	HF3228 + HF1699	HF3228 + HF3229	HF3228, HF3229
Δ70	HF3061 + HF1699	HF3304 + HF3305	HF3304, HF3305
Δ71	HF3061 + HF1699	HF3061 + HF3062	HF3061, HF3062
Δ72	HF3306 + HF1699	HF3306 + HF3307	HF3306, HF3307
Δ73	HF3308 + HF1699	HF3308 + HF3309	HF3308, HF3309
Δ70-72	HF3061 + HF1699	HF3304 + HF3307	HF3304, HF3307
Δ71-73	HF3061 + HF1681		
SL3Vγ9 between *ORF75* and H-DNA	HF759 + HF1690	HF2378 + HF3051	HF 2378, HF 3051, HF3173
Vδ2 under *StpC* promoter	HF2731 + HF3059	HF3048 + HF1850	HF1847, HF3048, HF3059, HF2731

HotStarTaq® DNA polymerase was mainly used for PCRs directly after virus passages in tissue culture, where viral DNA was still packed within their virions. This Taq-based polymerase had to be heat-activated and thereby limited oligonucleotide self-binding prior to

PCR. HotStarTaq® DNA Polymerase 5x buffer was diluted to 1x by mixing it to final concentrations of 0.2 µM dNTPs, 1 µM of each oligonucleotide, 0.1 U/µl HotStarTaq® DNA Polymerase, and water, to a reaction volume of 50 µl. Initial denaturation was achieved with 10 min at 95 °C, followed by 25-42 cycles of denaturation (95 °C, 30 s), primer annealing (50-70 °C, 30 s), elongation (70 °C, 1 kb/min), with a final elongation for 10 min at 72 °C.

Taq polymerase had a good general sensitivity and specificity and was mainly used for colony PCRs. The master mix contained $(NH_4)_2SO_4$ buffer 1x, as well as 4 µM $MgCl_2$, 0.2 µM dNTPs, 1 µM of each oligonucleotide, 0.5 U/µl Taq polymerase, and water. The reaction volume amounted to 25 µl. The runtime protocol did not vary from the HotStar®Taq DNA Polymerase protocol. DNA was either used at a concentration between 10 pg-1 µg, or, a small quantity of directly picked bacterial cells of one clone (one colony) were used where DNA was released during the initial denaturation of PCR.

Phusion® polymerase had the lowest, and thus, best error rate and offered the advantage of fast amplification. It was primarily used to amplify recombinant PCR products for the *en passant* mutagenesis and for cloning. Phusion® high fidelity 5x buffer was used at 1x concentration, additionally 0.2 µM dNTPs, 0.5 µM of each oligonucleotide, 0.02 U/µl of Phusion® high fidelity polymerase and water up to 50 µl were added. Initial denaturation was achieved with 30 s at 98 °C, followed by 25-40 cycles of denaturation (98 °C, 10 s), primer annealing (50-70 °C, 30 s), elongation (72 °C, 1 kb/20-40 s), and final elongation for 10 min at 72 °C.

2.2.6 Agarose gel electrophoresis and purification from gel

To determine size or concentration of DNA, or to select a specific band and purify it, DNA was run in TBE-agarose gels containing 0.5 µg/ml ethidium bromide. Agarose concentration depended on the products size and varied between 1.5 % and 0.6 %. Voltage and runtime depended likewise on the gel size, percentage, and the DNA products size. Small gels were run with 100-120 V for up to 2 h, while the larger gels for restriction fragment length polymorphism (RFLP) analysis were run at 50 V for 18-48 h. Purification was performed using NucleoSpinExtract® II kit (Macherey-Nagel). Elution from the anion-exchange column was achieved using 15-30 µl molecular pure water. DNA concentration was estimated by running another gel and comparing the isolated DNA's concentration to that of an appropriate DNA ladder.

2.2.7 Determination of the transcription start of *ORF75*

WTf HVS C488 virus was used to infect 5x 10^5 permissive OMK cells with a multiplicity of infection (MOI) of 4. Five different points of time (1-5 dpi) were chosen for total RNA isolation. At the indicated points of time, the infected cells were scraped off the 6-well plate and

the supernatants with cells collected and then centrifuged for 10 min at 460 x g. The cell pellets were flash frozen in liquid nitrogen and stored at -80 °C until further use.

The total RNA of 1-5 dpi was later on isolated by the RNeasy® kit (Quiagen). Subsequently, cDNA synthesis was performed according to the manual using the provided ingredients of the SMARTer® RACE 5'/3' kit (Takara). The gained cDNA was used to run a PCR amplifying the desired sequence with oligonucleotides provided by the manufacturer, and the additionally designed *ORF75* specific oligonucleotide HF3130 (table 17). The recommended controls were included. First, five cycles of denaturation for 30 s at 94 °C, followed by 2 min of elongation at 72 °C were performed. Second, another five cycles followed, consisting of 30 s denaturation at 94 °C and 30 s elongation at 70 °C and 2 min at 72 °C. Lastly, 25 cycles of 94 °C for 30 s, 68 °C for 30 s and 72 °C for 2 min followed.

Table 17: Oligonucleotides for determination of *ORF75* transcription start

Designation	location	orientation	oligonucleotide (5' - 3')
HF3130	pRACE ,*ORF75*	for	G ATTA CGC CAA GCT TAG AAG GTG ATG CAG CGT TGA A CAT GAC C
HF1381	pRACE	rev	GGA GAA AAT ACC GCA TCA G
HF3051	*ORF75*	for	GCG GTG AGT GGG AGC TGC TAG CCC TT

The PCR product was analysed via gel electrophoresis and all products within a reasonable size range were purified from the gel with the NucleoSpinExtract® II kit. In-fusion cloning was subsequently performed with the supplied, linearised pRACE vector in Stellar competent cells, according to manufacturer protocol. The transformed clones were later subjected to colony PCR and Sanger sequencing (Institute for Clinical Molecular Biology, Kiel) with oligonucleotides HF1381 and HF3051.

2.2.8 RNA isolation and cDNA synthesis

For RNA isolation, 1x 10^6 T cells were centrifuged (120 x g, 10 min) and the supernatant discarded. The cells were resuspended in 1 ml Trizol and frozen at -80 °C. To proceed, the samples were thawed and incubated at room temperature for 5-10 min. Subsequently, 200 µl of chloroform were added and the samples shaken for 15 s and further incubated at room temperature for 3-5 min. To separate the phases, the samples were centrifuged at 17,000 x g and 4 °C for 15 min. The aqueous phase containing both viral and cellular nucleic acids was transferred into a newly prepared tube containing 550 µl isopropanol (100 % v/v) to precipitate the nucleic acids. The sample was inverted several times and centrifuged at 17,000 x g for 15 min at 4 °C. The supernatant was discarded and the precipitate washed with 1 ml ethanol (75 % v/v) (10 min, 4 °C). Subsequently, the ethanol was removed and the sample air-dried for several min at room temperature. The purified nucleic acids were resuspended

in 30 µl molecular pure water for 15-20 min on ice. The concentration was measured via NanoDrop™ 2000.

To remove cellular and viral genomic DNA, 1.6 µg RNA were digested with DNaseI (Roche) at 37 °C for 30 min, and subsequently, the DNAse inactivated at 75 °C for 10 min. The samples were either stored at -80 °C or further proceeded with.

To ensure the complete removal of residual genomic or episomal DNA, the samples were split in half; both were treated similarly, except for the addition of reverse transcriptase (RT) in the end. Samples were incubated at 65 °C for 5 min, and immediately cooled down afterwards. Transcription buffer (5x) and 0.1 M DTT were added to both and the samples incubated further at 42 °C. One half of each sample received RT (+) while the other remained without (-) and served as a control for residual DNA contamination. All samples were further incubated at 42 °C for 50 min. Subsequently, the enzyme was inactivated at 70 °C for 10 min. The stable cDNA could be stored at -20 °C or subjected to PCR right away.

All samples were tested by PCR and gel electrophoresis for transcription of the ORFs and genes as indicated in table 18, the expected fragment sizes are included. Usually, *Taq* polymerase was used to detect the transcripts of interest. The presence of *Tip* (HF2729 + HF2730) and *eGFP* (HF3470 + HF3471) transcripts was checked with Phusion® polymerase, since PCR using Taq polymerase did not yield signals even for the positive controls.

Table 18: Oligonucleotides to detect transcription

Target	oligonucleotides	expected band size	Polymerase used
GAPDH	HF3211 + HF3212	581 bp	Taq
ORF75	HF742 + HF743	356 bp	Taq
Tip	HF2729 + HF2730	173 bp	Phusion®
eGFP	HF1836 + HF1837	670 bp	Taq
	HF3470 + HF3471	310 bp	Phusion®
RFP	HF3298 + HF3299	350 bp	Taq
Vδ2	HF3466 + HF3467	300 bp	Taq
Vγ9	HF3468 + HF3469	362 bp	Taq

2.2.9 Real-time PCR for detection and copy number quantitation

To establish a DNA standard for HVS, BAC DNA was isolated via maxi kit and the DNA concentration measured via NanoDrop™ 2000. The DNA was diluted to fit to the optimal ranges for subsequent use for real-time PCR with Fast Advanced® Taqman Kit (0.001-100 ng). In order to mimic samples isolated from HVS-transduced T cells, the standards were spiked with defined amounts of cellular DNA, isolated from of 1x 10^6 non-transduced K41 donor T cells. With support of the Biomers company, a Taqman probe was designed to bind in *ORF9*, which encodes for the viral polymerase (table 19).

Table 19: Oligonucleotides and probes designed for HVS-detection

Designation	location	orientation	oligonucleotide (5' - 3')
HF3402	*ORF9*	for	6fam -TTA CAG GAG TTG CGT CAG GCT TGCT- BMN-Q535
HF3403		for	TTC TAG ATA AAC AGC AAC TCG C
HF3404		rev	TTC TTG AAG TGT ATC AGG TGT C

Semi-quantitative PCR was performed by using the prepared BAC DNA standard as a reference. After normalisation to the glyceraldehyde-3-phosphate dehydrogenase gene (*GAPDH*), the DNA concentration was determined in ng/µl and used to calculate copy numbers for infected or transformed cells. The Taqman Fast Advanced® master mix (Applied Biosystems) was used with the settings provided in table 20.

Table 20: Taqman Fast Advanced semi-quantitative PCR mix and runtime settings

Component	final concentration	µl
Taqman FA Master Mix (2x)	1x	10
HF3402	0.5 µM	1
HF3403	0.5 µM	1
HF3404	0.1 µM	1
DNA	1 pg-100 ng	1
water		ad 20

step	temperature	time	cycles
I	95 °C	120 s	
II	95 °C	3 s	40
III	60 °C	30 s	

The average copy numbers per cell were calculated by using the dsDNA calculator web tool provided by the University of Rhode Island of URI Genomics & Sequencing Center. The calculator assumed an average weight of a base pair (bp) of 650 kDa and put the Avogadro's constant at 6.022 x 10^{23} molecules/mole. The copy number was determined by using the following formula.

$$\text{copy number} = \frac{\text{mass [ng]} \times 6.022 \times 10^{23}}{\text{size [bp]} \times 10^{9} \times 650}$$

All non-transduced donor T-cell lines as well as uninfected permissive OMK cells were measured as negative controls to exclude unspecific positive results. Non-transduced donor cells further served as a positive control for GAPDH, while uninfected OMK cells were, again, used as the negative control. As expected, signals were not detectable.

For the controls, 1x 10^5 OMK cells per well were seeded in a 6-well plate. The following day, the cells were infected in triplicates at the MOIs of 0.01 and 0.1 and incubated at 37 °C (95 % humidity, 5 % CO_2). After 24 h the cells were scraped off and the triplicates were pooled. These samples served as a positive control for HVS, and as a negative control for GAPDH. Copy numbers within infected OMK cells were calculated based only on initially deployed cell numbers for infected OMK cells.

2.2.10 DNA sequencing

DNA was Sanger-sequenced at the Institute for Clinical Molecular Biology of Kiel University. The amount of DNA was calculated following the rule of using 3 ng per 100 bp of sequence to be determined. The concentration was estimated in comparison to an appropriate band of similar size of GeneRuler Mix in gel electrophoresis (1 %, 1 h, 120 V) or via NanoDrop™ 2000. PCR was performed according to table 21.

Table 21: BigDye™ terminator v1.1 sequencing and runtime settings

component	final concentration	µl
5x sequencing buffer	1x	2
Big Dye™ v1.1		1
for primer	0.5 µM	1
rev primer	0.1 µM	1
DNA	3 ng/100 bp	X
water		ad 10

step	temperature	time	cycles
I	96 °C	60 s	
II	96 °C	10 s	24
III	53 °C	5 s	
IV	60 °C	240 s	
V	4 °C	∞	

2.3 Cell culture methods

2.3.1 Culture of permissive epithelial and T cells

Thawing of frozen cells had to be performed quickly at 37 °C to avoid damage due to the DMSO-containing freezing medium. A volume of 10 ml of the preferred cell culture medium was added and the cells centrifuged (260 x g, 10 min) to remove the DMSO completely. Permissive epithelial OMK cells were grown with D10, T cells with TC50 media. The cells were washed once more, counted, and an appropriate amount of medium, and a cultivation container (flask or plate-well) were chosen to account for the cells preferred density. T cells were kept in TC50 medium at > 1x 10^6 cells/ml and twice a week, one third up to one half of the medium volume was renewed. OMK 637 cells were split once a week 1:2 at a density of approximately 3.2x 10^5 cells/cm^2 and new medium was applied every 3-4 d.

For cryopreservation, cells were concentrated via centrifugation at 260 x g for 10 min and resuspended in the required amount of FBS with 9 % v/v DMSO. The cells were cooled down in a -80 °C freezer using an isopropanol box, allowing a slow reduction of the temperature of 1 °C per hour to -80 °C.

2.3.2 Transfection and virus reconstitution from BACs

Transfection with Lipofectamine™ reagent: One day prior to transfection, 5.5x 10^5 OMK cells were seeded in a 25 cm^2 flask in D10 medium. Via mini preparation, BAC DNA was isolated and stored over night at 4 °C. The following day, 10 µl of Lipofectamin® reagent were mixed with 190 µl Opti-MEM™ to generate solution A, while solution B contained 5 and 10 µl of the isolated BAC DNA, respectively, in a final volume of 200 µl of Opti-MEM™. Solution A

was pipetted into solution B, briefly mixed, and incubated at room temperature for 35 min. Meanwhile the OMK cells were washed twice with 2 ml of Opti-MEM™. After 35 min a volume of 1.1 ml Opti-MEM™ was added to the solution A-B mix and the complete solution was trickled onto the OMK cells. The following day the medium was renewed with 5 ml D10. After 3-5 d, first cytopathogenic effects (CPEs) were visible and after 5-7 d almost all cells were infected by HVS, provided the reconstitution was successful.

Transfection with Lipofectamine™2000: One day prior to infection a total of 6.5x 10^5 OMK cells was distributed on three wells of a 6-well plate. A maxi-preparation of the viruses was prepared and stored over night at 4 °C. The following day the DNA concentration was measured via NanoDrop™ 2000 and solution A was prepared by adding 12 µg to Opti-MEM™ to a final volume of 750 µl. Solution A was rested for 5 min at room temperature. Solution B was generated by adding 30 µl Lipofectamine™2000 to 720 µl of Opti-MEM™ and briefly vortexing. Solution A was subsequently pipetted into solution B and the mixture incubated for further 20 min at room temperature. A volume of 500 µl per well was then slowly trickled into the cells' medium. The following day, the medium was renewed. After 2-4 d the cells were treated with trypsin and pooled in a T75 flask and grown until complete lysis was reached.

2.3.3 Virus stock generation

Once a passage of OMK cells was completely infected with HVS, the supernatant was harvested. Debris was removed by centrifugation at 260 x g for 10 min. The infectious supernatant was either used for immediate infection or stored at 4 °C until further use. In order to generate virus stocks, a 100 % confluent T175 flask of OMK cells was passaged by 1:6. The next day, all six flasks were incubated for 2 h with 250 µl of the infectious virus containing supernatant in 5 ml D10 at 37 °C. The flasks were swivelled several times during incubation. After 2 h, the medium was discarded and 25 ml of fresh D10 were applied. The flasks were kept at 37 °C until all cells were infected. After 5-7 d, lytic infection was complete and all cells dead. The supernatant was collected and the cellular debris removed once more by centrifugation (260 x g, 10 min). The virus-containing medium was first pooled and then sampled into cryotubes to be stored at -80 °C.

2.3.4 Titration and replication kinetics

The generated stock was titrated to determine the number of plaque forming units (pfu) per ml (pfu/ml). One day prior to titration, 4x 10^4 OMK cells were seeded in 400 µl D10 per well in a 24-well plate. The following day, three separate serial dilutions (10^{-1} to 10^{-6}) of the virus-containing supernatant were produced. A volume of 100 µl of the respective virus dilution was added to the cells in medium. The following day, the supernatant was discarded and the cells were supplied with 1 ml fresh D10. CPEs were counted 3-7 dpi. The pfu were calculated

by multiplying the mean CPE count with the dilution used, divided by the volume used for infection, resulting in the titre in pfu/ml.

For the viral replication kinetics, 4x 10^4 permissive OMK cells were seeded in 1 ml of D10 per well on a 24-well plate one day prior to the experiment. The following day, infection was performed by removing the medium and adding 400 pfu in 250 µl D10 of the respective virus (MOI 0.001). The cells were incubated for 1 h, and every 15 min the plate was gently shaken. Subsequently, the virus-containing supernatant was discarded and the cells were washed with PBS three times and supplied with 1 ml fresh D10 medium. To estimate virus replication, the supernatants were collected every two days until complete lysis was reached, and frozen at -80 °C. To estimate the virus titre per time point, the supernatants were thawed and used to perform titrations. Three separate serial dilutions ranging from 10^{-1} to 10^{-6} were prepared per time point collected and used to infect new OMK cells. The plaques were counted 3-5 d later and pfu were calculated. All kinetics were to be repeated at least thrice.

2.3.5 Transduction of T cells

The T cells previously isolated from buffy coats of blood donations were thawed quickly and mixed with R10 medium. The cells were centrifuged for 10 min at 260 x g and the supernatant discarded. To ensure removal of all DMSO, the cells were washed once with R10. Afterwards the T cells were transferred into T75-flasks and grown in 15 ml R10 containing 4 µl/ml concanavalin A (1 mg/ml). The following day, the same amount of TC50 medium (containing interleukin 2) was added. Transduction with recombinant HVS was performed 3 d later via spinoculation (460 x g, 26 °C, 2 h) and an MOI of 3.

All transduced T-cell lines were named after month and year of transduction, *e.g.,* July 2016 was designated 0716, January and July 2017 were designated 0117 and 0717, respectively, and the transductions from January 2018 and September 2019 were abbreviated 0118 and 1019.

2.3.6 Flow cytometry and apoptosis staining

Cells were harvested, counted, and washed with PBS at room temperature (50-260 x g, 5-10 min). To initiate apoptosis, the cells were incubated with the respective inductor for 4 or 24 h and washed in ice-cold PBS (260 x g, 10 min), subsequently.

In order to study the apoptosis induction in HVS-transformed T cell-lines, 1x 10^6 cells were harvested and washed in PBS (50 x g, 5 min). The cells were resuspended in 5 ml phenol red-free R10 and either camptothecin (CPT) or H_2O_2 were added to final concentrations of 6 µM and 200 µM, respectively. The cells were incubated at 37 °C, 5 % CO_2, and a relative humidity of 95 % for 4 h and 24 h. The cells were washed twice with PBS at room temperature (260 x g, 5 min) and resuspended in 1 x binding buffer (FITC Annexin V Apoptosis De-

tection Kit I, Becton Dickinson). A volume of 5 µl of fluorescein isothiocyanate (FITC)-conjugated annexin V was used to assess induction of early apoptotic cells, while 5 µl of propidium iodide (PI) were used to identify late-apoptotic and dead cells. In the early stages of apoptosis, the membrane phospholipid phosphatidylserine, usually maintained on the inner leaflet by flippases, is presented on the outer leaflet to induce efferocytosis by phagocytes. The PI staining is included to stain late-apoptotic or dead cells, since it cannot pass the cell membrane of viable cells. Compensation was performed using single stained FITC and PI controls of transformed K39 WT(29fDX) T cells at a low flow rate.

Antibody staining of cells was performed by removing the cell culture medium and washing in ice-cold PBS (260 x g, 10 min), followed by resuspension in flow-cytometry buffer (PBS, 5 % v/v FBS) containing the antibody at a suitable dilution. The cells were incubated on ice for 60 min and washed twice to remove unspecifically bound antibodies. The pelleted cells were then resuspended in flow-cytometry buffer and stored on ice until measured.

For all measurements, the flow speed was set to low, raw data for forward scatter, side scatter, FITC-A, phycoerythrin (PE-A), and Peridinin chlorophyll protein-cyanine 5.5 (PerCP Cy 5.5) was generated, depending on the experiment. The FACS® Canto I instrument was used with its laser *Sapphire® Solid State 488 20*. Emission of FITC, eGFP and Alexa®488 was measured using the 530/30 bandpass filter, PI-emission was measured using the 670 longpass mirror, for measurement of mRFP- and PE-emission, the 585/42 bandpass filter was used. For all samples the area under the curve was measured, indicated by the A (*e.g.* PE-A). Since the FACSCanto™ I is not capable of measuring the signal peak (also height or H), doublet exclusion could not be performed.

3. Results

3.1 Copy number determination for herpesvirus saimiri genomes

In order to estimate the copy numbers of the herpesvirus saimiri genomes in infected cells, a protocol for a semi-quantitative real-time PCR was developed. A probe and oligonucleotides for GAPDH (Brunnemann, 2016) were used as cellular controls, and a probe and oligonucleotides for HVS polymerase, *ORF9*, were developed with support from the Biomers company and used for detection of the virus genomes.

DNA was isolated from permissive OMK cells which were infected with MOIs of 0.01 and 0.1. The cells were harvested at 24 hpi and their DNA was used as a positive control to establish the protocol. On average a copy number of 0.03 ± 0.01 copies/cell was detected when an MOI of 0.01 was used and at an MOI of 0.1, 1.31 ± 0.19 copies/cell. Normalisation to GAPDH could not be performed in OMK cells since these cells are of non-human origin and do not express human GAPDH. Instead the cell number at the time of infection (0 hpi) was used.

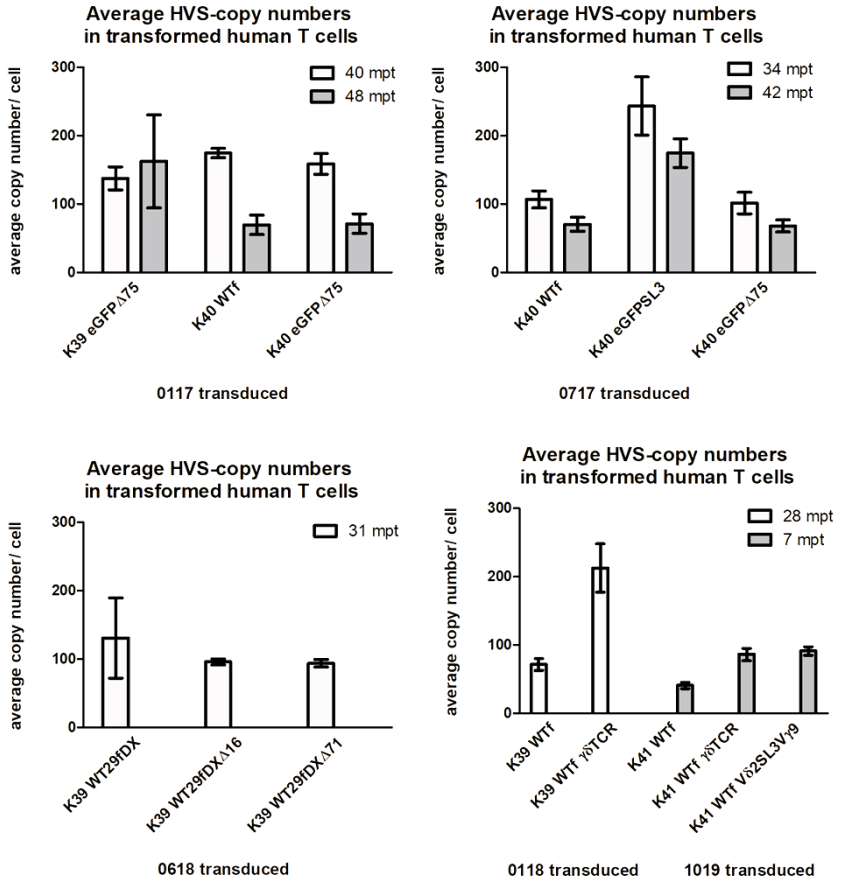

Fig. 5: HVS DNA copy numbers in transformed human T cells. DNA of 1x 10^6 transformed human T cells was isolated at the indicated time point with the DNeasy Kit and concentrations were determined thrice by semi-quantitative real-time PCR in comparison to a standard. Based on concentration and genome size, copy numbers could be calculated using the tool provided by URI Genomics & Sequencing Center. Cell numbers were normalised in relation to GAPDH signals. Depending on cell proliferation, one or more time points could be analysed. Dates of transduction were abbreviated as month and year, *e.g.*, cells transduced in January 2017 were designated 0117. Graph and statistics generated with GraphPad Prism® 5.

The HVS-DNA standard was evaluated by running three individual dilution series in parallel, spiked with different amounts of cellular K41-DNA to simulate real samples. The efficiency varied between 86-92 %, while the coefficient of determination R^2 was > 0.99. To determine the precision, the coefficient of variation was calculated and amounted to < 0.043 for all samples. In human T cells, normalisation to GAPDH was performed to establish the average copy numbers per cell using the web tool provided by the University of Rhode Island URI Genomics & Sequencing Center.

The copy numbers isolated from the T-cell lines varied at different time points of isolation after initial transduction (fig. 5, upper row). Changes varied from small to drastic and no trends were observed. For example, 0117 K39 eGFPΔ75 had 137 copies/cell at 40 mpt and at 48 mpt 162 copies/cell, while 0117 K40 WTf carried 175 copies/cell at 40 mpt and eight months later less than half with 70 copies/cell. However, the statistical power is low since only one sample of one experiment could be included per time point, which then was measured thrice. At least three copies per cell were expected since all analysed transformed cell lines were initially transduced with an MOI of 3.

These results provide an orientation on the range of the copy numbers within transformed T cells. Before, only rough estimations based on radioactive DNA hybridisations from decades ago were available which remained unpublished in the original studies. The average copy numbers of all transformed cell lines analysed were determined to range between 41 to 273 copies per cell, and therewith, by far exceeded the initial three copies used for transduction. The established protocol was convenient and reliable for semi-quantitation of DNA copy numbers isolated from HVS-transformed human T cells in relation to GAPDH DNA.

3.2 Artificial expression of a γδ T-cell receptor in transformed T cells

To evaluate the potential of HVS vectors in anti-cancer treatment, a human γδ TCR was inserted into the HVS genome via *en passant* mutagenesis under control of the *StpC/Tip* promoter (Linda Bremer), thus, generating a tetracistronic BAC. The Vγ9 chain was followed by the internal ribosomal entry site (IRES) from poliovirus and the Vδ2 chain by IRES from encephalomyocarditis virus. From here on, the IRES derived from poliovirus will be termed PolioIRES and the IRES derived from encephalomyocarditis virus will simply be termed IRES. Human donor T cells were transduced in nine independent experiments but did not grow to cell numbers as T cells transformed by WTf. Potentially the tetracistronic expression construct was too long for the expression of additional reading frames under the comparably weak *StpC/Tip* promoter.

Therefore, a new virus variant was generated. The Vδ2 chain with the corresponding IRES was inserted again under control of *StpC/Tip* promoter at the very left end of the HVS ge-

nome (fig. 6A). The Vγ9-Polio-IRES sequence was placed under the control of the comparably strong retroviral SL3 promoter at the right-most end of HVS genome, between ORF75 and H-DNA (fig. 6B). Both, the WTf γδTCR and the WTf Vδ2SL3Vγ9 BAC, were then used to transfect permissive OMK cells and reconstitute the respective virus. Replication kinetics showed no relevant differences compared to replication kinetics of the HVS C488 wild-type virus WTf (fig. 7C).

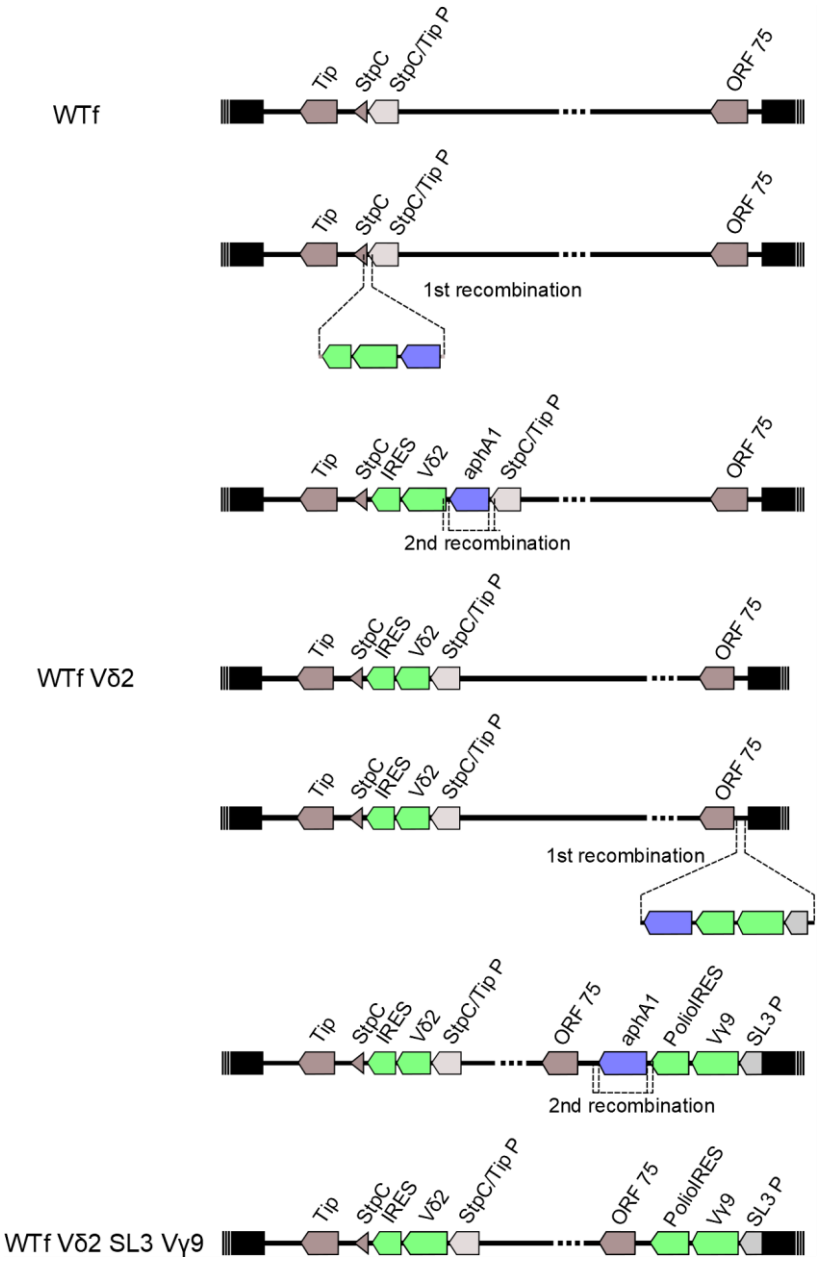

Fig. 6: Generation of the WTfVδ2SL3Vγ9 BAC in four steps. Upper panel: During the first recombination, the WTf BAC served as a backbone to insert *Vδ2*, *IRES* and *aphA1*, under control of the *StpC/Tip* promoter (StpC/Tip P) at the left-most end of HVS C488. The positive selection marker *aphA1* was released during second recombination from the viral genome and the BAC was termed WTf Vδ2. Bacteria carrying this BAC were made electro- and recombination-competent. Lower panel: A purified PCR product, consisting of the *Vγ9* chain gene and poliovirus IRES under control of SL3 promoter, and *aphA1* (blue) as the positive selection marker, was inserted at the right-most end of the genome during first recombination, between *ORF75* and H-DNA (black blocks). The positive selection marker was subsequently released during the second recombination and the final BAC was termed WTf Vδ2SL3Vγ9.

RFLP analysis showed the expected band patterns for the coding L-DNA for all three BACs, WTf, WTf γδTCR and WTf Vδ2SL3Vγ9 for both restriction enzymes (fig. 7; green arrows). However, the fragments consisting of non-coding H-DNA were altered during *en passant* mutagenesis (fig. 7; red arrows). For the BcuI-digest in BACs WTf and WTf γδTCR, a band of 40.7 kb, and for WTf Vδ2SL3Vγ9, one of 42.8 kb was expected. In the WTf BAC, an additional band above 40.7 kb was observed. The BAC WTf γδTCR met all expectations. The variant WTf Vδ2SL3Vγ9, however, seemed to have suffered a loss of approximately 27 kb, the fragment of 42.8 kb appeared to run at a size of around 13 kb. Additionally, a faint band of the expected band size was observed in the BcuI digest. The same loss of approximately 30 kb was observed in the SacI digest. Instead of the expected 42.8 kb H-DNA band, a fragment of approximately 13 kb could be distinguished.

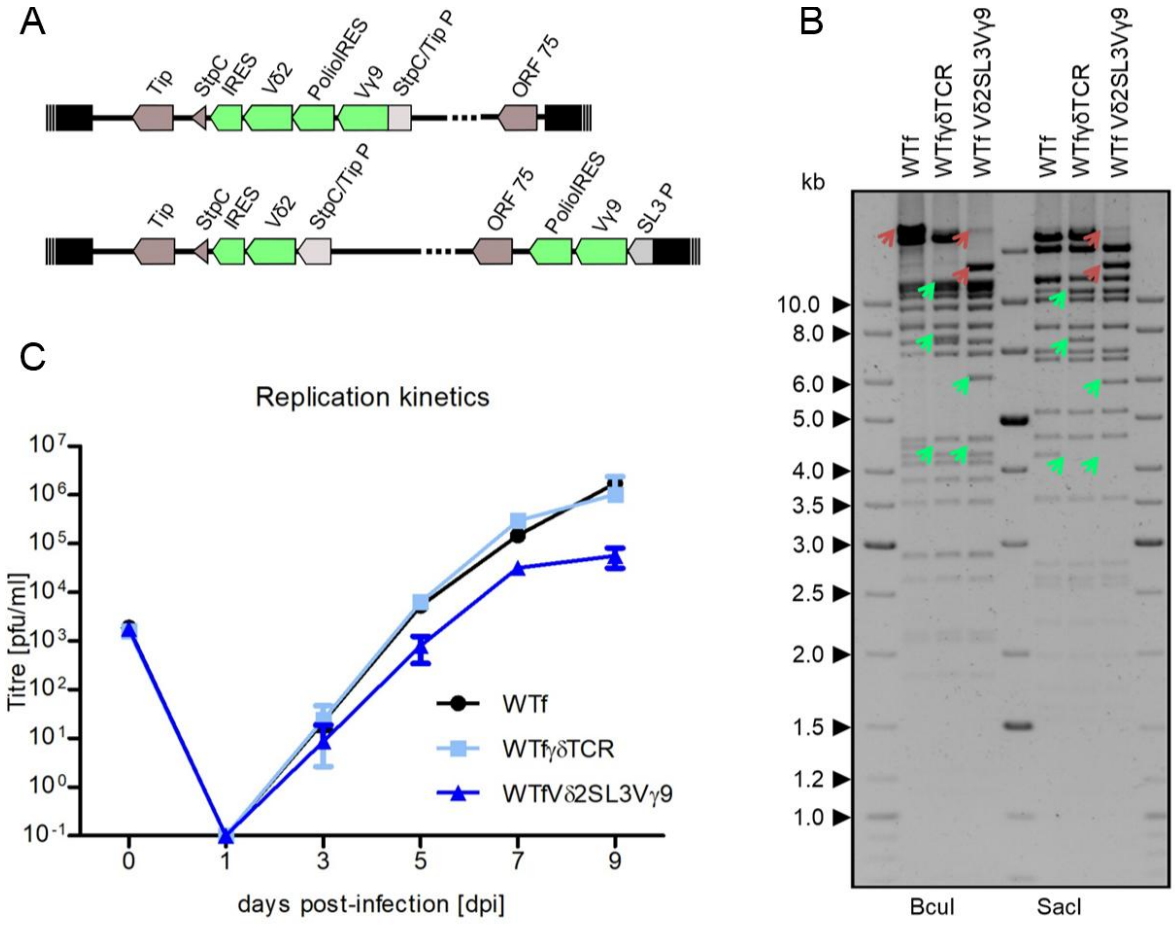

Fig. 7: Genomic structure, RFLP analysis, and replication of WTf γδTCR and WTf Vδ2SL3Vγ9. A Structure of the genomic organisation of HVS C488 BACs WTf γδTCR (top) and WTf Vδ2SL3Vγ9 (bottom). WTf γδTCR has a tetracistronic transcript under control of the *StpC/Tip* promoter, while WTf Vδ2SL3Vγ9 has a tricistronic one. **B** Restriction enzyme digest fragment patterns of BACs WTf, WTf γδTCR, and WTf Vδ2SL3Vγ9 cleaved with BcuI and SacI, respectively, were subjected to gel electrophoresis at 50 V on a 0.6 % agarose gel for 18 h. Changes in band size of H-DNA containing fragments are indicated with red arrows, changes in the coding L-DNA are visualised with green arrows. Grey shades are displayed in inverted mode. **C** Exemplary replication kinetics of both variants compared to wild-type virus, WTf, in permissive OMK cells are shown. Graph and statistics generated with GraphPad Prism® 5.

Sequencing after the *en passant* mutagenesis confirmed the correct insertion into the intended locus between *ORF75* and H-DNA. Taking the size of one repeat of approximately 1.4 kb into account, this would mean that instead of approximately 30 repeats, in WTf Vδ2SL3Vγ9 approximately nine repeats remained.

Nevertheless, transfection and sequencing confirmed a replication-competent virus with the desired insertions. Replication kinetics of the two variants were compared to that of the wild-type virus WTf. Major changes could not be found, however, the newly generated virus variant WTf Vδ2SL3Vγ9 seemed to replicate marginally slower and less efficiently compared to WTf virus. Both viruses produced titres in the range of 10^5-10^6 pfu/ml and were in so far eligible to transform human T cells.

Table 22: Average numbers of HVS C488 genome copies per cell normalised to GAPDH (SD, standard deviation)

time point of transduction	months post transduction	cell line	copy numbers run 1	copy numbers run 2	copy numbers run 3	copy number/ cell, mean ± SD
0118 (January 2018)	28	K39 WTf	81.25	54.71	78.99	**71.65** ± 14.71
		K39 WTf γδTCR	n.d.	177.35	248.18	**141.85** ± 50.08
1019 (October 2019)	7	K41	n.d.	n.d.	n.d.	
		K41 WTf	48.00	32.29	42.86	**41.05** ± 8.01
		K41 WTf γδTCR	n.d.	95.48	77.02	**86.25** ±13.05
		K41 WTf Vδ2SL3Vγ9	100.66	79.67	93.58	**91.30** ±10.68

Donor T cells K38, K39, K40 and K41 were transduced in different experiments at different time points with the all three viruses. WTf-transduced human T cells were reliably transformed. Meanwhile, both WTf γδTCR- and WTf Vδ2SL3Vγ9-transduced T cells died approximately at the same time as their non-transduced donor cell line did (3-9 months post-transduction, mpt). Twice, the transformation of T cells was successful with these variants. K39 T cells were transformed with WTf γδTCR and could be cultured for approximately 36 months after transduction with the virus variant (transduction 0118). K41 T cells could be successfully transformed (transduction 1019) with both TCR expression vectors and were grown for approximately a year. The cell line K41 WTf Vδ2SL3Vγ9 did not tolerate reductions in cell numbers for experiments, and as a result died at 11 mpt.

All cell lines were initially established by spinoculation of activated donor T cells with the respective virus at an MOI of 3. All of the cell lines had average copy numbers per cell exceeding three by far, ranging from 41 to 142 (table 22). As a negative control, non-transduced K41 donor cells were used and found negative for HVS genomes. To analyse the transcription of the two human TCR chains Vγ2 and Vδ9, total RNA was isolated whenever the available cell numbers allowed it, and did not endanger the survival of the cell line.

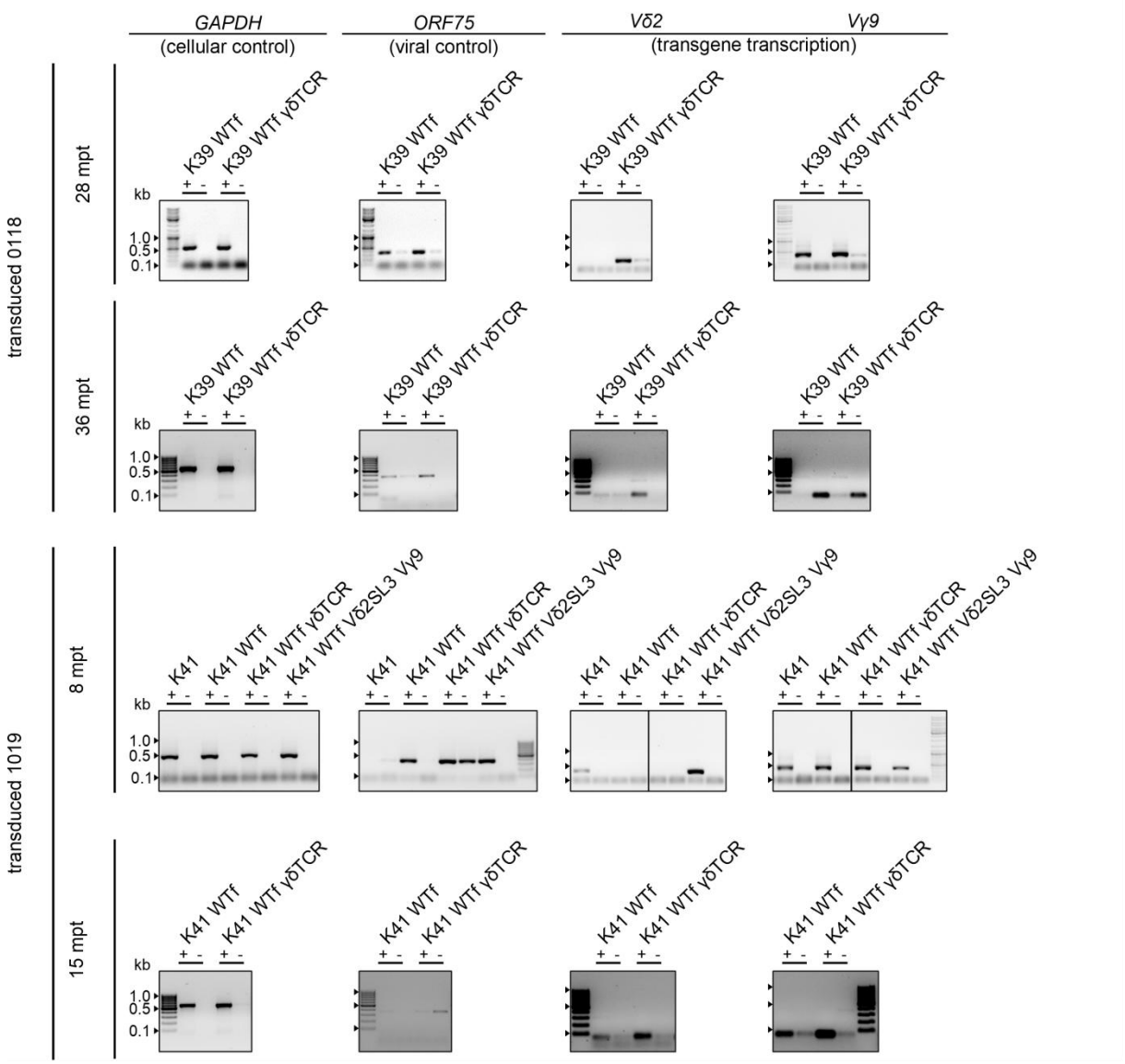

Fig. 8: RT-PCRs of RNA isolated from transformed human T cells. RNA was isolated from 1x 10^6 transformed human T cells per cell line. Genomic DNA and residual HVS episomal DNA were aimed to be removed by DNaseI digest. The RNA was reverse-transcribed into cDNA and subjected to PCR. To control for residual DNA after DNaseI digest, samples were processed in parallel with (+) and without (-) addition of reverse transcriptase. *GAPDH* served as a cellular control, *ORF75* as a viral control. Two different time points of transduction (0118, 1019) and two different donor lines (K39, K41) lead to successful growth transformation in transduced T cells. K39 cell lines could only be harvested at 28 and 36 mpt, K41-derived lines were growing faster and could be collected earlier at 8 and 15 mpt. The non-transduced K41 donor line was still alive at 8 mpt and was included as a negative control. All bands were displayed at the expected sizes (*GAPDH*: 581 bp, *ORF75*: 356 bp, *Vδ2*: 300 bp, *Vγ9*: 362 bp.) Black arrows indicate 1 kb, 0.5 kb and 0.1 kb bands. Grey shades are displayed in inverted mode.

Isolated total RNA was reverse transcribed into cDNA and PCR performed to prove the presence of transcripts (fig. 8). Transcripts of cellular GAPDH served as a cellular control and were reliably detected in samples with RT, while samples without mostly remained negative (faint band only at 15 mpt for K41 WTf γδTCR). *ORF75* transcription proved the persistence of the HVS episomes within the transformed human T cells. Predigestion of the RNA with DNaseI did not remove HVS DNA completely, since samples without RT turned out positive during PCR. However, most of the bands from samples without RT were fainter than

from the samples with RT, indicating at least a reduction of HVS DNA by predigestion with DNaseI. The exception was again the sample collected at 15 mpt for K41 WTf γδTCR. Unexpectedly, a faint signal for *ORF75* was detected in the sample of non-transduced T cells without RT, which might be a result of a spill-over from the high signal intensity sample from 8 mpt K41 WTf, since the test run performed prior to this final agarose gel electrophoresis did not show this band (data not shown).

Transcription of the transgenes *Vδ2* and *Vγ9* was monitored in all cell lines and positive signals for these genes, originally derived from the human genome, were expected in non-transduced or WTf-transduced T cells, too. It was anticipated, however, that transcription in T cells transformed with WTf γδTCR or WTf Vδ2SL3Vγ9 would be higher than in non-transduced or WTf-transduced cells. These expectations were more or less met by transcription of *Vδ2* under the control of *StpC/Tip* promoter but not by transcription of *Vγ9* which was regulated by the *SL3* promoter. A positive signal for the transcription of *Vγ9* in the sample without RT at 15 mpt for K41 WTf γδTCR indicates residual genomic DNA.

Expression of the transgenes was controlled for by flow-cytometry analysis and was performed at 7 mpt, 18 mpt, 26 mpt, and 38 mpt. For the first three time points, an antibody against the γδ TCR (FITC) was used in addition to antibodies against CD3 (PE) and the αβ TCR (PE). All samples had strong CD3- and αβ-TCR signals but γδ TCR expression could not be demonstrated (data not shown). After 38 months of cultivation, antibodies for γδ TCR verification were changed to antibodies specific for Vδ2 and Vγ9, respectively. The negative results presented in fig. 9 for cells at 38 mpt were nonetheless exemplary for the results gained for the other time points as well.

As a non-transduced control, K39 cells were thawed and analysed along with 38-month old T-cell lines K39 WTf and K39 WTf γδTCR (fig. 9). Measurement continued, until 5x 10^4 living cells were collected in the gate (speed setting: low). The raw data were processed using FCS express 6. The whole population was newly gated for living cells only, and the unstained control was compared to stained samples. Anti-CD3 (PE) revealed approximately 86 % of all living cells were CD3 positive in non-transduced K39 T cells, 97 % in K39 WTf-, and 80 % in WTf γδTCR-transduced cells. The presence of αβ TCR was indicated by anti-αβTCR (PE) and revealed 89%, 96 %, and 99 % positive rates in non-transduced, WTf-, and WTf γδTCR-transduced T cells, respectively. Conversely, the αβ TCR-negative cells were not observed to be positive for γδ TCR expression which was tested with anti-γδ1 (FITC) and non-conjugated anti-Vδ2 and anti-Vγ9 antibodies. Non-conjugated antibodies were secondarily stained with anti-mouse Alexa488. False positive rates were measured and totalled < 0.1 % for all cell lines.

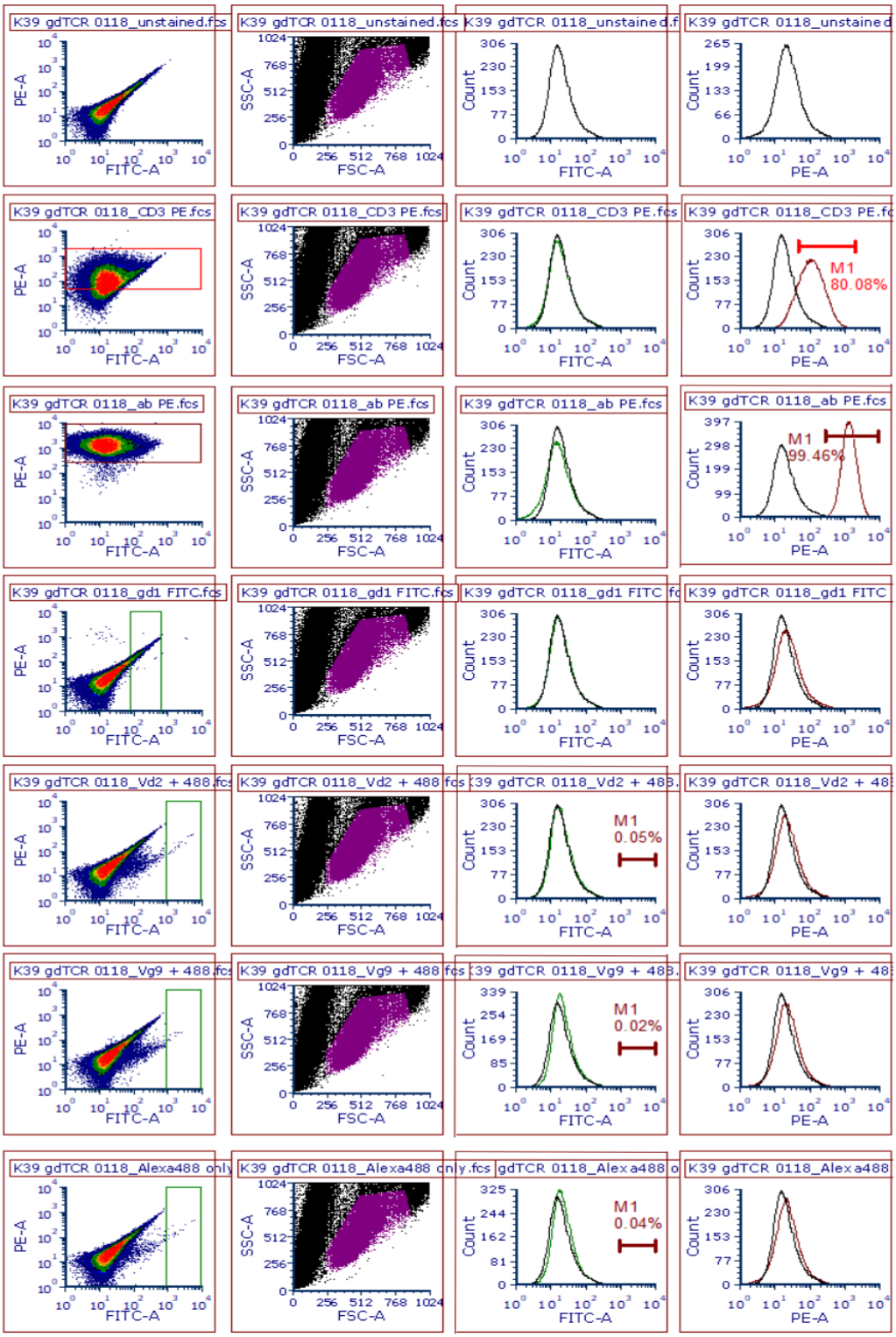

Fig. 9A: Flow-cytometry results of WTf γδTCR-transduced cell lines and their WTf counterparts at 38 months after transduction in comparison to native K39 donor T cells. A Flow-cytometry plots of WTf γδTCR transformed T cells at 38 mpt (continued).

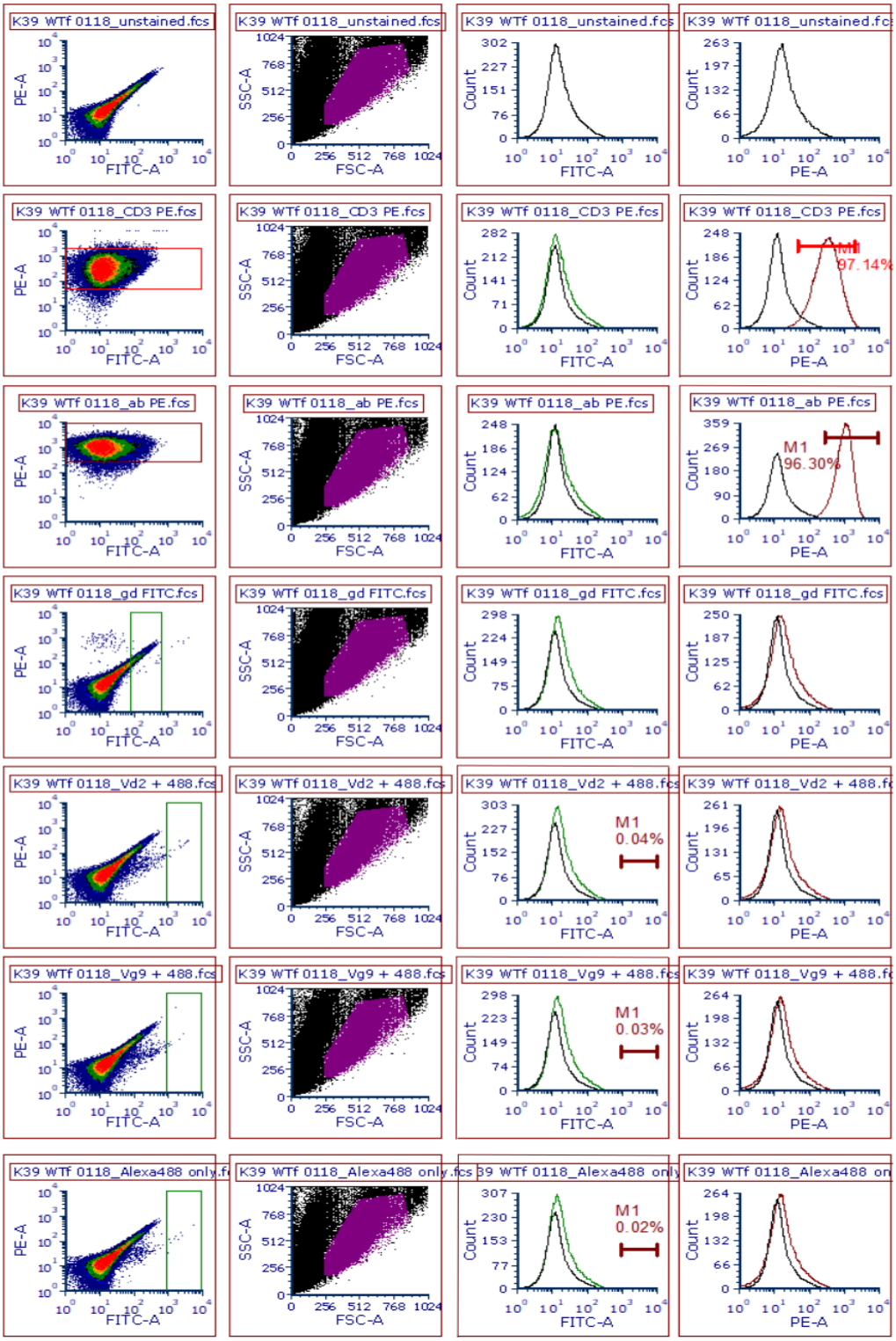

Fig. 9B: Flow-cytometry results of WTf γδTCR-transduced cell lines and their WTf counterparts at 38 months after transduction in comparison to native K39 donor T cells. B Flow-cytometry plots of K39 WTf transformed T cells at 38 mpt (continued).

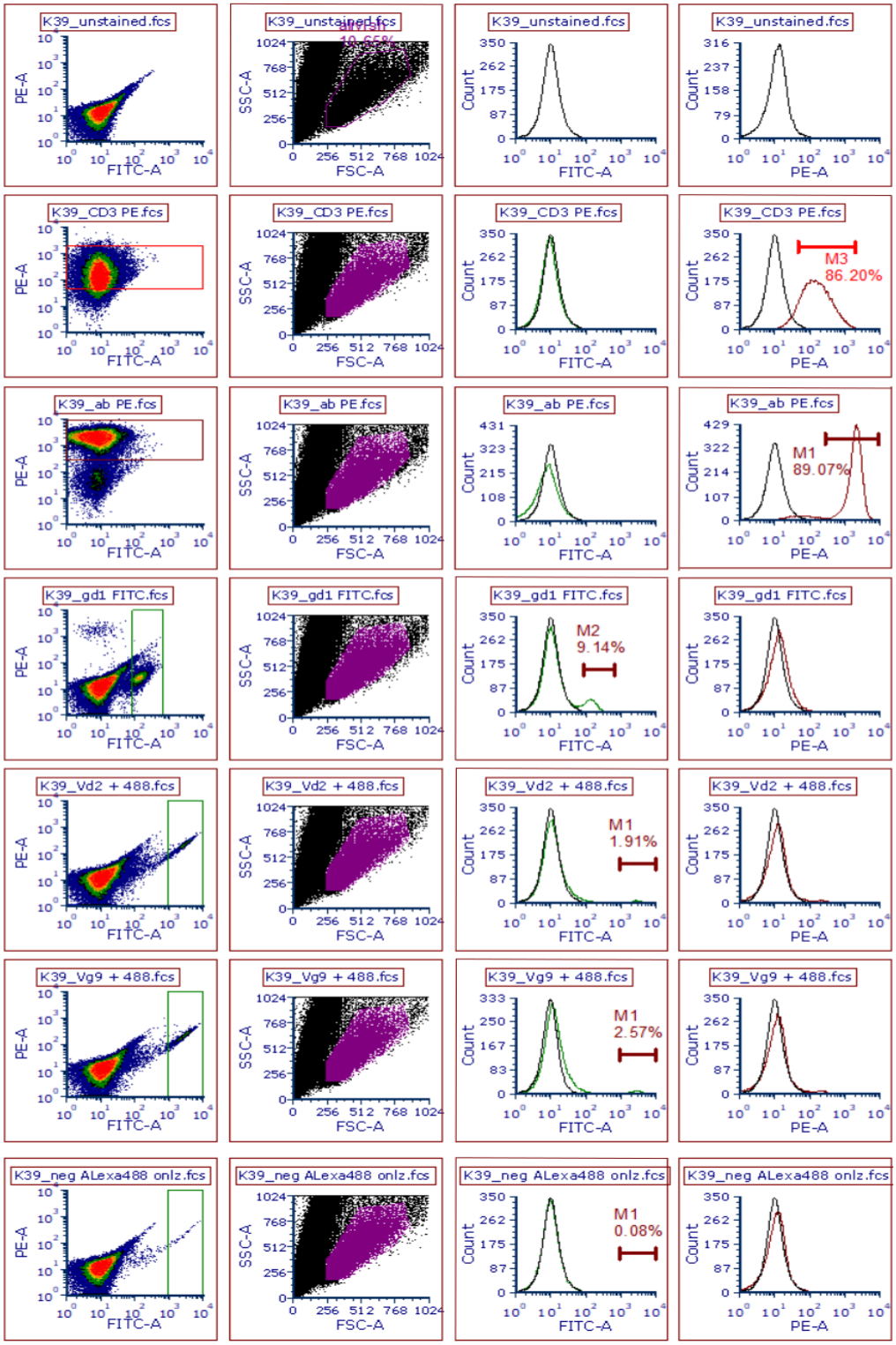

Fig. 9C: Flow-cytometry results of WTf γδTCR-transduced cell lines and their WTf counterparts at 38 months after transduction in comparison to native K39 donor T cells. Measurement during flow cytometry continued until 1x 10^6 living T cells were counted. Subsequently, cells were gated for living cells only (purple gate) and evaluated concerning their surface antigens, shown in rows, in the following order from top to bottom: unstained control; anti-CD3-PE, anti-αβ-TCR-PE; anti γδ1-TCR-FITC; anti-Vδ2, and anti-Vγ9, stained with secondary anti-mouse Alexa488. The lowest rows show unspecific binding of secondary antibody Alexa488 anti mouse, percentages were determined to be < 0.1%. Compensation was performed using CD3-PE and γδ1-FITC stained donor cells. Analysis was performed using FCS Express6. **A** Flow-cytometry plots of WTf γδTCR-transformed T cells at 38 mpt. **B** Flow-cytometry plots of K39 WTf-transformed T cells at 38 mpt. **C**. Flow-cytometry results of the non-transduced, native K39 T cells.

Three years (38 months) after the initial transduction, 97 % and 80 % of the transduced human T cells and 86 % of the non-transduced T cells presented CD3 on their cell surface. The αβ TCR was found to be expressed exclusively on transduced T cells (K39 WTf: 96 %; K39 WTf γδTCR: 99 %), in contrast to non-transduced T cells, where 89 % of the cells expressed αβ TCR and 9 % were found to be positive for expression of a γδ TCR. More specifically, 1.9 % of the cells showed expression of Vδ2 chain and 2.6 % expressed Vγ9 chain on their cell surface. In 38-month-old transformed T cells a γδ1-FITC positive subpopulation could not be detected in the dot plot. Instead, a slight shift to the right on the FITC-axis could be observed for both populations of T cells with WTf or WTf γδTCR. The shift is most likely due to autofluorescence emitted by dying cells.

In WTf- and WTf γδTCR-transformed T cells at 38 mpt, variations in the percentages of Vδ2-positive cells and Vγ9-positive cells could not be detected. Instead, both populations were found to show between 0.02 and 0.05 % cells positive for either TCR chain. They were, thus, in the same range as negative control samples for unspecific binding of the secondary anti-mouse antibody Alexa488. Without the use of a first antibody, binding of Alexa488 to human T cells occurred for 0.02-0.04 % of the cells. The flow-cytometry results confirm those received from cDNA PCRs (fig. 8), indicating that artificially induced expression of Vδ2 and Vγ9 chain in transformed human T cells was not achieved.

3.3 Determination of the transcription start site of *ORF75*

The *ORF75* promoter had been observed before to be active in HVS-transformed human T cells (Toptan, 2010). However, the transcription start site was not yet known. The SMARTer® RACE 5’/3’ Kit was used to determine the transcription start site for HVS *ORF75* in order to allow the appropriate use of the *ORF75* promoter for transgene expression in human T cells. The schematic sequence of the working steps is shown in fig. 10A. Total RNA of HVS-infected permissive OMK cells was subjected to RT-PCR using oligo(dT) primers amplifying from the 3' polyA tail of the mRNAs and adding an extension tail to the 5' end of the newly generated strand. This tail is recognised by the SMARTerII A oligonucleotides which in turn add another specific region at the end of the newly developing complementary strand. This complementary strand is then amplified with a specific primer for *ORF75*, adding yet another specific sequence, resulting in a product with two highly specific regions added on both 5' and 3' ends and ready for insertion via in-fusion cloning into the linearised vector pRACE provided in the kit. The resulting clones were tested via PCR and restriction enzyme digestion and subsequently sequenced (fig. 10B). The assumed structure of *ORF75* promoter is shown in fig. 10C. The transcription start is indicated in grey and orientated on the reverse strand. Black font on grey background indicates *ORF75* and white font on grey the identified transcribed start sequence 30 bp upstream of the start codon.

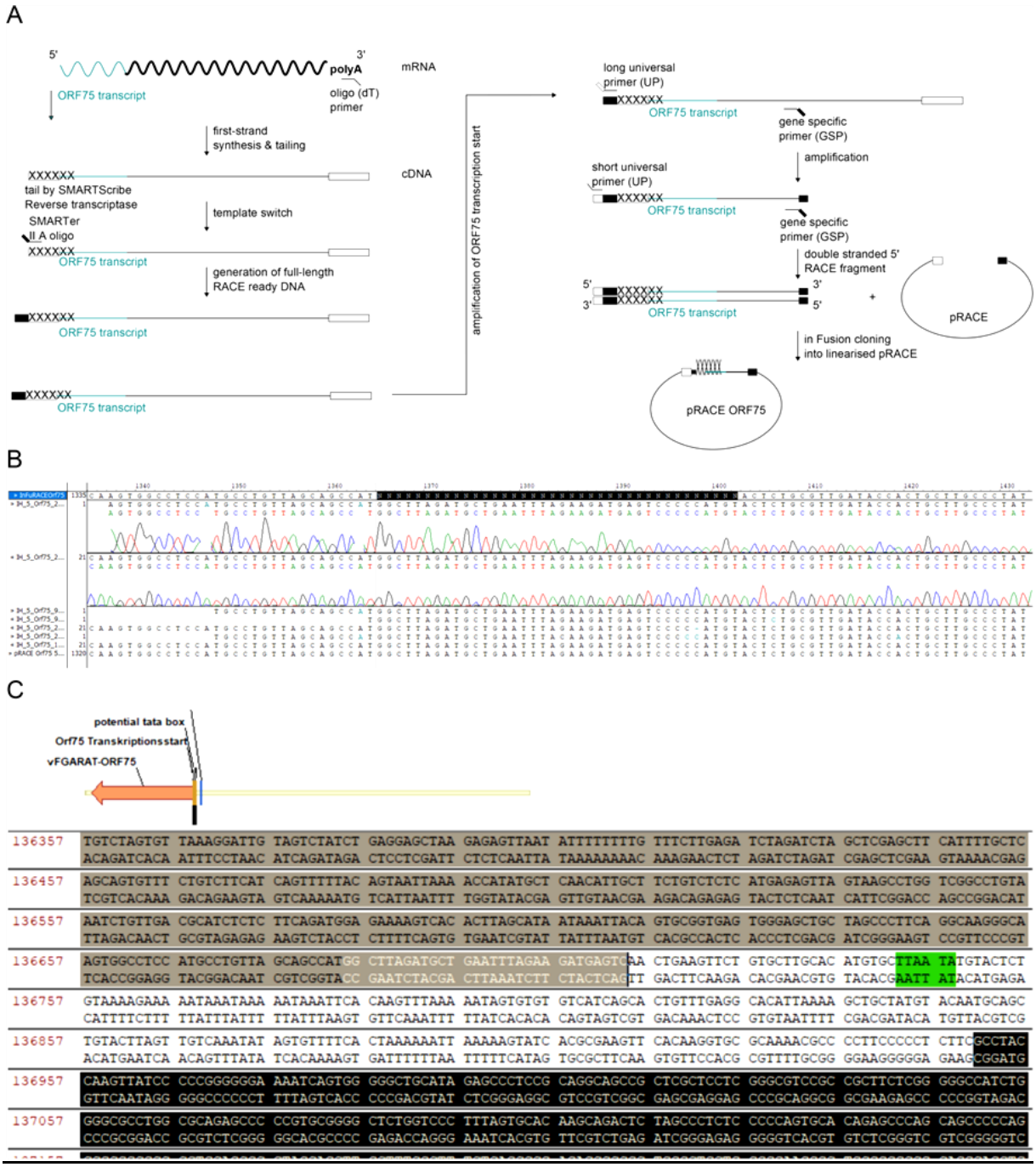

Fig. 10: Identification of the *ORF75* transcription start site of HVS C488 WTf BAC. A Permissive OMK cells were infected with WTf HVS C488 and cells harvested at different time points. Total mRNA was isolated 72 hpi and reverse-transcribed into cDNA while adding specific oligonucleotide sequences to both 3' and 5' ends in consecutive steps. Via PCR the transcript of interest was amplified by using an *ORF75*-specific oligonucleotide, allowing for subsequent ligation into pRACE vector. Colony PCR identified four positive clones that were sequenced and aligned using Contig Express. The experiments were done with the SMARTer® RACE 5'/3' Kit (Takara). **B** Alignment of InFuRACEORF75 (showing pRACE after ligation with unknown bases N) and sequences of clones 22, 9, 11 and 24, sequenced from both, 3' and 5' prime end. At the bottom lane the resulting construct, termed pRACEOrf75 is shown. **C** The transcription start of *ORF75* (grey, white font) lays 30 bp upstream of its ATG-codon (grey, black font, *ORF75* orientated reversely in accordance with standard nomenclature). A potential TATA box (green) was identified further 28 bp upstream. H-DNA is indicated in black with white font. Image generated with Vector NTI.

Further upstream, several TA-rich sequences can be found of which one, indicated in green, is highly likely to constitute the TATA box. A core promoter recognised by the DNA-

dependent RNA II polymerase usually spans 20-35 bp and consists of an initiator sequence and a TATA sequence (Flint et al., 2015). Between *ORF75* transcription start and the 7 bp TA-rich sequence indicated in green lay 28 bp, adding up to 35 bp from transcription start to end of possible TATA sequence. Additional local regulatory sequences might be located within the remaining 202 bp until the start of the H-DNA terminal repeats.

3.4 Reporter vector variants

Reporter gene cassettes were cloned in order to create HVS reporter variant viruses that could be used to test for long-term expression of transgenes in transformed human T cells. The already established transition site at the right-most end of the L-DNA, between *ORF75* and H-DNA was chosen to investigate the stability of transgene expression under different promoters. Therefore, first transfer vectors were cloned. The plasmid pepmRFP-in was used, whose *mRFP* open reading frame is interrupted by the positive selection marker *aphA1,* a kanamycin resistance gene. Subsequently, the polyA sequence of *bGH* was inserted at the 3' end downstream of the *mRFP.* Into the derived plasmid pepmRFPpolyA, the different promoters were then inserted. The correct structure of the derived transfer vectors pepSL3mRFPbGH, pepHTLVmRFPbGH and pepCD2mRFPbGH was confirmed through restriction enzyme digests, colony PCR, and Sanger sequencing. The PCR product to replace *ORF75* with an mRFP-Kan-polyA sequence was generated using precursor plasmid pepmRFPpolyA as a template.

Via *en passant* mutagenesis, the reporter cassettes were transferred into the chosen HVS BAC. Two different BACs were chosen to be manipulated into harbouring the reporter cassettes: WTf eGFP, with an eGFP under the control of the *StpC/Tip* promoter at the left-most end of the L-DNA, and WT29fDX, a HVS vector enabled to self-repair upon reconstitution. First, the expression of mRFP under the *SL3* promoter (476 bp), the HTLV long terminal repeat promoter (543 bp), and the newly localised HVS *ORF75* promoter (fig. 10) was to be studied in the context of WTf eGFP. The expression of eGFP under the *StpC/Tip* promoter served as a control for transformation. At the same time this allowed the documentation of long-term expression from this promoter more extensively than previously done. Later on, additional WT29fDX-based reporter vectors were created with HTLV and CD2 promoters controlling mRFP-expression. All generated BACs were confirmed in structure by RFLP analysis with at least two different restriction enzymes, by colony PCR, and sequencing of the insertion areas (data not shown). The generated BACs were used to transfect permissive OMK cells. The reporter genes helped to identify the transfected cells from 24 h on. Successfully transfected cells were grown until the cell monolayer was fully lysed by the virus and the supernatant used to generate stocks for transduction of human T cells and to perform replication kinetics (fig. 11C).

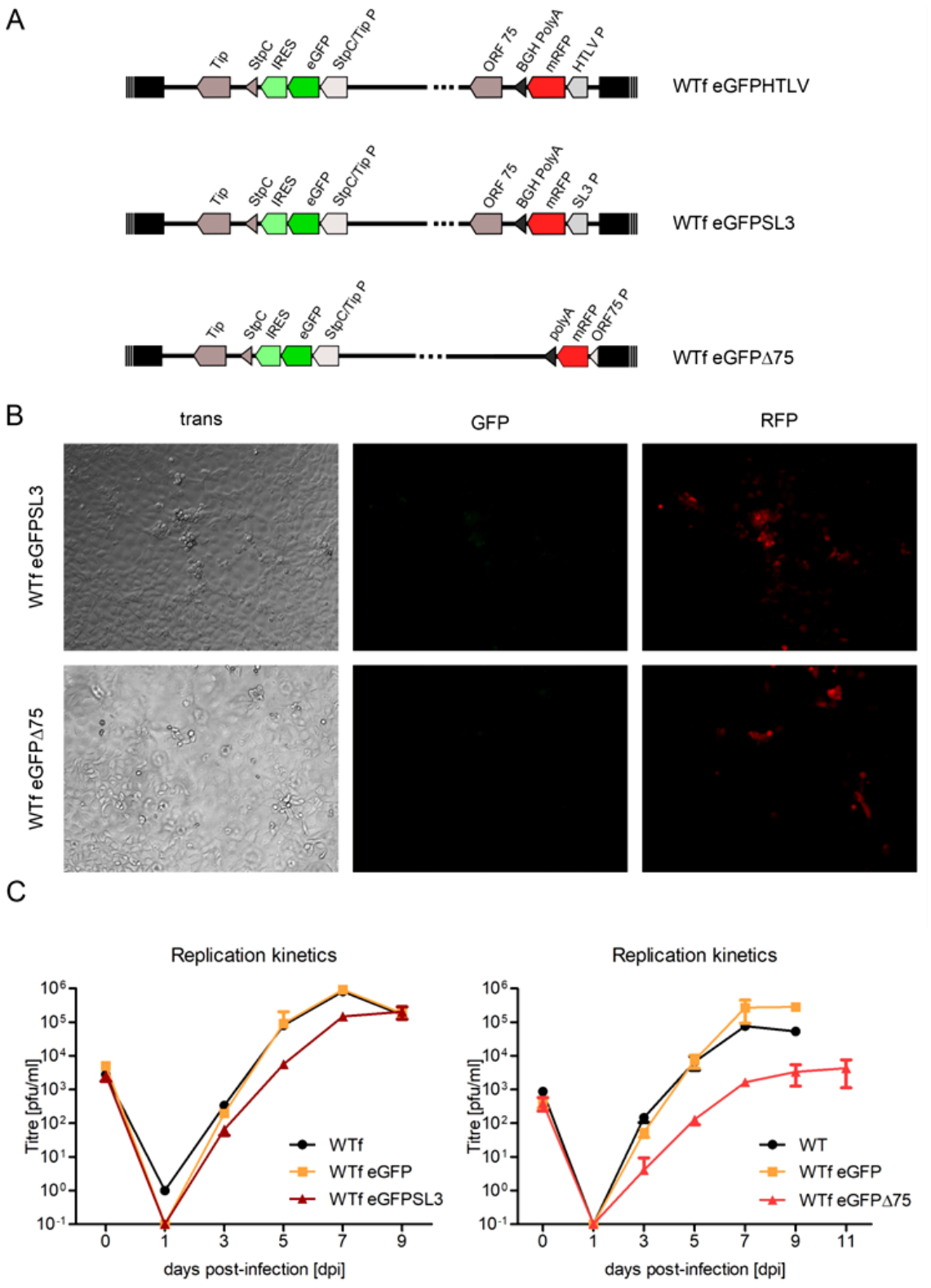

Fig. 11: Genomic organisation of reporter vectors WTf eGFP, WTf eGFPSL3, and WTf eGFPΔ75, and their replication kinetics compared to WTf. A The genomic organisation of reporter vectors is depicted, including the promoters (P) with the belonging fluorophore gene, and the respective location within the HVS C488 genome. The non-coding H-DNA at the 5' and 3' terminus is depicted as black boxes. **B** Photographs of permissive OMK cells infected with the reporter vectors WTf eGFPSL3 or WTf eGFPΔ75 in brightfield (trans), and under excitation using the GFP and RFP filter, respectively. The *StpC/Tip* promoter is highly active in T cells and not in epithelial cells, hence, eGFP signals were barely detectable in productively infected OMK cells. Expression of mRFP was very strong in OMK cells under both promoters, *SL3* and *ORF75*. **C** Replication kinetics of WTf eGFPΔ75 (left graph, red) and WTf eGFPSL3 (right graph, dark red) as compared to replication of WTf (black) and WTf eGFP (orange).

The genomic organisation of the generated WTf eGFP-based BACs is displayed in fig. 11A. Exemplary pictures of OMK cells at 3 d after transfection with WTf eGFPSL3 or WTf eGFPΔ75 are shown in fig. 11B. The expression of eGFP under control of the *StpC/Tip* promoter was weak to non-existent. Expression of mRFP was strong in cells infected with either virus variant but seemed stronger under the *SL3* promoter when assessed under the fluorescence microscope. The reconstitution of both BACs was easily accomplished, while the reconstitution of WTf eGFPHTLV could not be achieved in permissive OMK cells. In contrast, the reconstitution of the later generated WT29fDXHTLV was effortless. For the virus variant WT29fDXCD2, reconstitution could not be achieved as of yet.

The replication kinetics of WTf eGFPSL3 did not show relevant differences compared to the wild-type virus WTf (fig. 11C). The titre development of the deletion variant WTf eGFPΔ75, however, was impaired, replication was slower as compared to WTf and WTf eGFP and the titres did not reach similar levels. Usually HVS lytic replication within OMK cells (MOI of 0.01) took 7-9 d to complete lysis of the entire cell monolayer. For WTf eGFPΔ75, it regularly took 11-13 d. Titres normally ranged between 10^5 to 10^6 pfu/ml, when complete lysis was reached, while they regularly stayed between 10^3 to 10^4 pfu/ml for WTf eGFPΔ75.

The generated viruses WTf eGFPSL3 and WTf eGFPΔ75 were used to transduce different donor T cell lines (K38: n = 1, K39: n = 1, K40: n = 2) at different time points (July 2016, 0716; January 2017, 0117; July 2017, 0717) with an MOI of 3. WTf-transduced cells served as a positive control for successful growth transformation. Total RNA was isolated at different time points after initial transduction. Human donor T cells transformed with WTf eGFPΔ75 grew slowly and seemed to be more sensitive than cells transformed with the viruses WTf eGFPSL3 or WTf. Whenever cell density allowed it, total RNA of 1x 10^6 cells was isolated and the remaining cells were cultivated until they died or until the end of experiment at 48 mpt. Differences between the different donor lines were visible, cells of donor K39 that were transformed by HVS viruses appeared to be more sensitive compared to those derived from donor K40.

The isolated RNA was subjected to DNaseI digest and subsequently reverse-transcribed into cDNA and used as the template for PCR to study transcription of the transgenes. Subsequently, agarose gel electrophoresis was performed (fig. 12). Samples with added RT (+) and without RT (-) are indicated. Cellular control-PCR for *GAPDH* transcription proved positive for all samples. The precedent DNaseI digest failed twice out of 37 samples, proving good but not infallible for the removal of residual DNA before RNA isolation. As a preferred viral control *ORF75* was chosen, since its transcription in T cells is relatively strong.

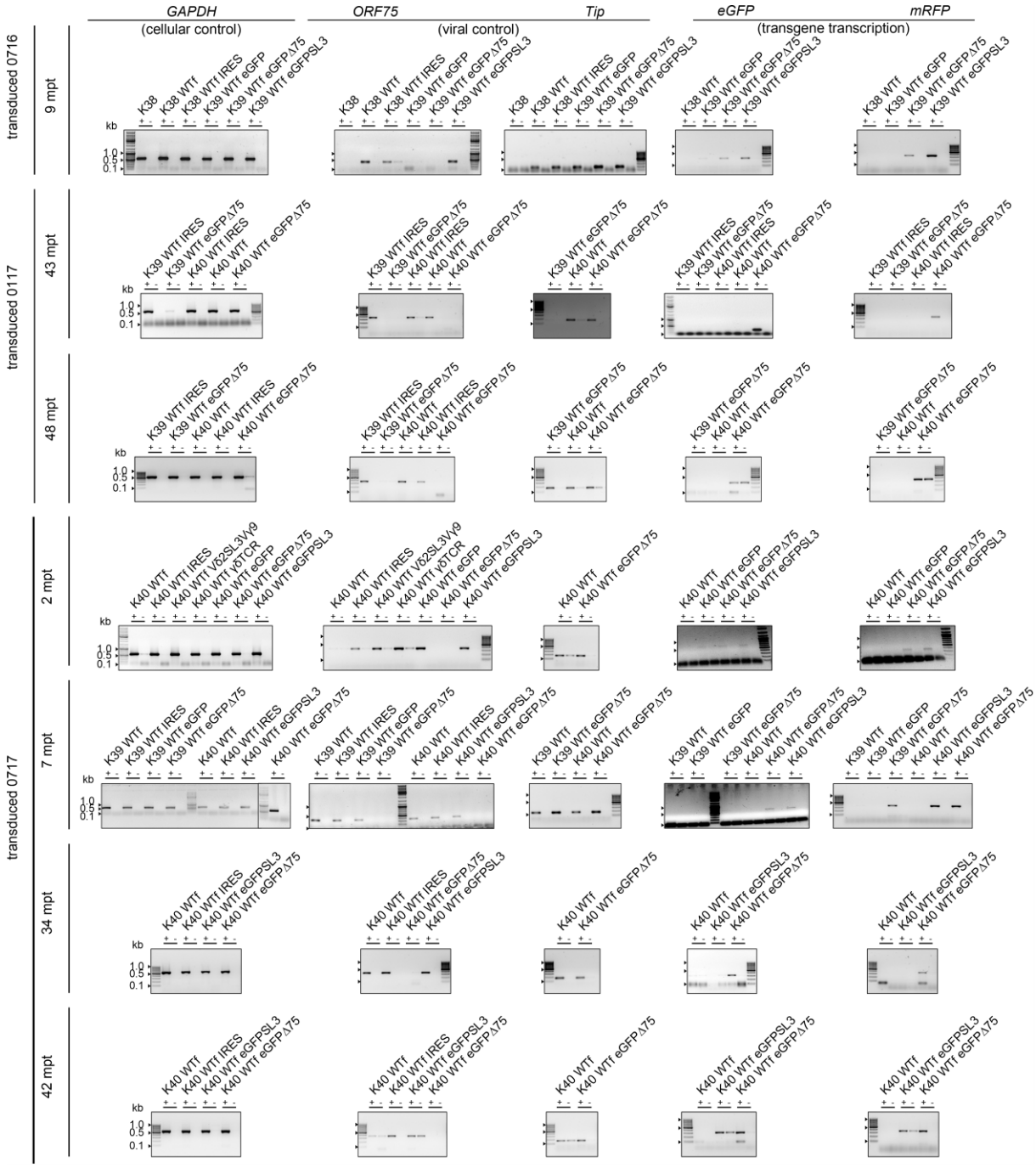

Fig. 12: Agarose gel electrophoresis of RT-PCRs. The observed band sizes coincided with the expected band sizes: *GAPDH* 581 bp, *ORF75* 365 bp, *Tip* 173 bp, *eGFP* 310 bp (or 670 bp for PCRs 0117, 48 mpt and 0717, 2 mpt), *mRFP* 350 bp. Cell line-variants WTf IRES carried the gene for a chimeric TCR (cTCR) but no fluorophore gene and were used alternatively to WTf as a negative control for transgene transcription. RT-treatment is indicated by (+), lack thereof is indicated by (-). Black arrows indicate 1 kb, 0.5 kb and 0.1 kb bands. Grey shades are displayed in inverted mode.

Since *ORF75* was deleted in variant WTf eGFPΔ75, *Tip* was used as a cellular control instead. Transcription of *Tip* was not detectable with the usually used Taq-polymerase, so Phusion® polymerase had to be used to verify transcription of this ORF. With increased sensitivity, however, more positive signals for DNA residues in the samples without RT were detected in *Tip*-specific PCR (10 out of 18) compared to *ORF75* specific PCR (11 out of 37).

As expected, cell lines transformed by the *ORF75*-deletion variant did not show *ORF75* transcription. Transcription of *eGFP* was first monitored with experimentally unreliable oligonucleotides HF1836 and HF1837 generating a product of 670 bp (fig. 12: 0717, 2 mpt). The oligonucleotides HF3470 and HF3471 were later used instead and generated a well reproducible band of 310 bp.

In cell lines derived from donor K39, *eGFP* and *mRFP* transcription were rarely and only weakly detected. Very faint signals for *eGFP* transcription can be seen in the cell lines K39 WTf eGFP and WTf eGFP∆75 transduced 0716 and isolated at 9 mpt, and in cell line K39 WTf eGFP∆75 transduced 0717 and isolated at 7 mpt. For the cell line K39 WTf eGFP∆75, transduced 0117 and isolated at 43 and 48 mpt, *eGFP* transcription could not be proven. The *mRFP* transcription in cell lines K39 WTf eGFP∆75 transduced at 0716 after 9 months and in cells transduced at 0717 after 7 months could be shown but not in cell line K39 WTf eGFP∆75 transduced at 0117 and isolated at 43 and 48 mpt.

Table 23: Transcription of indicated genes in transformed human donor K39 and K40 T cells. +, positive PCR; -, negative PCR; n.d., no data/cell line died/cell density too low.

	date of trans-duction	months post-trans-duction	K39 WTf/ WTf IRES, neg. contr.	K39 WTf eGFP	K39 WTf eGFP∆75	K39 WTf eGFPSL3	K40 WTf/ WTf IRES, neg. contr.	K40 WTf eGFP	K40 WTf eGFP∆75	K40 WTf eGFPSL3
eGFP	0716	9	-	+	+	+	n.d.	n.d.	n.d.	n.d.
	0117	43	-	n.d.	-	n.d.	-	n.d.	+	n.d.
		48	n.d.	n.d.	-	n.d.	-	n.d.	+	n.d.
	0717	2	n.d.	n.d.	n.d.	n.d.	-	n.d.	+	+
		7	-	+	+	n.d.	-	+	+	+
		34	n.d.	n.d.	n.d.	n.d.	-	n.d.	-	+
		42	n.d.	n.d.	n.d.	n.d.	-	n.d.	+	+
mRFP	0716	9	-	-	+	+	n.d.	n.d.	n.d.	n.d.
	0117	43	-	n.d.	-	n.d.	-	n.d.	+	n.d.
		48	n.d	n.d.	-	n.d.	-	n.d.	+	n.d.
	0717	2	n.d.	n.d.	n.d.	n.d.	-	-	+	+
		7	-	-	+	+	-	n.d.	+	+
		34	n.d.	n.d.	n.d.	n.d.	-	n.d.	-	+
		42	n.d.	n.d.	n.d.	n.d.	-	n.d.	+	+

Compared to the PCR signals of samples from K39-derived cell lines, more intense signals were observed from samples of K40-derived cell lines. The *eGFP* transcription in the cell lines K40 WTf eGFP∆75, transduced at the different time points 0117 and 0717, generally proved to be stable over time. Only 34 mpt no *eGFP* transcripts could be detected via PCR for 0717 K40 WTf eGFP∆75. K40 WTf eGFPSL3 cell line yielded strong signals in samples taken from 2, 7, 34, and 43 months after initial transduction. The exact same results could be observed for *mRFP* transcription at the same time points (fig. 12, table 23).

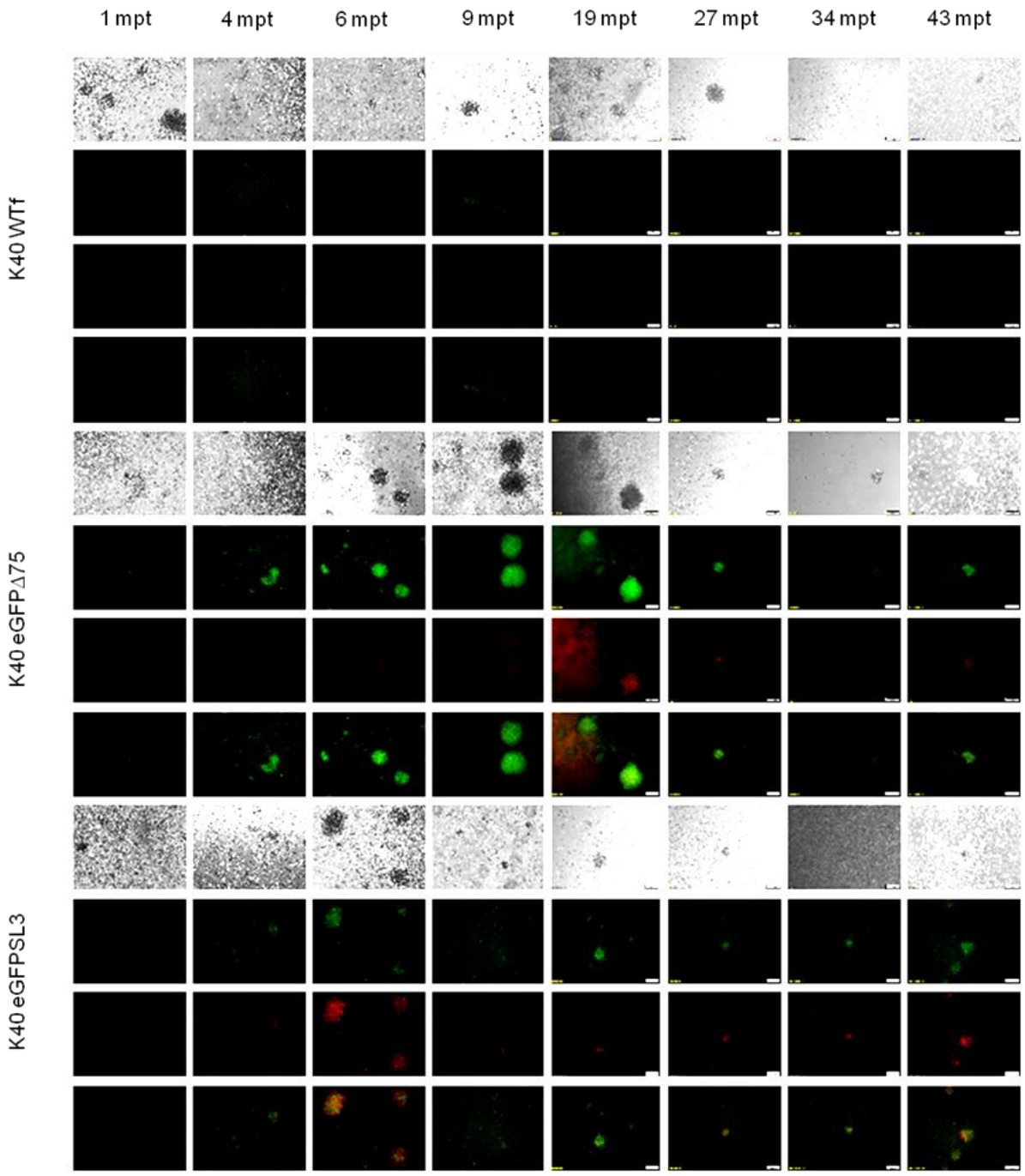

Fig. 13: Exemplary selection of fluorescence microscopy photographs of 0717 K40 HVS-transformed human T cells over time. The expression of fluorophores eGFP and mRFP under control of *ORF75* and *SL3* promoters was monitored by fluorescence microscopy. Pictures were taken regularly post-transduction. Cell line K40 WTf eGFP died before 6 mpt. Expression of the fluorophores seemed to peak around 6-14 mpt and afterwards subsided to low level expression until the end of experiment 43 mpt.

The results suggest a direct effect of the donor cell line on transgene transcription (fig. 12, table 23). Cell lines of donor K39 were more likely to not get transformed, died faster or grew slower, thus, preventing sampling. Cell lines derived from donor K39 in general did not seem well suited for *eGFP* or *mRFP* transcription, while cell lines based on K40 seemed to transcribe transgenes more reliably.

The fluorophore expression within the different cell lines was also documented via fluorescence microscopy. Exemplary pictures from four years of documentation were chosen of K40 donor-derived cell lines and presented in (fig. 13).Expression of the fluorophores eGFP and mRFP was fluctuating over time. Fluorescence of both was first observed 4 mpt and peaked in both donor lines around 6-14 mpt, to subsequently slowly subside to a low-level expression. In cells with extremely high signal intensities for mRFP or eGFP, the other fluorophore was mostly not found as intensely expressed. Fluorophore expression was mainly visible in clusters of aggregated cells. When cells were harvested, aggregates were separated and the proliferation of the remaining cells potentially impaired, depending strongly on the total cell number and, thus, the culture volume.

In case of transduced K39 cells, the repeated harvests of cells for experiments lead to the successive death of all transformed lines at latest 22 mpt. K39-derived cell lines transformed with HVS seemed to grow slightly slower, compared to K40-derived cell lines. The expression of mRFP was nearly not existent in K39-cell lines. K40-cell lines seemed stronger and cell propagation in general seemed faster.

These observations correlate with the cDNA results (fig. 12), where expression in K39-derived cell lines resulted in weaker PCR signals. It is conceivable that fluctuations were at least influenced, if not entirely due to, the harvest of cells for experiments. Transformed T cells were sensitive against changes in cell density and to reduction of total cell number within the culture, if it fell under 2x 10^6/ml. Comparison between *ORF75* and *SL3* promoters suggested that the expression levels under either promoter under ideal growth conditions is rather continuous, with *SL3* inducing stronger transgene expression levels (fig. 13).

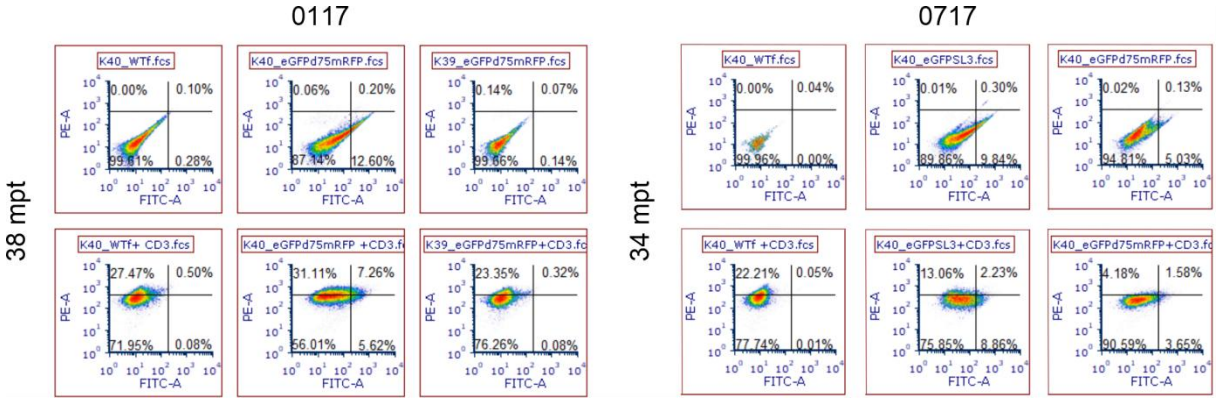

Fig. 14: Flow-cytometry results of HVS-transformed cell lines transduced 0117 and 0717. Density plots of transformed T cells. The cells were either measured untreated (upper row), in order to verify the percentage of cells expressing eGFP, or stained with anti-CD3 (PE), to attest they retained the expression of this T-cell marker (lower row). The cell lines K39 WTf eGFPΔ75, K40 WTf, and K40 WTf eGFPΔ75 were measured 38 mpt (left side) and the cell lines K40 WTf, K40 WTf eGFPSL3, and K40 WTf eGFPΔ75 were measured 34 mpt (right side).

Measurement of the expression of either fluorophore via flow cytometry was attempted. Previous analysis already implied a high probability of lacking signals for mRFP because condi-

tions were not ideal for its excitation (excitation maximum 584 nm; laser 488 nm, estimated excitation: 7.6% of maximum) and measurement with the bandpass filter available (emission maximum 607 nm; 585/42 bandpass filter (PE), estimated signal 22.8%). Expected excitation for eGFP under the FACS® Canto laser *Sapphire® Solid State 488 20* was almost perfect (99.8%), signal intensity with band pass filter 530/30 (FITC) was expected to be approximately 37.5% (evaluation with BD spectrum viewer).

The expectations were met: mRFP could not be detected but seen clearly under fluorescence microscope, whereas eGFP could barely be seen under fluorescence microscope but detected by flow cytometry (fig. 14). For 0117 cell lines, fluorophore activity was measured at 18, 32, and 40 mpt. For 0717 cell lines, it was performed 4, 8, 12, 26, and 34 mpt. Anti-CD3 staining was performed only once at the end of the experiments, after preliminary experimental results (not shown) suggested a constant expression of CD3 and TCR (almost exclusively αβ-positive). Autofluorescence of T cells was observed in all cultures and was taken into account by using K40 WTf- transformed cells as a negative control during compensation. Dot plots of transformed K40 cell lines were generated with FITC- on the x- and PE-signal intensities on the y-axis.

A slight shift of at least parts of the population to the right on the x-axis can be seen when the signal intensities of the WTf-transformed cell lines were compared to both (0117 and 0717) K40 WTf eGFPΔ75 lines as well as to 0717 K40 WTf eGFPSL3. CD3-stained samples confirm these results.

Table 24: Percentages of $FITC^+$ and $FITC/PE^{+/+}$ cells over time in HVS transformed T cells

0117					**18 mpt**		**32 mpt**		**38 mpt**	
					$FITC^+$	**$FITC^+/PE^+$**	**$FITC^+$**	**$FITC^+/PE^+$**	**$FITC^+$**	**$FITC^+/PE^+$**
K39 WTf					0.15	0.08	dead		dead	
K39 WTf eGFPΔ75					10.32	0.64	1.46	0.6	0.14	0.07
K40 WTf					0.04	0.08	0.75	1.22	0.28	0.1
K40 WTf eGFPΔ75					23.7	0.59	37.49	2.91	12.6	0.2
0717	**4 mpt**		**8 mpt**		**12 mpt**		**26 mpt**		**34 mpt**	
	$FITC^+$	**$FITC^+/PE^+$**	**$FITC^+$**	**$FITC^+/PE^+$**	**$FITC^+$**	**$FITC^+/PE^+$**	**$FITC^+$**	**$FITC^+/PE^+$**	**$FITC^+$**	**$FITC^+/PE^+$**
K39 WTf	n.d.	n.d.	0.0	0.00	0.00	0.00	dead		dead	
K39 WTf eGFP	0.06	0.06	0.2	0.00	1.64	0.01	dead		dead	
K39 WTf eGFPSL3	25.32	1.18	dead		dead		dead		dead	
K39 WTf eGFPΔ75	3.92	0.13	6.1	0.00	5.66	0.01	dead		dead	
K40 WTf	0.03	0.02	0.00	0.00	0.01	0.00	0.06	0.07	0.0	0.04
K40 WTf eGFPSL3	16.52	0.01	1.95	0.00	9.44	0.02	6.71	0.64	9.84	0.30
K40 WTf eGFPΔ75	1.83	0.01	1.74	0.00	6.90	0.01	7.69	0.45	5.03	0.13

In table 24, all generated results for the transduction 0117 and 0717 were summed up and the percentages of FITC-positive cells of unstained cells detected by flow cytometry with consistent settings at indicated time points after transduction were listed. Dot plots were analysed analogously to the dot plots shown in fig. 14. The percentage of cells positive for eGFP expression is fluctuating over time.

First, donor cell lines were compared concerning their eGFP expression. At both transductions (0117 and 0717), transformed cell lines derived from donor K39 died earlier than the K40-derived cell lines but had higher percentages of cells expressing eGFP when transformed with the same virus variant.

Second, the percentages of cell lines expressing eGFP were compared between the two transductions. For K40 cell lines transduced at 0117, it was observed that they had higher rates of eGFP expressing cells at all time points than their counterparts from the transduction 0717. For example, the percentage of eGFP-expressing cells of K40 WTf eGFPΔ75 amounted to 12.6 % FITC-positive cells for transduction 0117 at 38 mpt as compared to 5.03 % FITC-positive cells for transduction 0717 at 34 mpt. Unfortunately, K39 cells died too early and grew too poorly to allow thorough comparison. Only at 18 mpt and 12 mpt for 0117 and 0717 respectively, percentages of K39 WTf eGFPΔ75 cell lines could be compared to some extent: higher percentages were found in the 0117 transduced K39 WTf eGFPΔ75 cell line (10.32 %) than the 0717 transduced cell line (5.66 %).

Third, eGFP expression from the different virus variants was compared between transformed T cells from the same donor and the same time point of transduction. WTf eGFPSL3-transformed cells had mostly higher percentages of eGFP-expressing cells than WTf eGFPΔ75 (transduction 0717). Contrary to the expectations, 0717 K39 WTf eGFP showed almost no eGFP expression, only at 12 mpt percentages increased slightly.

For further evaluation, real-time PCR was performed to semi-quantitatively determine DNA copy numbers per cell and rule out the influence of strongly deviating DNA copy numbers per cell as an influence factor on expression. At the time points 34 and 43 mpt, 1x 10^6 transformed T cells were harvested and the DNA was isolated. Three separate semi-quantitative real-time PCRs were performed to validate the average copy number per cell, normalised to GAPDH (table 25). The mean average copy number per cell ranged from 68 up to 243. DNA from uninfected, permissive OMK cells and from non-transduced K41 donor cells acted as negative controls. Neither cell line proved positive. Copy numbers from DNA isolated from transduced T cells eight months apart were also compared to one another to search for changes (fig. 5).

Table 25: Average copy numbers per cell, determined from isolated DNA by real-time PCR.

Time point of transduction	months post-transduction	designation	copy numbers run 1	copy numbers run 2	copy numbers run 3	*average copy number/cell*
0117	40	K39 WTf eGFPΔ75	162.22	105.04	145.63	***137.63*** ± 29.42
		K40 WTf	176.09	185.79	162.35	***174.74*** ± 11.78
		K40 WTf eGFPΔ75	177.90	128.59	170.17	***158.89*** ± 26.52
	48	K39 WTf eGFPΔ75	295.37	70.10	122.05	***162.51*** ± 117.96
		K40 WTf	95.88	46.77	66.48	***69.71*** ± 24.72
		K40 WTf eGFPΔ75	96.87	47.27	70.23	***71.45*** ± 24.83
0717	34	K40 WTf	124.70	82.94	113.37	***107.00*** ± 21.60
		WTf eGFPSL3	310.10	164.53	255.96	***243.53*** ± 73.57
		K40 WTf eGFPΔ75	129.50	74.64	100.55	***101.56*** ± 27.44
	42	K40 WTf	86.99	51.80	73.29	***70.69*** ± 17.74
		K40 WTf eGFPSL3	215.52	145.06	163.15	***174.57*** ± 36.59
		K40 WTf eGFPΔ75	86.08	58.21	60.18	***68.16*** ± 15.55

All samples, except for 0117 K39 WTf eGFPΔ75, show a drop in average copy number per cell within the eight months between sampling. Standard deviation for that sample however is higher than for the others. The average copy number per cell within WTf eGFPSL3-transformed cell lines was higher than in WTf eGFPΔ75. An impact of copy numbers on expression is unlikely, since numbers are similar within 0117 K39 WTf eGFPΔ75 and its K40 sibling line, despite them having an almost two-fold difference in cells expressing eGFP. It is improbable that a copy number difference of approximately 20 copies would induce such a strong effect.

Taken together, the results indicate a stable and long-term transcription and expression of fluorophores under control of the viral promoters *SL3*, *StpC/Tip,* and *ORF75* is achievable in mature human T cells transformed with HVS C488 vectors. Between 2-37 % of the transformed cells were observed to express eGFP, for mRFP percentages could not be quantified. The donor cell line seemed to influence the transcription. The experimental settings were not ideal to quantify fluorophore expression exactly, however, the activity of the *SL3* promoter seemed subjectively higher than that of the *ORF75* promoter. PCR signals were stronger and the mRFP signal intensities appeared higher in T cells transformed with WTf eGFPSL3 than in WTf eGFPΔ75 transformed cells. The average DNA copy numbers in transformed T cells were determined to range from 68 to 243 copies per cell and excluded as a cause for lack of transcription or vastly differing levels of transgene transcription in human T cells.

3.5 Self-repairing bacterial artificial chromosomes

Self-repair of viruses which were reconstituted from BACs was mediated by homologous regions and enabled the viruses to remove the miniF sequence from their genome during replication. Upon direct orientation these regions were labelled DR and if inserted inversely, they were termed DX. Several variants were generated using *en passant* mutagenesis. Correct insertion and subsequent release of the selection marker were proven by colony PCR. The RFLPs were checked using suitable restriction enzymes and compared to the wild-type band pattern (fig. 15). Furthermore, the modified locus of insertion was confirmed by Sanger sequencing at the Institute for Clinical Molecular Biology in Kiel. The two BACs WT22fDR and WT29fDX were used as a basis and upon self-repair and removed miniF sequence were termed WT(22fDR) and WT(29fDX), respectively.

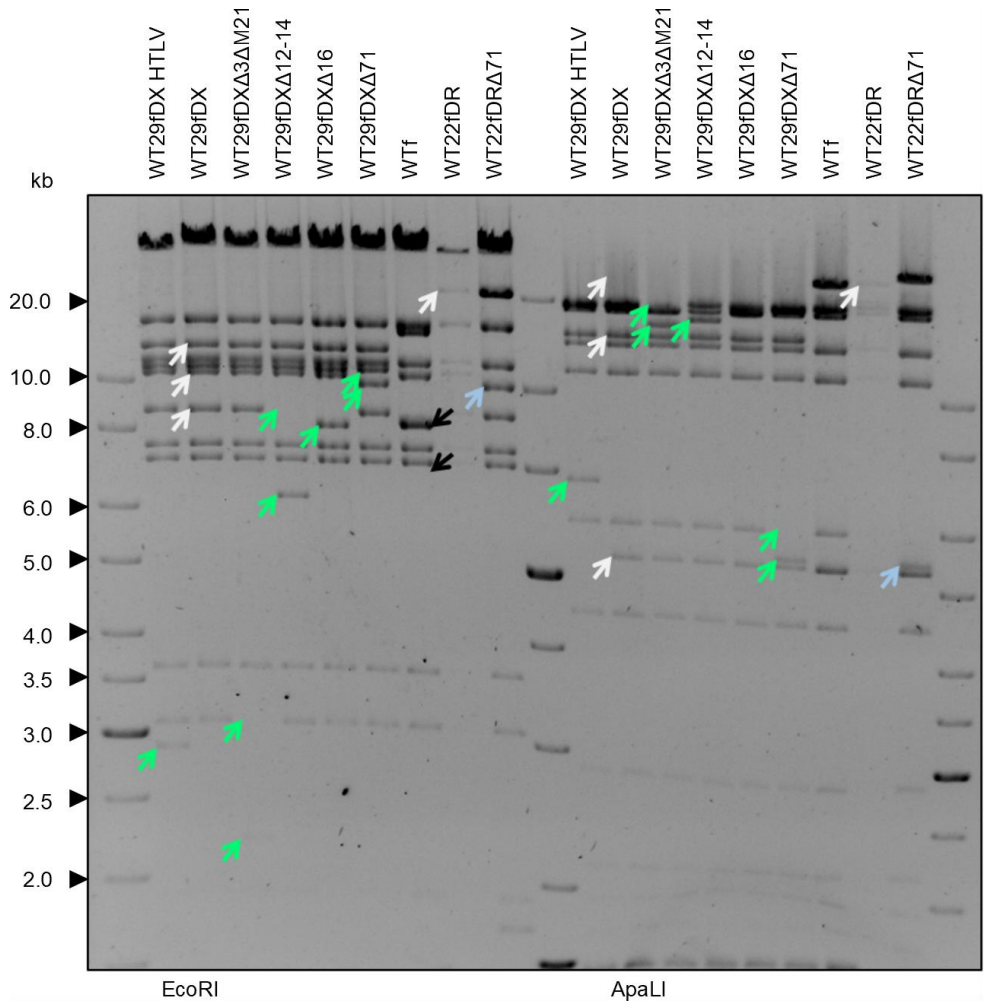

Fig. 15: RFLP analysis of all generated self-repairing BACs. BAC DNA was digested using EcoRI or ApaLI. The band pattern was compared to *in silico* digests generated with VectorNTI and corresponds with the expected patterns and band shifts, apart from divergences already seen in the wild-type from the expected pattern (black arrows pointing down, indicating missing or additional bands). Band-shift changes of all successor variants of WT29fDX compared to their predecessor WT29fDX are indicated by green arrows, changes of successor variants compared to WT22fDR are indicated in blue and differing bands of WT29fDX and WT22fDR compared to WTf are shown in white. Differences between the original and the predicted WTf BAC band pattern are indicated by black arrows pointing down. Grey shades are displayed in inverted mode.

The results from the restriction enzyme digest overall met the expectation. The anticipated changes in band patterns compared to the predecessor are indicated via arrows (fig. 15). White arrows signify the differences of the self-repair enabled BACs WT22fDR and WT29fDX compared to the WTf BAC. Green arrows visualise the band shifts compared to the WT29fDX predecessor BAC, while light blue arrows do so for the WT22fDR BAC. In general, the band pattern mirrors the expected pattern generated by using Vector NTIs *in silico* restriction enzyme digest function. Unfortunately, the passaged viral DNA pattern did not, most likely due to methylation after at least nine passages in permissive OMK cells (fig. 16).

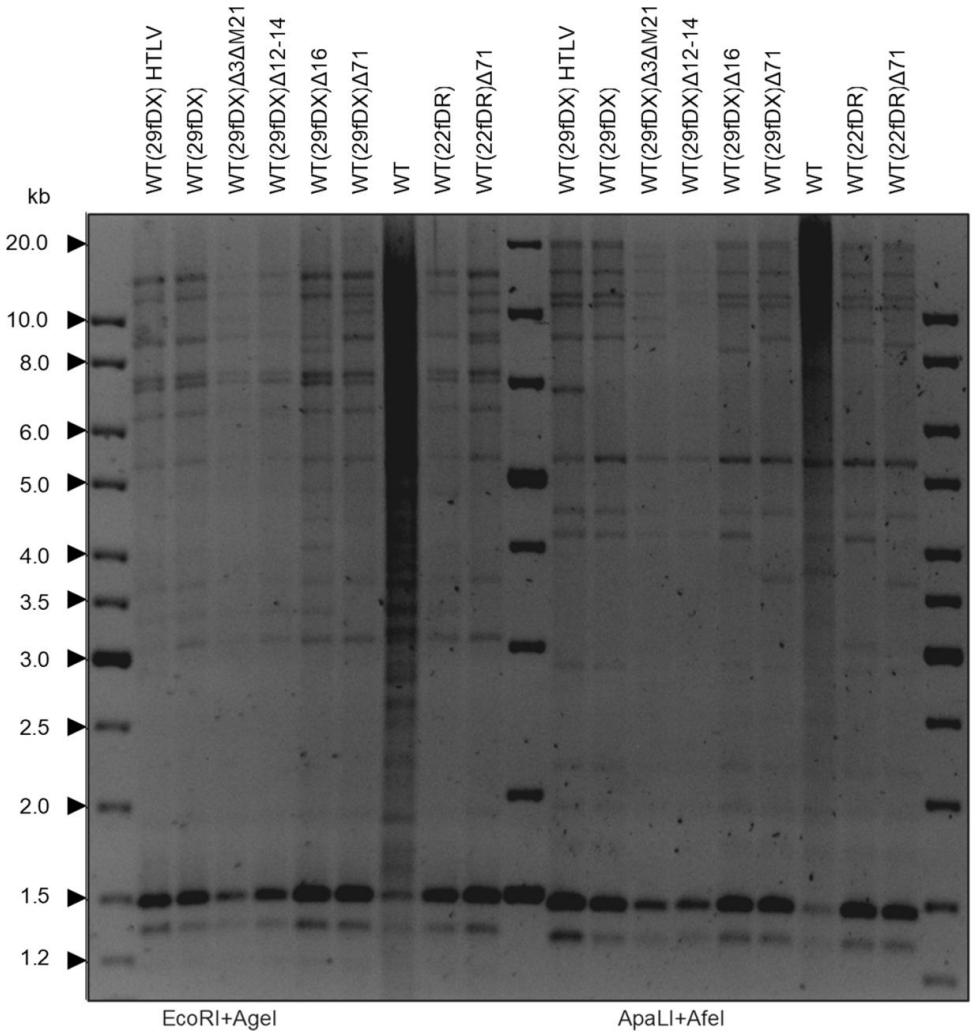

Fig. 16: RFLP analysis of self-repaired viral DNA after at least nine passages in OMK cells. Restriction-enzyme digest patterns of isolated viral DNA after completing at least nine passages in OMK cells. The DNA of WT HVS C488 virus unfortunately yielded low results in quality and concentration whenever isolated. The expected changes were not indicated, since the pattern mostly divert greatly from the expectations, most likely due to methylation of CpG islands, preventing enzyme cleavage.

Double digestion of the isolated viral DNA was performed using either EcoRI and AfeI or ApaLI and AgeI (fig. 16). Especially AfeI and AgeI seemed greatly impaired in their endonuclease activity, probably due to epigenetic modifications such as methylation. On the right side for example, digested with ApaLI and AfeI, multi-copy bands were expected at 959 bp

and 468 bp caused by AfeI cutting within the H-DNA repeats. Instead, strong bands are visible at approximately 1.5 kb, indicating the predicted restriction enzyme cleavage site within was either blocked or the available sequence data is not accurate. Many of the expected bands can be observed, some can be explained by failed restriction enzyme site recognition, while others cannot be explained without further analysis using other methods. For these reasons, the verification of viral self-repaired DNA via digest was of limited value.

In order to ensure the correct sequence of the virus genome and to exclude the possibility of incorrect sequence data distorting the expected digest-patterns, the WT virus and the self-repaired WT(29fDX) virus were subsequently subjected to next generation sequencing at Eurofins Genomics (NGS, Illumina platform Novaseq 6000). The sequence of the original WTf BAC was derived from the published sequence and pyrosequencing in 2014 (Bremer, 2014; Ensser et al., 2003). Two mutations were found via pyrosequencing compared to the published sequence. In *ORF46* and *47,* point mutations were detected leading to amino acid exchanges of aspartic acid to asparagine and of alanine to valine (Bremer, 2014).

Table 26: Nucleotide polymorphisms in coding regions identified by NGS of isolated viral DNA

WT			self-repaired WT(29fDX) virus (p9)		
site of mutation*	**ORF**	**frequency of exchange**	**site of mutation***	**ORF**	**frequency of exchange**
			46,379G>A	Leu216Leu (ORF26 capsid protein VP23)	32% of reads
55,412 T>G	Leu402Leu (ORF36, phosphotransferase)	30% of reads			
66,446 C>T	Asp65Asn (ORF46, DNA glycosylase)	100% of reads	66,446 C>T	Asp65Asn (ORF46, DNA glycosylase)	100% of reads
66,884 G>A	Ala50Val (ORF47, glycoprotein L)	50% of reads	66,884 G>A	Ala50Val (ORF47, glycoprotein L)	50% of reads
106,869 C>T	Gly149Glu (ORF73, LANA homologue)	22 % of reads	106,869 C>T	Gly149Glu (ORF73, LANA homologue)	36 % of reads
			106,872 T>C	Glu148Gly (ORF73, LANA homologue)	30 % of reads

*reference genome is the published sequence of WT genome of HVS C488 (Ensser et al., 2003; GenBank: AJ410493.1)

Evaluation of the NGS data confirmed these two mutations for the wild-type virus and the self-repaired wild-type virus. For the WT(29fDX) virus, this was to be expected since the WT29fDX BAC was derived from the WTf BAC (Heyn, 2015). Additionally, two more mutations were detected in the WT sequence and three more in coding regions in the self-repaired wild-type virus WT(29fDX), accessible in table 26. Three additional mutations were found in the self-repaired virus in non-coding regions (nucleotide 4 C>T or single-base deletion, nucleotide 28,380 C>T, and nucleotide 29,761 C>T; reference: GenBank: AJ410493.1). Sequencing of the H-DNA unfortunately was not possible using NGS. The high GC-content prevented amplification and the number of reads obtained for the H-DNA as a whole was extremely low.

Meanwhile, the generated virus mutant BACs were isolated by maxi-preparation and used to transfect permissive OMK cells with Lipofectamine™2000. Reconstituted virus was grown on permissive epithelial OMK cells until almost all cells were dead and, subsequently, a fresh culture of OMK cells was infected for 1 h, using the collected supernatant. Medium was then renewed. Directly from the supernatant, virions could be pelleted by centrifugation and re-suspended in water to be subjected to passaging PCR in order to determine progress of the self-repair and removal of miniF sequence from the viral genome. The virion structure was destroyed during the initial denaturation and PCR was performed using the freed viral dsDNA as a template. Two separate recombination events had to occur to release the miniF sequence from the viral genome during replication in permissive cells (fig. 17). The self-repair was monitored by PCR and was usually completed after two to eight passages (fig. 18A), depending on the virus and propagation method.

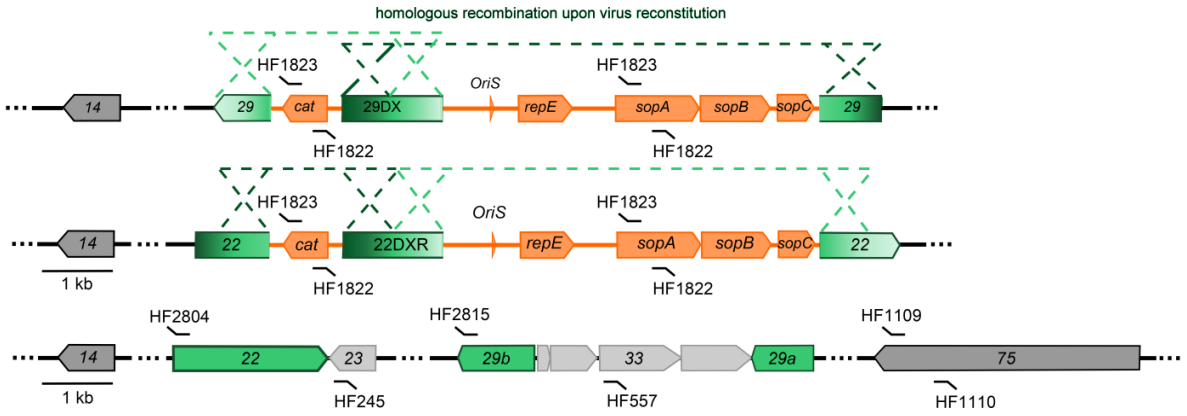

Fig. 17: Self-repair and monitoring PCRs after virus passages. Two separate homologous recombination events are necessary for the release of the miniF sequence from the viral genome and the restoration of *ORF22* and *ORF29b*, respectively. In the upper row WT29fDX is shown, in the middle WT22fDR, and in the lowest row the self-repaired WT genome without any miniF sequence. The Oligonucleotides used to monitor the presence of miniF genes *sopA* and *cat,* as well as the viral *ORF75* are indicated, as are the primer combinations applied to monitor the self-repair of *ORF22* and *ORF29*.

Mostly, self-repair was completed in passage 3. WT22fDRΔ71 took until passage 5, while for WT29fDXΔ12-14 the complete removal of the miniF sequence and restoration of *ORF29* took until passage 7 (fig. 18A). Although WT29fDXΔ16 seemed equally slow to lose the miniF sequence, it is not comparable to the others as it was passaged differently. Instead of only allowing the fittest and fastest virions to propagate, by limiting the infection of permissive OMK cells to 1 h, the virus containing inoculums were incubated with permissive cells until the cell layer was lysed completely. Similarly long self-repair results were obtained for WT29fDX when using this method (data not shown), proving a short infection period more efficient for quickly obtaining self-repaired virus. Exemplary replication kinetics of these viruses after passage 9 can be seen in fig. 18B.

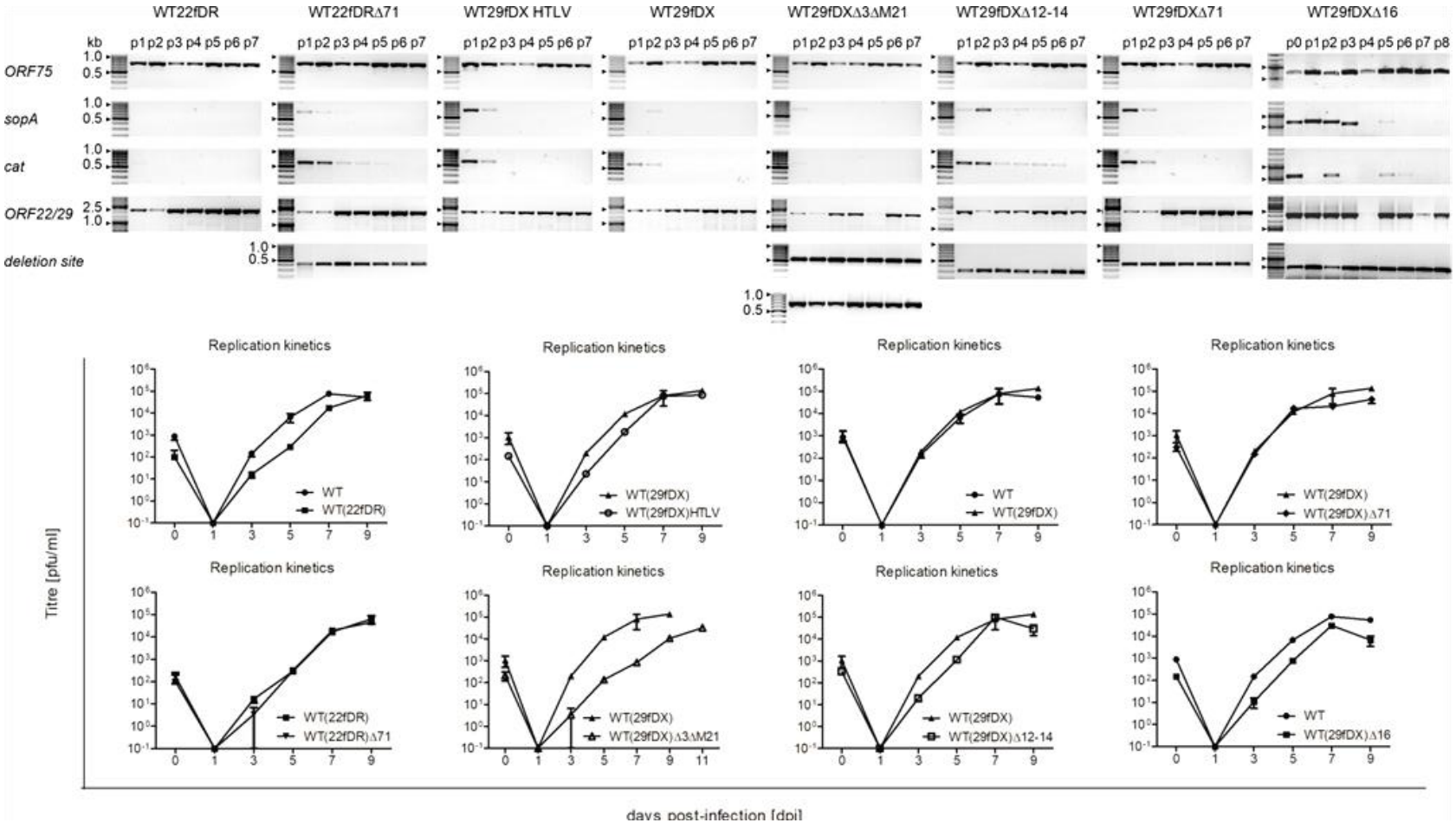

Fig. 18: PCR results of passaged self-repairing viruses and their respective replication kinetics after passage 9. All self-repairing viruses were passaged nine times on permissive OMK cells. **A** The self-repair was monitored by conventional PCR, followed by gel electrophoresis. Grey shades were depicted invertedly. *ORF75* served as a viral control, decreasing signals for *sopA* and *cat* served as markers for completed recombination events, positive signals for *ORF22/29* PCR indicated complete removal of the miniF sequence and restoration of the respective ORF. Additionally, a PCR spanning the deletion site was performed to ensure the stability of the deletion during passaging. For the virus variant W29fDXΔ3ΔM21 both, deletion of *ORF3*, and the partial deletion of the *ORF21* is demonstrated. All bandsizes were of the expected size (*ORF75*: 0.7 kb, *sopA*: 0.66 kb, *cat*: 0.58 kb, *ORF22*: 2.17 kb, *ORF29*: 2.07 kb, *Δ71*: 0.42 kb, *Δ3:* 0.6 kb, *ΔM21*: 0.68 kb, *Δ12-14*: 0.32 kb, *Δ16*: 0.5 kb). **B** Supernatant of passage nine of all viruses was collected, stored, and subsequently replication kinetics of the self-repaired viruses were performed. Replication kinetics of WT(22fDR), WT(22fDR)Δ71, WT(29fDX), WT(29fDX)Δ16, WT(29fDX)Δ71 and WT(29fDX)HTLV were repeated at least thrice and exemplary kinetics are displayed. Replication kinetics of WT(29fDX)Δ12-14 and WT(29fDX)Δ3ΔM21 could only be performed once as of now.

The replication of the generated mutants was compared either to that of the WT, or to the self-repaired, wild-type like predecessors WT(22fDR) or WT(29fDX). Between WT, WT(29fDX) or WT(22fDR), differences in replication time or in endpoint titre were not observed, in at least three separate experiments with each three independent dilution series.

Deletion of *ORF71* was performed in both self-repairing variants, WT22fDR and WT29fDX, and did not result in a change of viral replication. For the HTLV-mRFP-insertion variant WT29fDXHTLV, and deletion variant WT29fDXΔ12-14, the replication kinetics were unchanged, too, compared to the wild-type. The deletion of *ORF3* in WT29fDXΔ3ΔM21 virus slowed down the replication by two days but allowed the virus to grow to comparable endpoint titres as the wild-type. This coincides with the observations gained during virus passaging and stock generation. Deletion variant WT(29fDX)Δ16 showed the same replication dynamic as its predecessor WT(29fDX). For all self-repairing variants, titres after complete lysis varied around 5x 10^4 to 5x 10^5 pfu/ml.

Deletion of the apoptosis-relevant *ORF16* and *ORF71*

Replication of HVS was not affected by single deletion of *ORF16* or *ORF71* (replication kinetics see fig. 18B) but was abolished by double deletion of both ORFs. K39 T cells transduced with the self-repaired deletion viruses WT(29fDX)Δ16 or WT(29fDX)Δ71 were analysed 31 months post-transduction (mpt) for their average number of HVS genome copies per cell by use of the newly established semi-quantitative *ORF9*-specific real-time PCR. All samples were normalised to GAPDH and average copy numbers per cell ranged from 93 to 131 copies per cell (see fig. 5).

Up until now, the effect a deletion of these ORFs has on apoptosis in transformed human T cells has not been studied. Therefore, apoptosis was induced in these HVS-transformed cells, and the number of apoptotic cells measured at different time points after induction (fig. 19). Hydrogen peroxide (H_2O_2) was applied to stimulate the intrinsic apoptosis pathway and camptothecin (CPT) to induce apoptosis via DNA damage. The apoptosis rates at 4 and 24 h after induction were quantified by the combined use of flow cytometry and FITC-Annexin V/PI staining.

During measurement the gate was set to stop when 5x 10^4 living cells were measured. Compensation was performed using non-transduced FITC- or PI-stained T cells with induced apoptosis as positive controls. Dot plots (fig. 20) were generated with FCS express 6 and used for data evaluation. FITC-A was plotted on the X-axis and PerCP-Cy5.5-A on the Y-axis. Unstained viable cells presented in the lower left quadrant. FITC-Annexin positive cells, indicating early apoptosis, were accumulating in the lower right quadrant, while PI-positive cells, marking dead cells, could be located in the upper left quadrant. Late-apoptotic, double-positive cells were observed in the upper right quadrant.

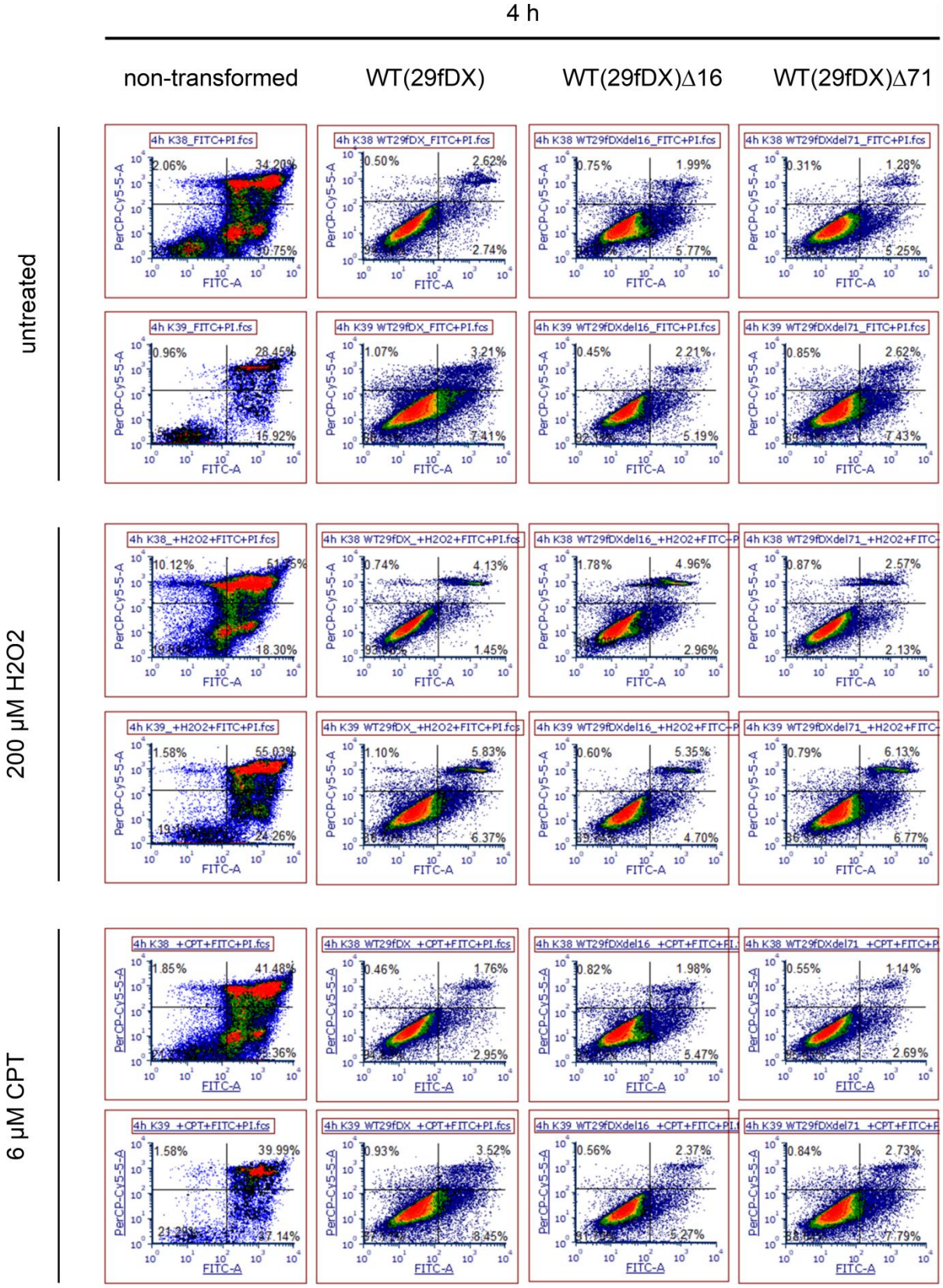

Fig. 19: Apoptosis induction in 32-months-old HVS- transformed human T cells after 4 h. (continued)

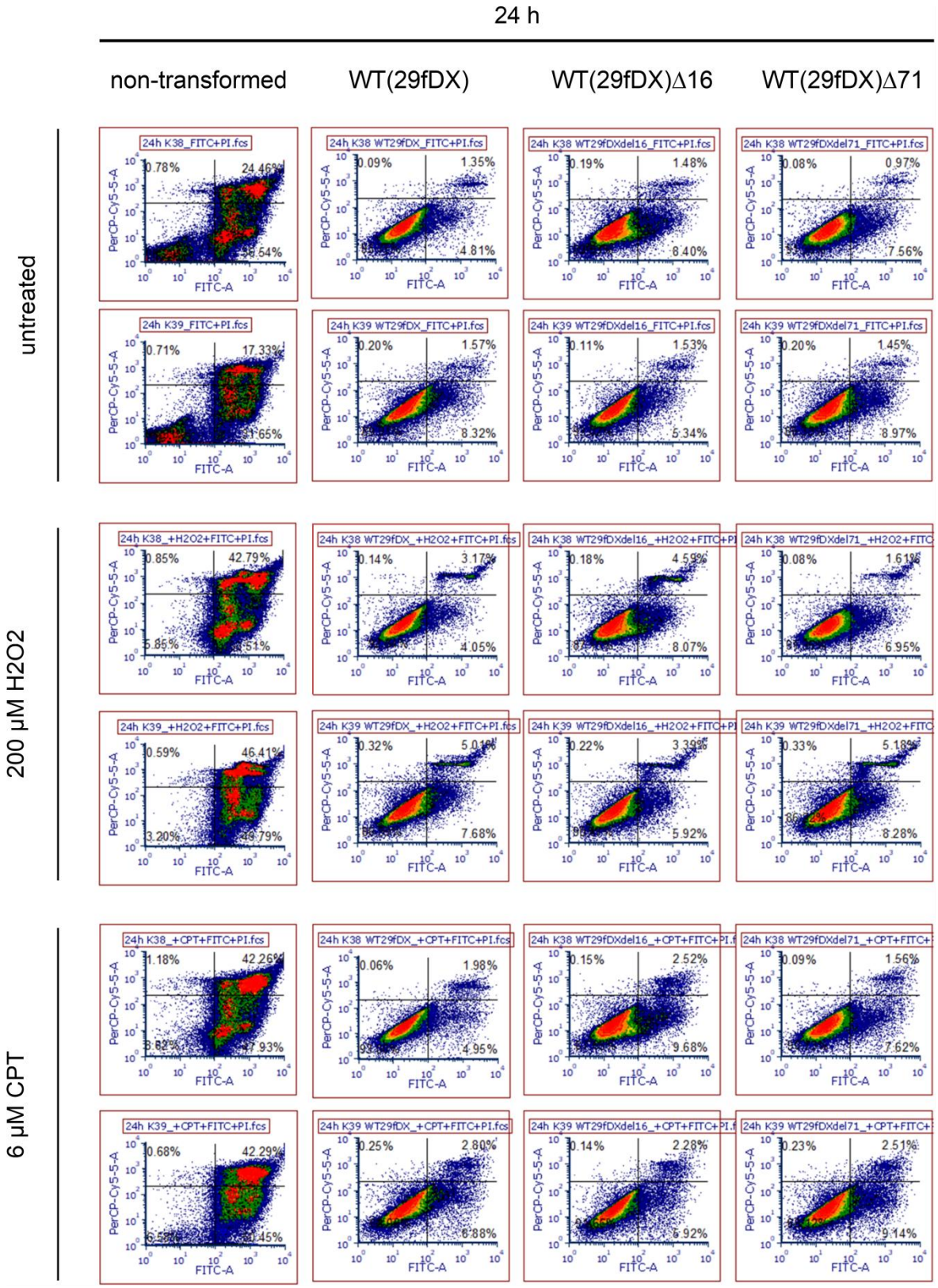

Fig. 19: Apoptosis induction in 32-months-old HVS- transformed human T cells after 24 h. The total apoptosis rates were measured using cell flow cytometry and FITC-AnnexinV/Propidium Iodide staining. Two different donor cell lines, K38 (upper rows) and K39 (lower rows), were transduced (0618) with self-repaired HVS WT(29fDX) and deletion variants WT(29fDX)Δ16 and WT(29fDX)Δ71 and stably transformed. At 32 mpt, apoptosis was induced in these cell lines by treating them with either 200 µM hydrogen peroxide (H_2O_2), or topoisomerase inhibitor camptothecin at 6 µM. FITC-A is plotted on the X-axis, PerCP-Cy5.5-A on the Y-axis. Rates of apoptosis were measured 4 h and 24 h after induction and monitored for effects resulting from the deletion of *ORF16* and *ORF71*. Unstained cells in the lower left quadrant were still viable.

For analysis, all FITC-positive human T cells, transformed by different self-repaired deletion variants WT(29fDX), WT(29fDX)Δ16, and WT(29fDX)Δ71, were categorised as apoptotic (fig. 19). Non-transduced T cells were included as a control for physiological apoptosis induction. The initial percentage of dying, non-transduced T cells was high. The effect of the different inducers at different time points is still clearly visible. Percentages of viable cells dropped for K38 from 34 % to 17 % (H_2O_2) and 20 % (CPT) after 4 h of treatment, and even further from 38 % to 6 % (H_2O_2) and 9 % (CPT) after 24 h. For K39, similar decreases were observed.

The percentages of FITC-positive cells in non-transduced cells by contrast increased due to the treatment. After 4 h, an increase from 56 % to 62 % (H_2O_2) and 65 % (CPT) was observed for K38, and after 24 h an increase from 61 % to 93 % (H_2O_2) and 90 %(CPT). For K39 cell lines, the percentages elevated from 40 % to 74 % (H_2O_2) and 69 % (CPT) after 4 h, and after 24 h from 49 % rose to 96 % (H_2O_2) and 93 % (CPT) due to treatment. In non-transformed T cells, induction of apoptosis with either inducer increased apoptosis rates and decreased the amount of viable cells. After 4 h these effects were more prominent than after 24 h.

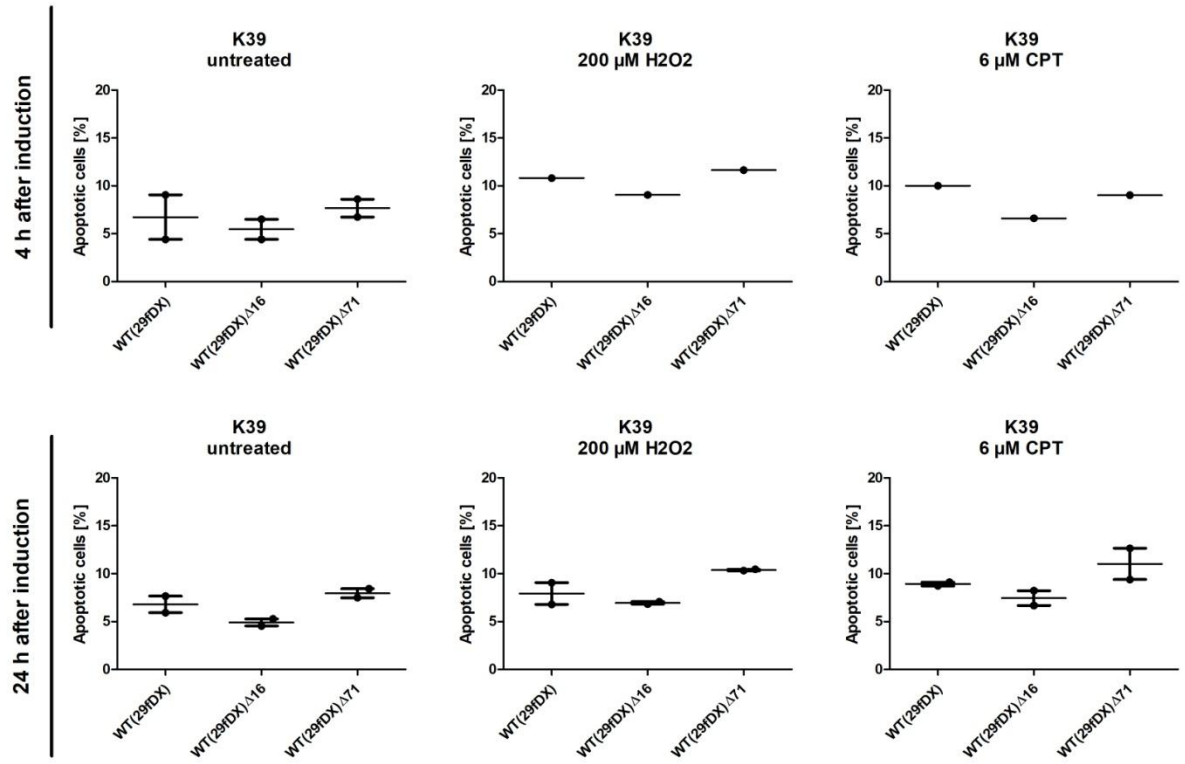

Fig. 20: Apoptosis rates 4 and 24 h after induction of apoptosis by H_2O_2 and CPT in K39 donor cell lines. Donor cell line K39 transformed cells were analysed concerning their response to induction of apoptosis by H_2O_2 (200 mM) and CPT (6 µM) by use of FITC-AnnexinV/PI staining. FITC positive cells, including FITC-AnnexinV/PI double-positive subpopulations, were counted as apoptotic. Apoptosis rates were measured via flow cytometry 4 h (32 mpt) and 24 h after induction (30 and 32 mpt). Three different self-repaired viruses were initially used for transduction WT(29fDX), WT(29fDX)Δ16 and WT(29fDX)Δ71. Apoptosis rates for the transformed cells under different conditions with their respective mean and standard deviation are depicted.

In transformed human T cells the induction was not as effective. Transformation of human T cells with the HVS vectors clearly had an effect on the efficacy of apoptosis induction via reactive oxygen species or DNA damage. The number of viable cells in transformed cell lines, independent from the applied virus variant, stayed more or less the same during treatment and ranged from 88-95 %. Induction of apoptosis did not result in drastic changes of the overall-amount of viable cells in any of the cultures. Evaluation of percentages of FITC-positive cells revealed minor differences between the cell lines transformed with the deletion variant viruses WT(29fDX)Δ16 or WT(29fDX)Δ71, and the WT(29fDX)-transformed cell lines (fig. 19). The results for K39-derived cell lines can be seen in fig. 20.

Preliminary results for K39-derived T cell lines, transformed with different deletion variants of HVS, showed minor changes in the percentage of apoptotic cells. Cells transformed with deletion variant WT(29fDX)Δ16 mostly showed lower percentages than the wild-type transformed control cell line K39 WT(29fDX), while deletion variant WT(29fDX)Δ71 showed a slight increase in the percentage of apoptotic cells. However, results from one experiment with K38-derived cell lines did not support this finding. Time and cell density only allowed for this experiment to be performed once but a conclusive assessment of the induced effects demands at least three repetitions. Preferably the experiment should include more donor cell lines to investigate a possible effect the donor T-cell line might have. In table 27 an overview of means and standard deviations of apoptosis rates within the gated cell population in the different donor lines under specific treatment modalities is given.

Table 27: Mean apoptotic cells in % in K38- and K39- transformed cells 4 and 24 h after induction of apoptosis

		mean ± SD (4 h)*						mean ± SD (24 h)*					
		WT(29fDX)		WT(29fDX)Δ16		WT(29fDX)Δ71		WT(29fDX)		WT(29fDX)Δ16		WT(29fDX)Δ71	
K38	untreated	**5.94**	±0.81	**7.42**	±0.49	**10.92**	±6.21	**4.92**	±0.00	**8.88**	±0.00	**6.75**	±0.00
	200 µM H_2O_2	**5.58**	±0.00	**7.92**	±0.00	**4.7**	±0.00	**5.07**	±0.00	**10.7**	±0.00	**6.35**	±0.00
	6 µM CPT	**4.71**	±0.00	**7.45**	±0.00	**3.83**	±0.00	**5.71**	±0.00	**11.01**	±0.00	**7.46**	±0.00
K39	untreated	**6.73**	±3.28	**5.46**	±1.48	**7.67**	±1.32	**6.79**	±1.22	**4.91**	±0.52	**7.96**	±0.66
	200 µM H_2O_2	**10.8**	±0.00	**9.05**	±0.00	**11.65**	±0.00	**7.93**	±1.61	**6.95**	±0.18	**10.4**	±0.09
	6 µM CPT	**10.0**	±0.00	**6.61**	±0.00	**9.02**	±0.00	**8.92**	±0.27	**7.45**	±1.09	**11.03**	±2.31

* number of experiments for SD > 0: n = 2 and for SD = 0.00: n = 1.

The results presented for K39 cells indicate that induction of apoptosis works with both inductors at both time points, 4 and 24 h after the start of the experiment. For K38-transformed cell lines, induction did not seem to induce apoptosis after 4 h but slight increases were noticeable after 24 h. When comparing the different virus variants used for transformation and their effect on the cell lines' apoptosis response, it was surprising that responses were completely opposite. Since these are only preliminary results, however, this would have to be validated in further experiments.

In K38 transformed cells, the deletion of *ORF16* or *ORF71* seemed to increase spontaneous apoptosis at both time points. After 4 h, the apoptosis rate of K38 WT(29fDX)Δ16 was increased by 2-3 %, compared to K38 WT(29fDX). After 24 h the rate further increased and was found to be 5 % higher than in K38 WT(29fDX). For K38 WT(29fDX)Δ71, after 4 h the apoptosis rate was reduced by approximately 1%, while a slight increase of 1-2 % was observed after 24 h. The trends were consistent for both deletion variants for both inductors.

In K39 transformed cells, however, the deletion variant K39 WT(29fDX)Δ16 had a slightly reduced apoptosis rate after 4 h when compared with the wild-type transformed cell line K39 WT(29fDX). Both, spontaneous (1 % lower) and induced apoptosis rates (H_2O_2: 2 % lower, CPT: 3.5 %) were observed to be diminished. The same was observed after 24 h, where usually a drop of approximately 1-2 % was noted. The *ORF71* deletion variant had the opposite effect, where apoptosis rates were found to be slightly elevated by 1-3 % compared to K39 WT(29fDX). The only exception was the drop in apoptosis rate by 1 % after 4 h.

In summary, apoptosis rates were severely reduced due to transformation compared to non-transduced K38 or K39 cells in accordance with Kraft et al. (1998). Impacts on apoptosis rates were mostly found to be higher after 24 h. Between the differently transformed donor cell lines, distinctions in response to apoptosis-inducing drugs were observed. Though apoptosis could be induced in transformed human T cells, the increase in apoptosis rates was minor. The different deletions seemed to have little impact on the response to apoptosis, compared to cells transformed with the wild-type virus WT(29fDX). For WT(29fDX)Δ16 in K38 cells, an increase of apoptosis was found, while in K39 cells, a decrease was noticed at both time points under all conditions. WT(29fDX)Δ71-transformed cells instead had an increased apoptosis rate compared to WT(29fDX) in both donor lines, at both time points and under all conditions.

3.6 Minimised vectors

Packaging capacity is a limiting factor when it comes to vaccine generation and transgene expression via viral vectors. Four different BAC variants were used as a starting point to analyse the essentiality of ORFs for replication in OMK cells: WTf (miniF sequence in *ORF14*), *eGFP* (miniF sequence in *ORF14*, *eGFP* under control of *StpC/Tip* promoter), and self-repair-enabled BAC WT29fDX and WT22fDR (Heyn, 2015).

Deletions were mainly introduced in the WTf BAC, because reconstitution of deletion variants enabled to self-repair was slower and more laborious. The risk remained to evaluate a deletion essential when only the self-repair was responsible for an unsuccessfully reconstitution. Therefore, all deletion variants were first introduced in WTf BAC. Two master theses centred on the function and homology of *ORF63*, and the directly adjacent *ORF62* and *ORF64*

(Propp, 2015; Werny, 2016). One master thesis evaluated the deletion of ORF16 and ORF71 in the self-repairing virus variants (Zingler, 2015).

All generated deletion variants, based on WTf, with miniF sequence located in *ORF14*, showed the expected band shifts as a result of the deleted ORFs (fig. 21). Green arrows signify changes in band size compared to the WTf BAC, white arrows instead point out changes compared to the direct predecessor BAC. For restriction enzyme digest, SacI and BcuI were chosen. Both enzymes were insensitive to epigenetic modifications of the BAC DNA. All deletion variants, as well as their predecessors, with positive selection marker still integrated, were subjected to restriction enzyme digest with at least two different enzymes and subsequent sequencing spanning the sequence of interest, the deletion site (data not shown). All variants were found to show the correct structure.

Reconstitution of all generated variants was attempted by lipofection into permissive OMK cells. Not all virus variants could be reconstituted. In table 28, a complete list of all generated HVS C488-deletion variants is presented and whether reconstitution of the corresponding viruses in permissive OMK cells proved possible.

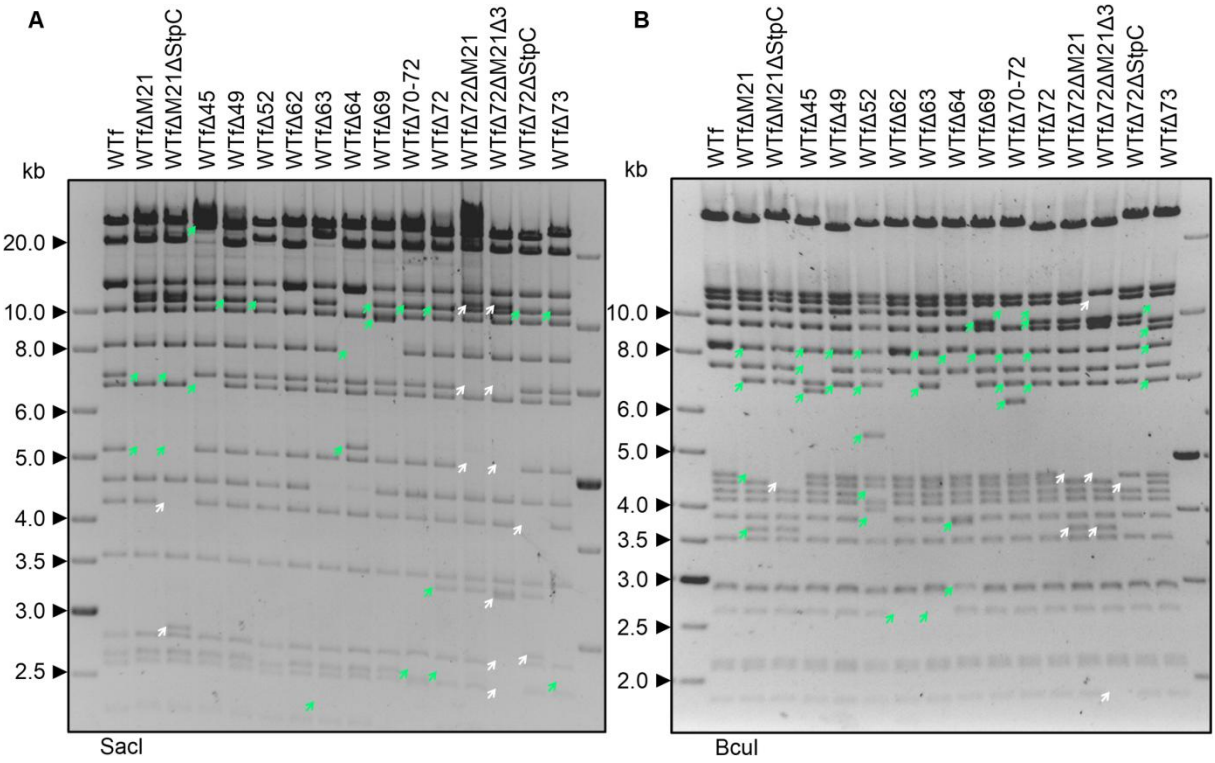

Fig. 21: RFLP analysis of all generated deletion-variants based on HVS C488 WTf. Isolated BAC DNA was cut with restriction enzymes SacI (**A**) or BcuI (**B**) and the resulting fragments were separated during gel electrophoresis at 50 V for 24-26 h on a 0.7 % gel. Grey shades are depicted invertedly. All patterns shown correspond with the expected in silico digest performed using VectorNTI. Arrows in green indicate band shifts compared to the wild-type. When more than one deletion was performed, arrows in white indicate band shifts compared to the predecessor variant (WTfΔM21 or WTfΔ72).

Virus variants which could be successfully reconstituted were subsequently grown to high-titre stocks and used to perform replication kinetics to assess the viral capacity for a productive infection. Lytic replication was measured over time and the viral propagation measured in plaque-forming units per ml (pfu/ml, fig. 7C, fig. 11C, fig. 18B, fig. 22).

Table 28: Complete list of all generated deletion mutants, ability to reconstitute, and source

Designation	BAC	reconstituted virus		source
WT29fDX	yes	yes		Heyn, 2014
WT22fDR	yes	yes		Heyn, 2014
WT22fDRΔ71	yes	yes		Zingler, 2015
WT29fDXΔ71	yes	yes		Zingler, 2015
WT29fDXΔ16	yes	yes		Zingler, 2015
WT29fDXΔ16 Δ71	yes		no	Zingler, 2015
WT29fDXΔ12-14	yes	yes		
WT29fDXΔ3	yes		no	
WT29fDXΔ3 ΔStpC	yes		no	
WT29fDXΔ3 ΔM21	yes	yes		
eGFPΔ75mRFP	yes	yes		
eGFPΔ75mRFPΔ3	yes		no	
WTfΔM21	yes	yes		
WTf ΔM21 ΔStpC	yes	yes		
WTfΔ45	yes		no	
WTfΔ49	yes		no	
WTfΔ52	yes		no	
WTfΔ63	yes		no	Propp, 2015
WTfΔM63	no		no	
WTfΔ62	yes		no	Werny, 2016
WTfΔM62	yes		no	Werny, 2016
WTfΔ64	yes		no	Werny, 2016
WTfΔ69	yes		no	
WTfΔ70-72	yes		no	
WTfΔ72	yes	yes		
WTfΔ72 ΔStpC	yes	yes		
WTfΔ72 ΔM21	yes	yes		
WTfΔ72 ΔM21 Δ3	yes	yes		
WTfΔ73	yes	yes		

The varying wild-type virus variants WT and WTf were shown to replicate similarly and were hence considered equal. Usually viruses with miniF sequence still within the viral genome were compared to WTf virus, while self-repaired virus variants based on the viruses WT29fDX and WT22fDR were compared to a self-repaired version of their predecessor virus. All generated self-repair enabled virus variants were passaged until at least passage nine to ensure the vast majority of virus genomes had lost the miniF sequence.

The replication of all deletion variants compared to the (self-repaired) wild-type (WT, WTf, WT(22fDR), WT(29fDX)) was within the expected fluctuation established for viral infections. Usually, lytic replication was completed after 9 d when infected with an MOI of 0.01 and reached titres between 5x 10^4 and 1x 10^6 pfu/ml.

The deletion of *ORF71* did not show any influence on viral replication in both generated virus variants, WT(22fDR)Δ71 and WT(29fDX)Δ71, as compared to their respective self-repaired predecessor. The same held true for the deletion of *ORF73* from the WTf genome.

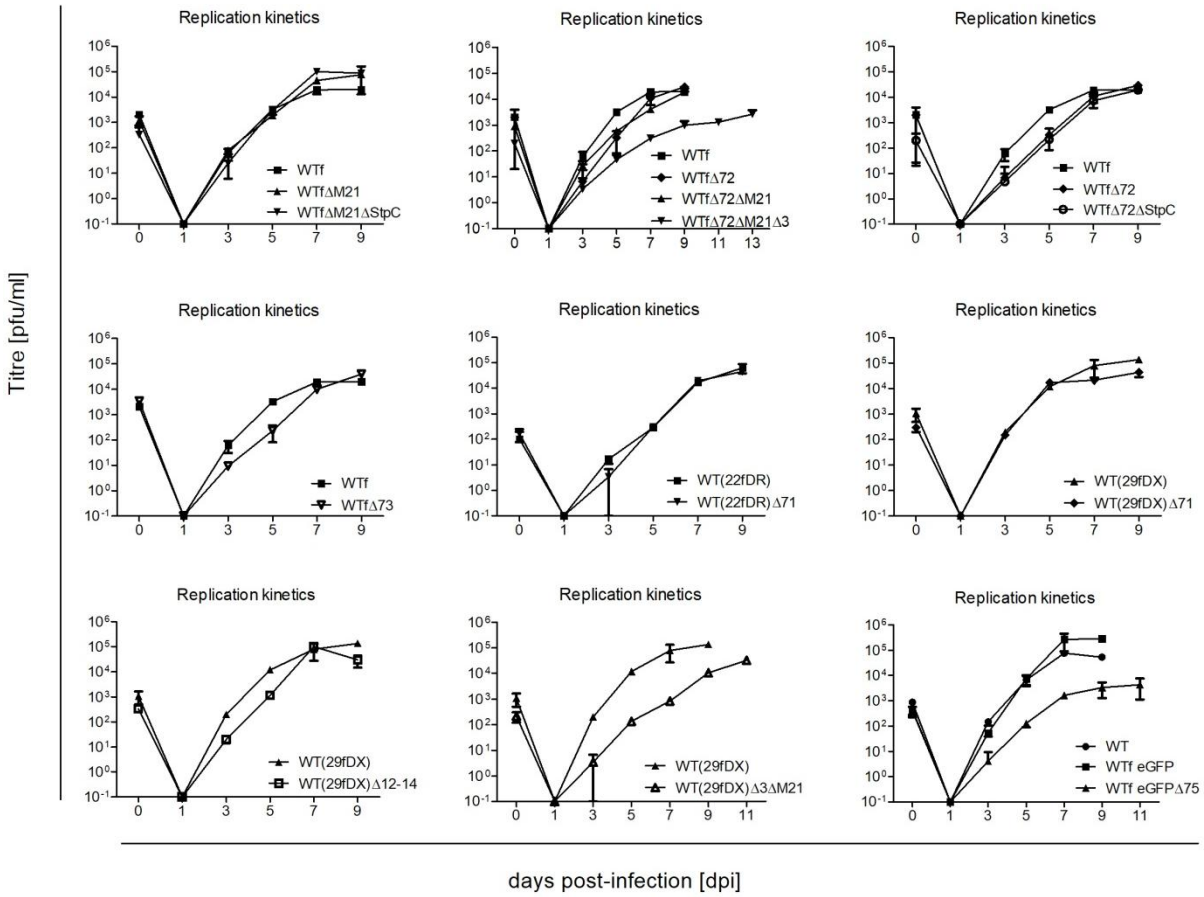

Fig. 22: Representative replication kinetics of all generated deletion variants. OMK cells were infected on d 0 with an MOI of 0.01 and supernatants harvested at indicated time points. Three separate dilutions were prepared for each time point and used to infect OMK cells. The whole supernatant was added for the sample collected 1 dpi. CPEs were counted 4 dpi and titres calculated for each time point. The mean and corresponding standard deviation of triplicates was plotted with GraphPad Prism® 5. Experiments were repeated at least three times and showed comparable results. The exceptions were WT(29fDX)Δ3ΔM21, WT(29fDX)Δ12-14, and WTfΔ72ΔM21Δ3 which were only performed once. All WT29fDX or WT22fDR variants were used in passage 10 and had lost the miniF sequence as indicated by brackets.

Relevant differences concerning the lytic replication of neither WTfΔM21 nor its successor virus variant WTfΔM21ΔStpC when compared to WTf were not found (fig. 22). The same is true for WTfΔ72 and the successor virus variants WTfΔ72ΔStpC and WTfΔ72ΔM21. However, the additional deletion of *ORF3* in WTfΔ72ΔM21 lead to a replication delayed by 4 d and resulted in a reduced titre when lytic lysis was completed. The reduction was approxi-

mately one log phase. A similar delay in replication by 2 d and a reduction of viral propagation of approximately one log phase was seen in the virus variant WT(29fDX)Δ3ΔM21, compared to WT(29fDX).

Replacing *ORF75* with the *mRFP* expression cassette in virus variant WTf eGFPΔ75 had a similar effect on viral replication. The complete lysis of the OMK cell monolayer was reached 2 d later than in WTf virus and the direct predecessor virus WTf eGFP, respectively. Both, *ORF3* and *ORF75* encode variants of the viral protein formyl-glycinamide phosphoribosylamidotransferase (FGARAT).

Kinetics of viruses having either *ORF3* or *ORF75* deleted proved the slower replication, and a longer time period was needed to complete lysis at considerably lower titres compared to their predecessor virus variants or the wild-type (fig. 22). Expression of mRFP under *ORF75* promoter was well visible in infected OMK cells, while expression of eGFP under *StpC/Tip* promoter was weak to non-existent.

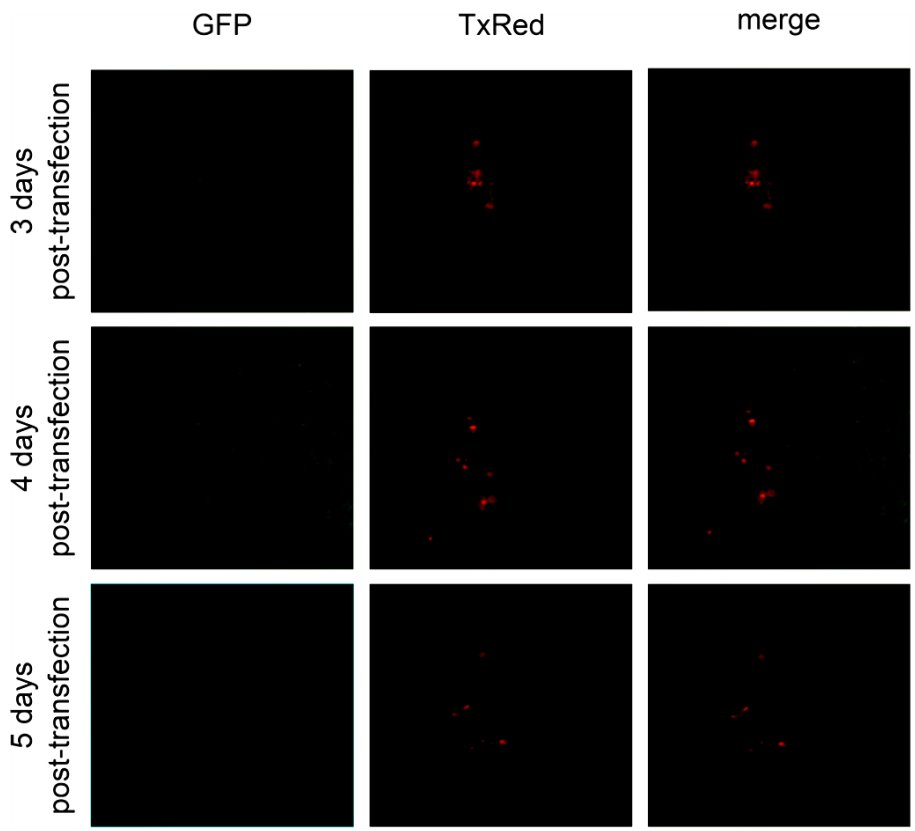

Fig. 23: Fluorescence imaging of WTf eGFPΔ75Δ3 transfected OMK cells. Permissive OMK cells were transfected with isolated BAC DNA of WTf eGFPΔ75Δ3. Expression of eGFP was very weak since it was controlled by the *StpC/Tip* promoter. Expression of mRFP under control of *ORF75* promoter was observed after d 1, very small CPEs were visible from d 3 on but did not expand over time like they do in the wild-type infection.

OMK cells transfected with the double-deletion variant WTf eGFPΔ75Δ3 expressed mRFP and proved that the transfection procedure worked (fig. 23). Nevertheless, spread of the infection through the monolayer could not be observed although CPEs were seen. Via live-cell

imaging over 5 d, the varying expression levels of mRFP could be documented over time by the change in intensity. The total number of mRFP expressing cells and CPEs, respectively, stayed the same. The virus did not spread further than the initially transfected cell(s) that were giving an mRFP signal. The fluorescence signal was not observable any longer at the latest 14 d post-transfection. Further cultivation of the transfected cells did not yield new CPEs or fluorescent signals and supernatant transferred to fresh OMK cultures did not lead to infection in those cells.

In summary, the loss of both viral FGARAT seems to severely impair viral replication and the deletion of the ORFs coding for it was not tolerated. Deletion of one ORF decelerated replication by 2-4 d and the titres were found to be at least one order of magnitude lower than the titres of the wild-type virus.

4. Discussion

4.1 Copy numbers of virus genomes in transformed T cells

An average copy number between 40 and 300 copies per cell was found to persist within transformed human T cells. These findings endorse previously published numbers of 50 to 300 copies (Biesinger et al., 1992). Here, an *ORF9*-specific real-time PCR was used for the direct semi-quantitation of HVS copy numbers in transformed human T cells. The established system is simple and convenient.

It is applicable as well in infected permissive OMK cells, however, an alternative to human *GAPDH* in OMK cells would be needed for semi-quantitation. Up to date, the cellular genome of owl monkeys (*Aotus trivirgatus*) is not yet available, *e.g.,* in the data base of the National Center for Biotechnology Information (NCBI). The gene for hypoxanthine-guanine phosphoribosyltransferase might be an alternative, since it was shown to be expressed similarly in transformed and non-transformed human T cells, and was commonly used as a control, although recent studies suggest a higher variability in gene expression in malignant tissues (Tamgüney et al., 2004; Panina et al., 2018; Townsend et al., 2019). A housekeeping gene which is suitable to normalise gene expression against in not only transformed and non-transformed human T cells but also productively infected cells of all varieties and species would be preferable. However, not many genes have been identified to stay stably expressed between non-transformed and transformed T cells, apart from the genes for hypoxanthine-guanine phosphoribosyltransferase and ribosomal protein 9 (Tamgüney et al., 2004).

4.2 Expression of a human γδ T-cell receptor in transformed T cells

The artificial expression of a γδ TCR in mature human T cells was not accomplished with the two generated HVS C488 variants WTf γδTCR and WTf Vδ2SL3Vγ9. The different virus variants carrying the genes for Vγ9 and Vδ2 were successfully established and proven to replicate similarly to the wild-type virus HVS C488 WTf. Different human donor T cell lines (K38, K39, K40, and K41) were transduced with both virus variants and the wild-type WTf in five separate experimental transductions. Simultaneously, the same virus was used to transduce more than one cell line (K38: n = 2, K39: n = 3, K40 n = 3, K41 n = 1). The wild-type WTf was reliably successful in transforming the donor cells in all five experiments in all donor cell lines. For the virus variants carrying the Vγ9 and Vδ2 chains, only three cell lines in total were found to be successfully transformed by HVS: K39 and K41 WTf γδTCR, and K41 WTf Vδ2SL3Vγ9, resulting in fairly low transformation efficiencies of 22 % (WTf γδTCR) and 11 % (WTf Vδ2SL3Vγ9).

Transcription of Vδ2 chain was mostly limited to either of the γδ TCR vector variants but a weak signal was also found in K41 WTf 15 mpt, while none was seen for K41 WTF γδTCR

any longer at that time point (fig. 8). This result is not surprising, as usually 2-5% of the non-transformed, freshly isolated T cells from donors K39, K40 and K41 carry the γδ TCR (for K39 see fig. 9C; for K38, K40 and K41 data not shown but similar). Thus, it was expected that some of the donors' own γδ T cells would be transformed or at least survive for some time within the transduced cell culture. These cells were most likely responsible for the positive RT-PCR signals seen in WTf transformed cells, although it is interesting, that the cells could not be detected unambiguously via flow cytometry. It might be that this small population of cells did not express the receptor chains on their surface although the genes were transcribed, or that the expressed TCRs were too few to be detected reliably. Sensitivity of the RT-PCR is generally high, while the sensitivity of flow cytometry is affected by the quantity of the structure to be detected, too. If the total number of the receptors on the cell surface is low, detection of the cell is aggravated. Transcription of Vγ9 was detected at all times for all variants including non-transduced cells. An exception were all cell lines 15 mpt, when only the -RT control seemed to be positive for Vγ9. This result argues for a DNA contamination. Similar results for transcription were gained from human T cells transformed with the transgene-expression vector virus variant WTf IRES carrying a murine chimeric receptor under control of the *StpC/Tip* promoter. The virus was included as a second control and in transformed human T cells the transcription of this receptor proved stable over 48 mpt (Bremer 2014, data not shown).

Drastically differing copy numbers might also have an effect on transcription, therefore, the average copy numbers per cell were determined whenever cell density allowed it (table 22). The donor lines K39 and K41 which were successfully transformed with the different virus variants, showed average copy numbers per cell ranging from 41 to 142 copies, with WTf-transformed cell lines always showing lower copy numbers (K39 WTf 72 copies/cell, K41 WTf 41 copies/cells) than the TCR variants (K39 WTF γδTCR 142 copies/cell, K41 WTF γδTCR 86 copies and K41 WTF Vδ2SL3Vγ9 91 copies/cell). Thus, a small quantity of copy numbers per cell was excluded as a reason for low transcriptional activity in transformed cells. Furthermore, all cells were transduced with an MOI of 3 but now carried a much higher average copy number per cell, indicating replication of the episomal viral genomes as is usual for human T cells transformed with HVS strain C488 (Fickenscher et al., 1997). Supernatants of transformed human T cells did not prove infectious for HVS permissive OMK cells, hence, the possibility of productive infection within the T cells was excluded, endorsing previously published studies (Calderwood et al., 2004b; Weber et al., 1993).

Enhanced expression of the γ and δ chains could not be observed during 38 months of monitoring. The assessed cell lines K39 WTf and K39 WTf γδTCR at 38 mpt proved almost exclusively positive for αβ TCR with 96% and 99 %, respectively, while expression of either Vγ9 or Vδ2 were below 1 % and within the same range as the control for non-specific binding of the

secondary antibody. CD3 expression was retained by the transformed cell lines K39 WTf with 97 %, and WTf γδTCR with 80 % CD3-positive cells in accordance with previously published studies (Bröker et al., 1993; Fickenscher et al., 1997).

In contrast to the efficient transcription of a murine chimeric T-cell receptor, the coexpression of the pre-existing phenotypic TCR and the artificial Vγ9Vδ2 TCR was not feasible. This is somewhat surprising, since double-positive T cells were recently reported in humans and mice, carrying both, αβ and γδ TCR, termed αβ-γδ T cells. These newly found cells amounted to less than 1 % of peripheral blood mononuclear cells (Edwards et al., 2020). Consequently, coexpression of both receptors is physiologically possible and the lacking transcription observed in our experiments might simply be due to insufficient activation in human T cells under the *SL3* and *StpC/Tip* promoters. For further experiments, a human TCR gene promoter, *e.g.,* the Vbeta6.7 promoter, might be useful (Deng et al., 1998).

However, extensive functional testing would be necessary with such transformed cells, should artificial expression of the Vγ9Vδ2 TCR by a HVS vector in mature T cells prove successful eventually. The previously mentioned double positive αβ-γδ T cells were reported to express a hyperinflammatory phenotype, on the one hand able to protect against a *Staphylococcus aureus* infection, on the other hand able to trigger autoimmune pathology in the central nervous system in mice. In human peripheral blood mononuclear cells, 10 % of the CD3-positive αβ-γδ T cells were found to be Vδ2-positive (Edwards et al., 2020). After activation by phosphoantigens the Vγ9Vδ2 T-cell is usually associated with a Th1 profile subset and low production of interleukin-17, while dermal γδ-positive cells, mostly Vδ1-positive cells, were found to be able to produce high interleukin-17 levels and probably initiate and drive autoimmune responses (Eberl et al., 2003; Hintz et al., 2001; Shiromizu & Jancic, 2018). However, the Vγ9Vδ2 T-cell subset was also reported to be recruited into inflamed skin tissues psoriasis patients (Laggner et al., 2011). It is for these reasons, that antigen redirection and artificial increase of γδ T cells has to be exhaustively evaluated with regard to adverse events.

In conclusion, the evidence gained by this experiment suggests that the cells were transformed successfully but transcription of the human Vδ2 and Vγ9 genes from the episomal HVS-vector was neither reliable nor long-lasting.

4.3 Reporter vector variants

Five reporter vector variant BACs were established successfully. Three were based on the BAC WTf eGFP and express eGFP and mRFP in parallel, the other two are self-repair enabled upon reconstitution and were only modified to carry the *mRFP* gene. Only three of those five variants proved reconstitutable and two of them were studied in human T cells to analyse long-term transgene expression.

Expression of mRFP in permissive OMK cells was achieved under control of *ORF75*, SL3*,* and HTLV promoters. The murine retrovirus-derived SL3 promoter seemed to induce a stronger expression in these primate cells, than the HVS *ORF75* promoter did. The expression of mRFP in OMK cells under the HTLV promoter could only be evaluated with a virus variant with WT29fDX backbone, since the virus variant WTf eGFPHTLV was not reconstituting, although transfection was successful. Nevertheless, mRFP expression in OMK cells infected with WT29fDXHTLV subjectively seemed equally strong as expression under SL3 promoter in WTf eGFPSL3 infected cells.

The transcription in transduced human T cells of different donors was furthermore assessed over time under the same experimental settings in order to achieve comparable results. Total RNA was reverse-transcribed into cDNA and subjected to PCR analysis. The cellular control *GAPDH* was reliably positive, although samples without RT were found to have residual DNA contaminants giving weak signals, too. *ORF75* was used as a viral control. This ORF is known to be actively transcribed in human transformed T cells (Toptan, 2010). Additionally, since *ORF75* was deleted in WTfeGFP∆75 variant-transformed cell lines, *Tip* was included as a second viral control, although its expression is much lower than that of *ORF75* and a more sensitive polymerase had to be used for its detection (Fickenscher *&* Fleckenstein, 2001). Digestion with DNaseI did not always result in removal of all DNA contaminants but when both samples indicated positive PCR results, the strength of the bands without RT was generally weaker than the signals with RT. Non-successful removal of DNA might be related to higher copy numbers in those isolates, resulting in much higher transcription levels. As expected, *ORF75* transcription was not detectable in all *ORF75*-deletion variant-transformed cell lines.

The results suggest that transcription of *eGFP* from *StpC/Tip* promoter is rather weak. Often the bands were faint and almost imperceptible. Transcription under *ORF75* promoter is weak, too. Transcription was mostly steady, although sometimes no transcripts were detected under its control, especially in K39-derived cell lines. The SL3 promoter was found to reliably induce transcription, although at varying levels.

Furthermore, compared to bands derived from the WTf eGFP∆75 transformed cell line at the same time point, the transcript levels of mRFP always seemed to be higher. The transcription levels differed depending on the donor line. Cell lines derived from donor K39 showed lower (or no) expression of eGFP and mRFP compared to K40-derived transformed cell lines at the same time point (fig. 12).

Expression of mRFP was compared to expression of eGFP in order to gain a first impression of the continuity of transgene expression under the respective promoter and the strength compared to *StpC/Tip* promoter. Transcription of the bicistronic product under the *StpC/Tip*

promoter und subsequent expression of the viral proteins StpC and Tip was previously described as strong in transduced human T cells (Fickenscher et al. 1996; Medveczky et al. 1993). Fluorescence microscopy photographs regularly taken confirm the transcription results. In general, stronger signals of both fluorophores were only observed in viable T cells that formed aggregates. The bigger the aggregate, the better the detected signal. Weak fluorophore signals could be noted in cells accumulating at high density at the bottom edge of the culture flask. The expression of eGFP was subjectively stronger in WTf eGFPΔ75 transformed cell lines, while mRFP expression was higher in WTf eGFPSL3 transformed cell lines and was also visible earlier in most cell lines transformed with the virus. Unfortunately, a direct comparison of both virus variants and their fluorophore expression in human T cells was only possible for the transduction from 0717 in K40 donor cells.

In order to validate the amount of cells expressing eGFP and mRFP, flow cytometry was performed. As expected, the mRFP signal was too weak to be detected with our FACS® Canto. Thus, the percentages of eGFP expressing cells were evaluated. Additionally, a CD3 staining was added to estimate the amount of viable CD3 positive T cells in culture.

Gating ensured that only viable cells were analysed for this experiment and the results demonstrated that different levels of eGFP were expressed. The weak autofluorescence of transformed human T cells was accounted for by using WTf-transformed cell lines as a negative control during compensation. In the density plots, a shift towards the right on the FITC-A axis was observed in cell lines transformed with a reporter virus variant but not in the wild-type transformed cell lines (fig. 14). At 38 mpt no shift could be observed in the unstained populations of K39 WTf eGFPΔ75 but in the CD3-positive cell population a small fraction was demonstrated to express eGFP (fig. 14). Histogram results suggested as well that the remaining reporter cell lines had eGFP expression in all cells at varying levels, since the population as a whole shifted to the right and no subpopulations were observed (data not shown). Meanwhile, CD3 staining confirmed that 100% of all cell lines were still carrying CD3 at 34 and 38 months after transduction with the HVS variants.

With the chosen parameters, it was demonstrated that the number of eGFP-expressing cells within the exact same cell lines fluctuated over the course of time. Percentages also varied between cell lines derived from different donors, yet transformed with the same virus (0117 and 0717, K39 or K40 WTf eGFPΔ75) in the range from 0- 40 % eGFP-positive (FITC) cells (fig. 24). No clear trend was observed, although expression of eGFP seemed to stabilise at approximately 10 % of the cells expressing eGFP. Quadrants were chosen very conservatively, though, and it is likely the actual percentage of eGFP-positive (FITC) cells was underestimated. Flow cytometry also confirmed the comparatively weak expression of eGFP be-

cause clear shifts in the population, as obtainable by antibody staining for example, were not reached.

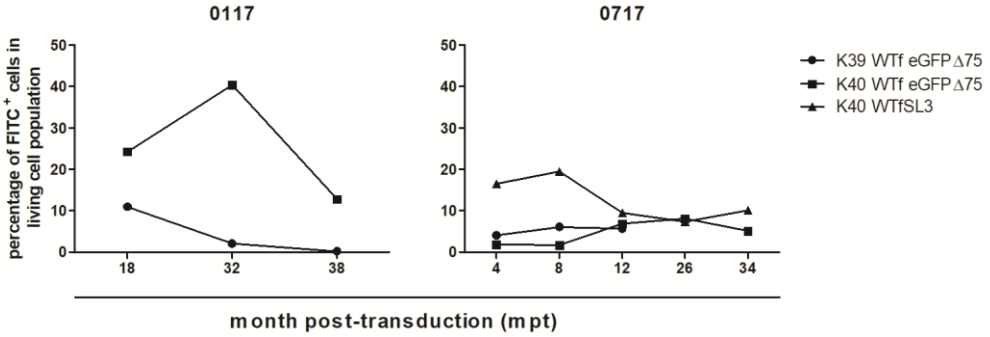

Fig. 24: Fluctuation of percentages of FITC-positive cells of living transformed cell lines over time. Human donor cells (K39 or K40) were transformed at different time points (0117, 0717) with indicated virus variants and the surviving cell lines were monitored via flow cytometry for eGFP expression using the FITC filter. The percentages of cells expressing eGFP were plotted against the time after initial transduction.

Taken together, the results suggest a successful transformation with not only the wild-type virus but also modified virus variants is possible for at least four years. The stably transformed T cells were found to have comparably weak transgene expression under *StpC/Tip* promoter in viable HVS transformed cells. The mRFP expression could not be monitored via flow cytometry but evidence from fluorescence microscopy suggested that the murine retrovirus SL3 promoter was stronger than the HVS *ORF75* promoter and better suited for long-term expression. The average copy number suggested abortive, non-productive episomal genome replication of HVS within transformed human T cells but did not exceed the average 300 copies per cell, matching the numbers routinely found in the the last five decades of research.

In the future, the experiment should be repeated with a flow cytometer with an appropriate filter to monitor mRFP-expression as well. Real-time PCR to quantify *mRFP* and *eGFP* transcription would be helpful as well. It would be beneficial to include more donor cell lines, ideally freshly isolated, and the self-repaired reporter virus variants. With a consistent microscope set-up, the quantitation of expression would also be conceivable.

4.4 Minimised vectors and self-repairing viruses

The generation of a minimised variant of HVS for use as a potential gene therapy vector has long been discussed and aimed at (Grassmann & Fleckenstein, 1989; Stevenson et al., 1999). Data collection revealed that many ORFs were already reported to be non-essential for viral replication in OMK cells, so the most likely candidates were targeted in the deletion strategy with hopes of a reduced pathogenicity. The aim was to generate one minimised vector virus variant with transforming genes *StpC/Tip,* and one without them. The single deletion approach was preferred, although deletion of multiple ORFs at once was also performed.

Deletions that proved essential for viral reconstitution

Not all deletion variants generated could be reconstituted successfully, for example, the double deletion of *ORF16* and *ORF71* proved lethal for virus replication, double deletion of *ORF75* and *ORF3* was not tolerated, deletion of the single *ORFs 45, 49, 52, 62, 63, 64, 69*, and the deletion of *ORF70-72* resulted in total loss of viral replication. Since reconstitution of the self-repairing BACs was more demanding and time consuming than the reconstitution of WTf-based BACs, first deletion variants based on the WTf BAC were generated to identify which deletions could be combined. At a later time point, the successful combinations were aimed to be collected in a self-repairing virus variant. To gain insight into putative functions of unidentified HVS proteins, their amino acid sequences were compared to homologues of other rhadinoviruses (fig. 1) such as murid herpesvirus 4 (MuHV-4, also known as Murine herpesvirus 68, MHV-68), Kaposi's sarcoma herpesvirus (KSHV), or Rhesus monkey rhadinovirus (RRV).

ORF45: Information is not yet available on the function of ORF45 in HVS viral replication. For KSHV it is known to serve as a regulatory function by binding KSHV ORF33, regulating virus progeny and ubiquitin-specific peptidase 7 (Gillen et al., 2015). However, according to NCBI blast, the protein identity (query coverage) of the two viral proteins is low (23 %), only the C- and N-termini seem to align but lead to an identity percentage of 52.17 % (E value = 1 e^{-6}). It is possible that the function was conserved over the two virus species and the function of ORF45 is in the promotion of lytic replication. The notion was supported by the role ORF45 plays in rhesus rhadinovirus lytic infection. Although it is not required for replication in this rhadinovirus, it is reported to be essential for KSHV replication, and apparently also for HVS replication (Gillen et al., 2015; Woodson et al., 2014).

ORF49: The deletion of *ORF49* resulted in the loss of viral replication. The function of HVS ORF49 is of yet unknown but in the distant relative KSHV, *ORF49* codes for the immediate-early (IE) transactivator Rta, known to interact amongst others with *ORF50* (Gonzalez et al., 2006; Whitehouse et al., 1997). HVS *ORF50* encodes the R protein and is suggested to be a transactivator of delayed-early *ORF6*, a part of major DNA binding protein, and of ORF57, another regulator of initiation of lytic replication (Schäfer, et al., 2003; Thurau et al., 2000; Whitehouse et al., 1997). In HVS strain A11, HVS *ORF49* and *ORF50* are transcribed reversely of each other and overlap, however, they do not do so in strain C488. The A11 ORF49 protein sequence and that of strain C488 shared a query coverage of 100 %, with an identity percentage of 94.7 % (E value = 0.00). It therefore might well be that deletion of HVS *ORF49* leads to an abortion in immediate-early gene transcription during replication.

ORF52: Not much is known about ORF52 in HVS or other closely related herpesviruses. In the more distantly related gammaherpesvirus MHV-68, *ORF52* codes for a tegument protein

involved in the viral envelopment and egress (Bortz et al., 2003). Query coverage for the two predicted protein sequences is 86 %, with an identity percentage of 42.16 % (E value =1e^{-20}). Similarly to MHV-68 ORF52, HVS C488 ORF52 seems to be essential for viral replication.

Deletion of *ORF62, ORF63, and ORF64:* The deletion of the putative NOD-like receptor homologue encoding *ORF63* proved to generate a non-replicating virus variant and was unable to be reconstituted in permissive OMK cells (Propp, 2015). However, it is as of yet unclear whether the effect is due to a crucial role the ORF63 protein plays in viral cell infection, or because the neighbouring *ORF62* and *ORF64* were influenced, since transcription for both ORFs starts within *ORF63* (Thies, 2016). Single deletion virus variants of both, *ORF62* and *64,* were generated and proved equally transfectable as *ORF63* deletion variant but did not result in infection (Werny, 2017). At least *ORF64* is, therefore, evidentially essential for viral replication. More likely, however, is that all three of them are essential. Unfortunately, these suspicions could not be confirmed, since the creation of a deletion variant leaving 500 bp of the C- and N-terminal sequences, respectively, intact failed. Four different operators attempted the deletions and various approaches were used to improve recombination efficiency (prolonged homologous region to the insert locus by PCR or by a generated transfer vector) but to no avail. Similarly, the generation of a virus variant with a single point mutation within *ORF63,* altering the base triplet to encode a termination signal in the central protein region could not be generated.

These three ORFs are densely packed and transcriptionally interwoven. Former studies found *ORF62* to probably code for a capsid assembly and maturation protein, and *ORF64* for a large tegument protein. It is highly likely that all three ORFs are expressed during late stage of infection and are probably involved in packaging of new virions, since the slightest change of sequence in either ORF lead to an abortive infection (Propp, 2015; Thies, 2016; Werny 2017).

ORF69: The putative function of ORF69 for the gamma herpesviruses RRV, KSHV, MHV-68, or HVS is unknown. MHV-68 and HVS C488 *ORF69* share 41.38 % identity while the query coverage amounts 97 % (E value = 5 e^{-70}). Between RRV and HVS A11, ORF69 protein sequences have 57.5 % identity and 49 % query coverage (Searles et al., 1999). From its location it is highly likely that it belongs to the late genes as well and might serve in packaging or as a tegument protein.

***ORF70* and origin of lytic replication.** The deletion of *ORFs 70-72* was expected to cause abortive infection, since it was previously published that the origin of lytic replication of HVS is located upstream of *ORF70*, which is transcribed from the reverse strand. By deleting the combination of ORFs, the origin of lytic replication was also lost. Furthermore, *ORF70*, coding for the cell-homologous thymidylate synthase, was previously published as essential for

virus replication (Honess et al., 1982; Nicholas et al., 1990). It was reported to exert functions in dMTP synthesis, DNA replication and repair and belongs to the late viral genes. Singularly, the *ORF71* and *ORF72* can be deleted without ramifications for viral replication. The triple deletion variant *ORF71-73* could not be generated via *en passant* mutagenesis, despite various attempts in various vector backbones (WTf, n = 6; WTf eGFP, n = 3; WT29fDX, n = 4).

Deletion of non-essential ORFs for viral replication

Apoptosis relevant *ORF16* and *ORF71:* Single deletion of either *ORF16* or *ORF71* is well tolerated to retain normal viral replication, transforming capacity and persistence in human T cells (Stevenson et al., 1999; Zingler, 2015). However, the deletion of both ORFs lead to an abortive infection of the double-deletion, self-repaired HVS variant WT(29fDX)Δ16Δ71 (Zingler, 2015). Similarly to the cellular homologue, vBcl2 was reported to protect HVS-infected cells from virus-induced apoptosis (Nava et al., 1997). The BH1 and BH2 domains were presented as highly conserved over the gammaherpesvirus subfamily and, thus, possibly important in the viral life cycle. Usually, cleavage of cellular Bcl-2 by caspase 3 leads to a loss of its anti-apoptotic function and was even suggested to exhibit proapoptotic properties instead. However, HVS vBcl-2 was found to be protected from this cleavage (Bellows et al., 2000).

After initial problems with the reconstitution of the virus variant WT29fDXΔ16, the deletion of *ORF16's* BH1 domain alone was found to be equally well tolerated with regard to replication competence (data not shown), as the complete deletion of this interaction partner of Bcl-2 family proteins, Bax and Bak (Nava et al., 1997). HVS *ORF16* was furthermore reported to be a suitable locus for insertion of transgenes, when a reporter gene cassette coding for *β-galactosidase* was inserted and viral replication was unimpeded (Stevenson et al., 1999).

ORF71 codes for the vFLIP, a homologue to anti-apoptotic cellular FLIP. The deletion of the two death effector domains (DED) of vFLIP/ORF71 sequence was reported to show anti-apoptotic properties in infected OMK cells but not in transformed T cells (Glykofrydes et al., 2000). Viral replication was not impaired due to partial or complete deletion of the vFLIP (Glykofrydes et al., 2000; Zingler, 2015). Both, wild-type and *ORF71*-deletion variant virus, lead to stably transformed cottontop tamarin T cells (*Saguinus oedipus*) still expressing the death receptor FAS/CD95 on their surface. Transcription of the tricistronically transcribed product *ORF73-71* (reverse strand) was shown in infected OMK cells, as well as in transformed human and simian T cells. However, expression of vFLIP in transformed human T cells was not observed (Glykofrydes et al., 2000). These results contradicted a previous study that reported neither expression nor transcription of apoptosis-relevant genes *vFLIP/ORF71* and *vBcl-2/ORF16* in transformed human T cells but only in cells were the vi-

rus could establish productive infection, specifically excluding human T cells (Kraft et al., 1998).

The complete deletion of both ORFs from self-repairing HVS vectors did not alter the capacity to replicate in OMK cells, nor did it impair transformation capacity for human T cells in accordance with previous reports (Glykofrydes et al., 2000, Kraft et al., 1998; Nava et al., 1997). The preliminary results from this study suggest stable and long-term transformation of human T cells over years and a remarkable protection from apoptosis due to transformation with HVS C488 compared to non-transduced cells of the same donor or Jurkat cells (data not shown). Compared to non-transduced cells, the cells transformed with either WT(29fDX), WT(29fDX)Δ16, or WT(29fDX)Δ71 had a severely reduced risk to be sent into apoptosis when apoptosis was induced with reactive oxygen species or a topoisomerase inhibitor. In two different donors, a slight increase in apoptosis rates was observed for WT(29fDX)Δ71-transformed cells, compared to WT(29fDX)-transformed cells, indicating, if at all, a minor role in the anti-apoptotic regulation in transformed T cells. The results differed for WT(29fDX)Δ16 transformed cells between two different donor cell lines and further experiments are required to validate those findings. The only consistency constituted the minor change in apoptosis rates, observed as a result of the deletion of *vBcl-2* in transformed human T cells to apoptotic stress.

Ideally, the experiments should be repeated with additional donor T-cell lines and longer induction periods, including more time points of measurement. Although close to 100% of non-transduced donor cells were apoptotic after 24 h, the change in apoptosis rate in transformed T cells was minor but might increase if the incubation time is increased and lead to more conclusive results. However, the changes observed so far were minor and it might equally well be that a deletion of either ORF does not have a crucial influence on apoptosis in transformed T cells.

***ORF3, ORF75,* and *ORF70* encoding proteins involved in purine metabolism:** It is a common principle in biology to establish redundancies of important genes within genomes. An example for this principle seems to be the expression of vFGARAT from HVS *ORF3* and *ORF75*. Previous reports that single-deletion virus variants of either ORF reach full lysis of the cell monolayer 2-6 d later and end with much lower titres compared to the wild-type virus could be confirmed by the results gained (fig. 22; Full et al., 2012). However, both ORFs differ in their sequence and were found to deploy different functions.

The central domain of *ORF3* was reported to interact with nuclear domain 10, a part of the host cells' intrinsic immunity against viral infections. It was also demonstrated to lead to depletion of Sp100, one of the proteins the nuclear domain 10 is composed of (Full et al., 2012). Nuclear domain 10 has been reported in the nucleoli of mammalian cells as a subnu-

clear structure with high dynamic concerning their protein composition and was suggested to be involved in major regulatory processes, such as apoptosis, transcription regulation, oncogenesis, and antiviral defence (Full et al., 2017). Composition of nuclear domain 10 (alternatively promyelocytic leukemia nuclear bodies, or promyelocytic leukemia oncogenic domains) is made up mainly by the already mentioned Sp100, and furthermore by ATRX, hDaxx, and PML (also known as TRIM19) (Tavalai & Stamminger, 2009). Other herpesviral proteins were found to target other components of nuclear domain 10 and severely interfere with the cellular ability to keep viral infections in check, or even to be able to turn the host cells' intrinsic immunity against itself. Productivity of viral replication or of long-term latency was found to be dependent on nuclear domain 10's presence and/or integrity. This was not only reported for the herpesviruses HSV, Epstein-Barr virus, KSHV but also for adenoviruses and papillomaviruses (Fada et al., 2021).

The vFGARAT is unlikely to mimic its cellular homologue, the enzyme phosphoribosyl-formyl glycinamidine synthase, which is involved in purine-metabolism. All gammaherpesviruses were reported to have at least one viral homologue for this cellular enzyme but lack its ATP-binding site, and several viral N-terminal domains differ from cellular protein while being homologous to each other (Fada et al., 2021, Full et al., 2012). For most gammaherpesviruses the vFGARAT was demonstrated to play an important role in disabling the host cells antiviral defence, and is furthermore suggested to give structural integrity to the virions (Full et al., 2017; Tsai et al., 2015). Thus, double deletion of both ORFs encoding for the protein lead to an abortive infection.

For these reasons, the deletion of either ORF can be considered a step into the generation of a safer HVS vector for transgene expression. Moreover, the results indicate long-term transgene expression under control of the *ORF75* promoter is stable and comparatively low. The quantitation of transcripts would be the next logical step in characterising the *ORF75* promoter to determine suitable transgenes possibly expressed by a HVS vector.

ORF72: HVS *ORF72* encodes for a viral cyclin D, a homologue most likely derived from the host's genome at one point during co-evolution. Deletion of *ORF72* is without consequences for viral replication in OMK cells and was reported to have no effect on transformation of human T cells (Ensser et al., 2001). The ORF was therefore a prime candidate to generate insert capacity for transgenes by deletion. For viral replication, the further deletion of the central sequence of *ORF21* (900 bp) was tolerated equally well as the additional deletion of *StpC/Tip*. The triple deletion virus variant WTfΔ72ΔM21Δ3 suffered from the replication impairments already established due to the *ORF3* deletion.

ORF21: *ORF21* is highly conserved over the herpesviruses and encodes for the viral thymidine kinase. The activity of the cellular thymidine kinase is usually observed during G_1-

to S-phase or whenever replication processes are initiated. Its function is the phosphorylation of deoxythymidine to deoxythymidine monophosphate. For gammaherpesviruses, the viral thymidine kinase was reported to have a conserved C-terminal kinase activity while the N-terminus is speculated to serve a yet undetermined additional function (Gill et al., 2005). The generated virus variants had a deleted central sequence of 0.9 kb (GenBank: AJ410493.1, *ORF21* c.318-1218 bp), since the promoters for *ORF19* (virion tegument protein, transcribed from reverse strand) and *ORF22* (gH) were very likely located in the 5' and 3' sequences of *ORF21*.

Although the ATP-binding domain was possibly still present in the generated viruses, the function of the viral thymidine kinase is nonetheless almost certainly disrupted by the implemented deletion, since all five of the conserved putative catalytic domains identified by alignment, including the putative nucleotide binding site were eradicated (Brunnemann, 2016; Cannon et al., 1999). So far, an *ORF21*-deletion variant has not been reported for HVS C488. The deletion of the central part of this ORF did not affect the replication in OMK cells, even combined with further deletions in the same vector (*StpC/Tip or ORF72*). Removal of the viral thymidine kinase is usually associated with reduced pathogenicity. It remains to be seen how, and if, the deletion results in differences in the growth or phenotype of transformed human T cells.

For alphaherpesviruses, the thymidine kinase was reported to be non-essential but its removal lead to attenuated viruses less virulent than their thymidine-kinase competent counterparts (Xie et al., 2019). While HSV thymidine kinase was reported to recognise and phosphorylate a broader spectrum of substrates, gammaherpesviral thymidine kinases seemed to be rather specific in their targeting of deoxythymidine (Gill et al., 2005; Honess et al., 1982). For MHV-68, a deletion of thymidine kinase did not affect the viral replication *in vitro* but lead to attenuation *in vivo* (Coleman et al., 2003). Given the enzymes role during genome replication, it might be that viral copy numbers per cell of human T cells transformed with a thymidine kinase-deletion variant virus might be lower than in wild-type transformed cells.

The difference of thymidine kinases of alpha- and gamma-herpesviruses became even more pronounced when a suicide gene system was established by replacing HVS thymidine kinase with its homologue from HSV-1 (Hiller et al., 2000a; Hiller et al., 2000b). *In vitro* experiments were initially promising when efficient elimination of tamarin (*Saguinus oedipus*) and human T cells, transformed with an HVS virus carrying the HSV-thymidine kinase, was achieved using low concentrations of ganciclovir (Hiller et al., 2000a). However, *in vivo* experiments in common marmosets (*Callithrix jacchus*) demonstrated an increased pathogenicity of the mutant HVS virus expressing HSV-thymidine kinase. The onset of disease in the infected animals happened within hours and was apparently accelerated by the HSV-

thymidine kinase. Thus, the disease progressed rapidly without inhibition since any therapeutic effects would have been expected to take a hold within a week of treatment (Hiller et al., 2000b).

In summary, the viral thymidine kinase was identified as a virulence marker, influencing pathogenicity. Hence, the partial deletion of this ORF was decided to be included in order to generate a safer, minimised vector that was aimed to retain unaltered maintenance of the viral episomes as well as transgene expression in transformed T cells. The replication within proliferating host cells was not affected by the deletion and an attenuation was not observed. It would be highly interesting how such a thymidine-kinase deletion variant influences transformation in human T cells. It is conceivable that the copy number per cell might be reduced. Then again, the hosts' cellular thymidine kinase turnover might be sufficient for the establishment of episomal HVS copies. So far, an influence on replication in OMK cells by deletion of the gene was not detected, which indicates a potential second function benefitting the viral life cycle. It might be informative to see how the thymidine-kinase deletion variants conduct infection in other cell lines, which might engage such a putative second function of the enzyme unnecessary for replication in OMK cells.

Role of *ORF1* and *ORF73* for transformation and persistence: The importance of the bicistronically transcribed *ORF1* genes *Stp* and *Tip* has long been established in the capacity of transforming HVS infected cells (Biesinger et al., 1992). Deletion of both genes does not limit viral replication in OMK cells but leads to the loss of oncogenicity (Desrosiers et al., 1984, Duboise et al., 1998). With regard to generating a potential viral vector for use in other than epithelial cells, the goal was to generate two distinct minimised variants of HVS C488, one containing the transforming genes and one without them. Since expression of *StpC/Tip* is known to be next to non-existent in OMK cells, it was anticipated that deletion of the *StpC/Tip* genes alone would not lead to abortive infection in OMK cells.

ORF73 is transcribed tricistronically conjoint with *ORF71* and *ORF72* (Schäfer et al., 2003). These three ORFs are known to be non-essential for viral replication in T cells (Calderwood et al., 2005; Glykofrydes et al., 2000; Jung et al., 1999), contradicting the essential role assigned to *ORF73* for viral replication by Verma and Robertson in 2003. The combined deletion of all three at once proved not possible as of yet. Although many bacterial colonies were found after first *en passant* recombination, not one was positive for deletion of the ORFs by insertion of the *aphA1*-cassette in its place. Single deletion variants of all three ORFs were successfully generated and did not impair viral replication. The deletion of all three should hence be attempted singularly.

Deletion variants without *ORF73* will be interesting to study in transformed human T cells with regard to their capacity to stably persist in the proliferating cells. Strong evidence sug-

gests a crucial role of H-DNA tandem repeats and *ORF73* for tethering the viral episomes to the host DNA and for viral persistence in proliferating cells (Calderwood et al., 2004a, 2005; Verma & Robertson, 2003; White et al., 2003). So far the loss of persistence has only been reported for a non-transforming A11 virus vector in dividing human colorectal cancer cells SW480 (Calderwood et al., 2005). It is therefore highly likely that human T cells transduced with an *ORF73* deletion virus variant would be able to provide short-term transient transgene-expression only. ORF73 was furthermore shown to suppress *ORF50* transcription. Transcription of *ORF50* leads to two splice variants, ORF50A and ORF50B, both described as strong transactivators for *ORF57* and *ORF6* promoters for HVS C488 (Thurau et al., 2000). Both were reported to be transcribed delayed-early in HVS infection (Whitehouse et al., 1997). Although gene expression is limited in HVS transformed human T cells and mostly restricted to varying levels of *StpC/Tip* and *ORF75*, other ORFs were shown to be inducible, *e.g., ORF14* (Fickenscher et al., 1996; Knappe et al., 1997; Toptan, 2010).

For these reasons, it is of interest to study the consequences of *ORF73* deletion in transformed human T cells. HVS *ORF73* was reported to serve regulatory functions, not only by maintaining episomal persistence in dividing populations but also by supporting the viral mRNA export from the nucleus (Boyne et al., 2008). Moreover, other herpesviral ORF73-homologues were proven to even benefit in translation (Larralde et al., 2006; Majerciak & Zheng, 2015). It is conceivable that by deletion of *ORF73* and, thus, the lacking suppression provided by it for transactivators ORF50A and ORF50B, the viral gene transcription in transformed human T cells might be affected as well.

4.5 HVS as a potential vector

HVS harbours the potential for being developed into a versatile vector for various applications and different variants have been suggested and studied over the years. The broad host cell spectrum of HVS allows the delivery of transgenes into different epithelial or haematopoietic cells but also cancer cell lines (Biesinger et al., 1992, Ensser et al., 2003; Smith et al., 2005).

Different strategies have so far been applied for the generation of HVS vectors with different goals and target cells. On the one hand, a HVS vector was used to target and kill cancer cells. One approach included elimination of grafted T cells via HSV-1 thymidine kinase, another the specific targeted infection of tumour cells, while carrying the suicide gene TRAIL (Hiller et al., 2000a; Hiller et al., 2000b; Stevenson et al., 2000; Turrell et al., 2012). While one caused an increase in pathogenicity *in vivo*, with expression of HSV-1 thymidine kinase accelerating the development of lymphoproliferative disease in the used primates, the other was successful in establishing a vector tool for functioning induction of apoptosis *in vitro* in cancer cells. Targeted infection of tumour cells especially was of interest after studies proved

that HVS can infect cells organised in tumour-like spheroids, and that the host specificity of HVS can be rendered experimentally (Smith et al., 2005; Turrell et al., 2012). For studies applying HVS as a kill-switch tool, usually a vector devoid of the transforming genes *StpC* and *Tip* was used.

A different approach was the use of transformation competent HVS vectors to transform human T cells for transgene expression. It is presumed that a number of gene defects in T lymphocytes, for example those collected under the term severe combined immunodeficiency, could putatively be treated by such a HVS-derived vector. Another field of application would be to use adoptive T-cell therapy to establish a HVS-vector mediated antigen redirection in order to specifically target cancer cells carrying tumour markers such as ErbB2 on their surface (Bremer, 2014).

The basis for HVS studies aimed for adoptive T cell therapy was established when full-length expression of bovine growth hormone (bGH) from a transformation-incompetent HVS virus variant was proven feasible in an inoculated white-lipped marmoset (*Saguinus fuscicollis*) and two owl monkeys (*Aotus trivirgatus*). These animals survived without adverse events for at least 16 months (Desrosiers et al., 1985). Another milestone in proving the potential of this virus as a vector was the demonstration of well-tolerated, autologous transfusion of HVS-transformed macaque T cells without it resulting in adverse events such as lymphoproliferative disease (Knappe et al., 2000).

Other herpesviral vectors have been proposed over the years for gene delivery, too. For example, an HSV-1 based vector is already in use for treatment of advanced melanoma in humans (Andtbacka et al., 2015). For another gammaherpesvirus, the Epstein-Barr virus, it was demonstrated for the first time that an episomal vector could be used as a tool to stably correct a deficiency in human cell *in vitro* (Wade-Martins et al., 2000).

4.6 Summary and outlook

To current knowledge, 12-18 months had been the longest observation period for HVS-transformed T cells (Biesinger et al., 1992; Weber et al., 1993). The results gained from the experiments presented in chapter 3.3 and 3.4 proved HVS to be a vector capable to transform human T cells to stable growth *in vitro*, allowing for transgene expression for up to 48 months. This suggests HVS has the ability to persist indefinitely, potentially lifelong, within transduced human T cells. The attempted antigen redirection of transformed T cells via an artificially expressed human Vδ2Vγ9 TCR did not prove possible, although transcription and expression of a chimeric TCR was possible at the same locus under control of the same promoter (Bremer, 2014, data not shown).

Over a period of up to four years, stable and long-term transgene expression under the viral promoters *SL3*, *ORF75,* and *StpC/Tip* was observed. A semi-quantitative real-time PCR was established, suited for the detection of average HVS genome copies per cell normalised to GAPDH. This system might also applicable to detect and measure viral polymerase activity in transformed human T cells.

Moreover, the generation of minimised variants with increased insert capacity due to the targeted and precise deletion of HVS ORFs was initiated. Although some of these ORFs were already known to be non-essential for viral replication, viral replication kinetics in permissive cells compared to the wild-type were so far mostly lacking, and often only partial deletions of the respective ORFs were generated. Proof of principle was therefore given in the WTf BAC to establish which combined deletions influence the viral replication the least and yield the highest increase in insert capacity. All deletions were ultimately aimed to be collected in the self-repairing variants WT22fDR or WT29fDX to enable the removal of the bacterial vector backbone, the miniF sequence, from the viral genome upon reconstitution in permissive OMK cells by a two-step homologous recombination. Various virus variants were generated, combining several deletions of non-essential genes for viral replication, for example, the double deletion variant WTfΔM21ΔStpC or the triple deletion variants WTfΔ72ΔM21Δ3 and WT29fDXΔ12-14.

Table 29: ORFs reported or demonstrated to be nonessential for viral replication in OMK cells

	ORF	function	size of deletion [kb]	source
	1	StpC/Tip, transformation of T cells	1.397	Desrosiers et al., 1984, Jung et al., 1999
	3	vFGARAT, induction of proteosomal degradation of Sp100 (cellular prohibitor of herpesviral replication)	3.741	Full et al., 2012
➡	4	C4b binding protein, complement inhibition	1.083	Stevenson et al., 1999
➡	12	putative regulatory function	0.510	Knappe et al., 1998a
➡	13	viral interleukin 17, immune regulatory function	2.422	Knappe et al., 1998a
➡	14	viral superantigen homologue, stimulation of CD4 cell proliferation	0.798	Knappe et al., 1997
➡	15	complement binding protein	0.351	Jung et al., 1999
➡	16	viral Bcl-2, apoptosis inhibition	0.483	Stevenson et al., 1999
➡	M21	viral thymidine kinase	0.900	
	71	viral FLICE interacting protein, apoptosis inhibition	0.504	Glykofrydes et al., 2000
➡	72	viral cyclin, inhibition of cell cycle arrest	0.765	Calderwood et al., 2005
	73	latency-associated nuclear antigen homolog, suppresses ORF50 to maintain latent state, inhibits p53 and pRb	1.506	Calderwood et al., 2005
➡	74	constitutively active G-protein coupled receptor	0.966	Jung et al., 1999; Schäfer et al., 2003
➡	75	see ORF3	3.900	Toptan, 2010

Table 29 lists all ORFs dispensable to viral replication at high titres in OMK cells. Additionally, the function, the insert capacity generated, and the sources were added. Arrows indicate

the intended deletions in order to create a self-repairing minimised variant with reduced pathogenicity and increased insert capacity.

So far, in its repaired state (miniF and ORF12-14 deleted), 8.848 kb additional insert capacity were generated in the triple deletion variant WT29fDXΔ12-14, compared to the WTf virus genome. The second triple deletion variant WTfΔ72ΔM21Δ3 had an increase in the potential insert capacity of approximately 5.4 kb, although replication was less efficient and did not reach end titres similar to the wild-type virus.

Deletion of all indicated ORFs (including introns between single ORFs) in table 29 would potentially increase the insert capacity by approximately 12.5 kb in addition to 7.4 kb that were made available by miniF removal and in addition to the basic insert capacity of at least 10 kb HVS offers by nature. In total, this would result in an insert capacity of approximately 30 kb. In case that the deletion of *ORF73*, a homologue to the latent nuclear antigen of KSHV, proved without consequence to episomal maintenance in transformed human T cells, the removal of the complete sequence of *ORF72-75* could be attempted which would add another 2 kb to the insert capacity.

Depending on the area of application, the safety profile of a HVS vector would be improved by the additional removal of both, *ORF73*, a homologue of the latent nuclear antigen of KSHV, and *ORF1*, encoding transforming proteins *StpC/Tip*. As mentioned before, *ORF1* genes *StpC* and *Tip* are absolutely necessary to establish transformation and without *ORF73* the virus cannot persist in a dividing cell population. Deletion of both would, thus, reduce oncogenicity and pathogenicity.

Studying the generated virus variant WTf Vδ2SL3Vγ9, it became obvious that an (involuntary) loss of H-DNA of approximately 27 kb is tolerated well with regard to viral replication and transforming capacity, even with an additional 3 kb of transgenes added to the viral genome. It was reported, that as little as one to four terminal repeats suffice for persistence in cells. However, more than three copies would prolong the time of persistence and increase the number of episomal copies within the host cell nucleus (Collins et al., 2002). In theory, a transgene capacity of a minimised HVS variant of at least 50 kb seems feasible.

Further experimental steps would include testing of the generated deletion variants in human T cells for their transformation competence and maintenance of episomes, especially WTfΔM21 and WTfΔ73. The combination of the deletions indicated in table 29 in a single, self-repair enabled vector and repeated testing in OMK and human T cells would have to ensue. Another aim would be to show long-term expression under the established long-term active *ORF75* or *SL3* promoters and to quantify the transcription under those promoters. For short-term transient expression, the additional deletion of *ORF73* could prove interesting,

since such a mutant remains replication-competent in OMK cells but is unable to persist in proliferating cells (Calderwood, 2005; Whitehouse, 2013).

5. Literature

Albrecht JC, Nicholas J, Biller D, Cameron KR, Biesinger B, Newman C, Wittmann S, Craxton MA, Coleman H, Fleckenstein B, and Honess RW (1992) Primary structure of the herpesvirus saimiri genome. *Journal of Virology 66*, 5047–5058

Allende LM, Hernandez M, Corell A, Garcia- Perez MA, Varela P, Moreno A, Caragol I, Garcia-Martin F, Guillen-Perales J, Olive T, Español T, and Arnaiz-Villena A (2000) A novel CD18 genomic deletion in a patient with severe leucocyte adhesion deficiency: A possible CD2/lymphocyte function-associated antigen-1 functional association in humans. *Immunology* 99, 440-450

Altare F, Durandy A, Lammas D, Emile JF, Lamhamedi S, Le Deist F, Drysdale P, Jouanguy E, Döffinger R, Bernaudin F, Jeppsson O, Gollob JA, Meinl E, Segal AW, Fischer A, Kumararatne D, and Casanova JL (1998) Impairment of mycobacterial immunity in human interleukin-12 receptor deficiency. *Science* 280, 1432-1435

Andtbacka RHI, Kaufman HL, Collichio F, Amatruda T, Senzer N, Chesney J, Delman KA, Spitler LE, Puzanov I, Agarwala SS, Milhem M, Cranmer L, Curti B, Lewis K, Ross M, Guthrie T, Linette GP, Daniels GA, Harrington K, Middleton MR, Miller Jr WH, Zager JS, Ye Y, Yao B, Li A, Doleman S, VanderWalde A, Gansert J, and Coffin RS (2015) Talimogene laherparepvec improves durable response rate in patients with advanced melanoma. *Journal of Clinical Oncology 33*, 2780–2788

Bellows DS, Chau BN, Lee P, Lazebnik Y, Burns WH, and Hardwick JM (2000) Antiapoptotic herpesvirus Bcl-2 homologs escape caspase-mediated conversion to proapoptotic proteins. *Journal of Virology 74*, 5024–5031

Biesinger B, Trimble JJ, Desrosiers RC, Fleckenstein B (1990) The divergence between two oncogenic Herpesvirus saimiri strains in a genomic region related to the transforming phenotype. *Journal of Virology 176*, 505-514

Biesinger B, Müller-Fleckenstein I, Simmer B, Lang G, Wittmann S, Platzer E, Desrosiers RC, and Fleckenstein B (1992) Stable growth transformation of human T lymphocytes by herpesvirus saimiri. *Proceedings of the National Academy of Sciences USA 89,* 3116–3119

Birnboim HC and Doly J (1979) A rapid alkaline extraction procedure for screening recombinant plasmid DNA. *Nucleic Acids Research* 7, 1513–1523

Bortz E, Whitelegge JP, Jia Q, Zhou ZH, Stewart JP, Wu TT, and Sun R (2003) Identification of proteins associated with murine gammaherpesvirus 68 virions. *Journal of Virology 77*, 13425–13432

Boyne JR, Colgan KJ, and Whitehouse A (2008) Herpesvirus saimiri ORF57: a post-transcriptional regulatory protein. *Frontiers in Bioscience 13,* 2928–2938

Bremer L (2014) Rhadinovirale Vektoren zum Transfer unter Latenz exprimierter oder induzierbarer Gene in primäre T-Lymphozyten Hepatozyten und sensorische Neurone und zur Umleitung der T-Zell-Spezifität auf ein Tumorantigen. *Dissertation* Christian-Albrecht University

Bröker BM, Tsygankov AY, Müller-Fleckenstein I, Guse AH, Chitaev NA, Biesinger B, Fleckenstein B, and Emmrich F (1993) Immortalization of human T-cell clones by herpesvirus saimiri. *Journal of Immunology 151*, 1184–1192

Brunnemann AK (2016) Aciclovir resistance phenotype of clinical isolates proven by targeted mutagenesis of recombinant herpes simplex and varicella zoster viruses. *Dissertation* Christian-Albrecht University

Calderwood MA, Hall KT, Matthews DA, and Whitehouse A (2004a) The herpesvirus saimiri ORF73 gene product interacts with host-cell mitotic chromosomes and self-associates via its C terminus. *Journal of General Virology 85*, 147–153

Calderwood MA, White RE, and Whitehouse A (2004b) Development of herpesvirus-based episomally maintained gene delivery vectors. *Expert Opinion on Biological Therapy 4*, 493–505

Calderwood M, White RE, Griffiths RA, and Whitehouse A (2005) Open reading frame 73 is required for herpesvirus saimiri A11-S4 episomal persistence. *Journal of General Virology 86*, 2703–2708

Cannon JS, Hamzeh F, Moore S, Nicholas J, and Ambinder RF (1999) Human herpesvirus 8-encoded thymidine kinase and phosphotransferase homologues confer sensitivity to ganciclovir. *Journal of Virology 73*, 4786–4793

Chang H, Wachtman LM, Pearson CB, Lee JS, Lee HR, Steven H, Vieira J, Mansfield KG, and Jung JU (2009) Non-human primate model of Kaposi's sarcoma-associated herpesvirus infection. *PLoS Pathogens 5*, 1–10

Coleman HM, Lima B, de Morton V, and Stevenson PG (2003) Murine gammaherpesvirus 68 lacking thymidine kinase shows severe attenuation of lytic cycle replication in vivo but still establishes latency. *Journal of Virology 77*, 2410–2417

Collins CM, Medveczky MM, Lund T, and Medveczky PG (2002) The terminal repeats and latency-associated nuclear antigen of herpesvirus saimiri are essential for episomal persistence of the viral genome. *Journal of General Virology 83*, 2269–2278

Corvaisier M, Moreau-Aubry A, Diez E, Bennouna J, Mosnier JF, Scotet E, Bonneville M, and Jotereau F (2005) Vy9Vd2 T cell response to colon carcinoma cells. *Journal of Immunology 175,* 5481–5488

Daniel MD, Silva D, and Ma N (1976) Establishment of owl monkey kidney 210 cell line for virological studies. *In Vitro 12*, 290 - 294

D'Asaro M, La Mendola C, Di Liberto D, Orlando V, Todaro M, Spina M, Guggino G, Meraviglia S, Caccamo N, Messina A, Salerno A, Di Raimondo F, Vigneri P, Stassi G, Fourniè JJ, and Dieli F (2010) Vγ9Vδ2 T lymphocytes efficiently recognize and kill zoledronate-sensitized imatinib-sensitive and imatinib-resistant chronic myelogenous leukemia cells. *The Journal of Immunology 184,* 3260–3268

Davison AJ (2002) Evolution of the herpesviruses. *Veterinary Microbiology 86,* 69–88

Davison AJ, Eberle R, Ehlers B, Hayward GS, McGeoch DJ, Minson AC, Pellett PE, Roizman B, Studdert MJ, and Thiry E (2009) The order Herpesvirales. *Archives of Virology 154*, 171–177

De Carli M, Berthold S, Fickenscher H, Müller-Fleckenstein I, D'Elios M, Gao Q, Biagiotti R, Giudizi MG, Kalden JR, and Fleckenstein B (1993) Immortalization with herpesvirus saimiri modulates the cytokine secretion profile of established Th1 and Th2 human T cell clones. *Journal of Immunology 151*, 5022-5030

Deng X, Sun GR, Zheng Q, and Li Y (1998) Characterization of human TCR Vβ gene promoter: Role of the dodecamer motif in promoter activity. *Journal of Biological Chemistry 273*, 23709–23715

Desrosiers RC, Burghoff RL, Bakker A, and Kamine J (1984) Construction of replication-competent Herpesvirus saimiri deletion mutants. *Journal of Virology 49,* 343-348

Desrosiers RC, Kamine J, Bakker A, Silva D, Woychik RP, Sakai DD, and Rottman FM (1985) Synthesis of bovine growth hormone in primates by using a herpesvirus vector. *Molecular and Cellular Biology 5*, 2796–2803

Duboise SM, Guo J, Czajak S, Desrosiers RC, and Jung JU (1998) STP and Tip are essential for herpesvirus saimiri oncogenicity. *Journal of Virology 72*, 1308–1313

Eberl M, Hintz M, Reichenberg A, Kollas AK, Wiesner J, and Jomaa H (2003) Microbial isoprenoid biosynthesis and human γδ T cell activation. *FEBS Letters 544,* 4–10

Edwards SC, Sutton CE, Ladell K, Grant EJ, McLaren JE, Roche F, Dash P, Apiwattanakul N, Awad W, Miners KL, Lalor SJ, Ribot JC, Baik S, Moran B, McGinley A, Pivorunas V, Dowding L, Macoritto M, Paez-Cortez J, Anderson G, Silva-Santos B, Hokamp K, Price DA, Thomas PG, McLoughlin RM, and Mills KHG (2020) A population of proinflammatory T cells coexpresses αβ and γδ T cell receptors in mice and humans. *Journal of Experimental Medicine 217*, 1-16

Elmore S (2007) Apoptosis: A review of programmed cell death. *Toxicologic Pathology 35*, 495–516

Ensser A, Glykofrydes D, Niphuis H, Kuhn EM, Rosenwirth B, Heeney JL, Niedobitek G, Müller-Fleckenstein IM, and Fleckenstein B (2001) Independence of herpesvirus-induced T cell lymphoma from viral cyclin D homologue. *Journal of Experimental Medicine 193*, 637–642

Ensser A, Thurau M, Wittmann S, and Fickenscher H (2003) The genome of herpesvirus saimiri C488 which is capable of transforming human T cells. *Virology 314*, 471–487

Fada BJ, Reward E, and Gu H (2021) The role of nd10 nuclear bodies in herpesvirus infection: A frenemy for the virus? *Viruses 13*, 1–19

Fickenscher H, Biesinger B, Knappe A, Wittmann S, and Fleckenstein B (1996) Regulation of the herpesvirus saimiri oncogene stpC similar to that of T-cell activation genes in growth-transformed human T lymphocytes. *Journal of Virology 70*, 6012–6019

Fickenscher H, Bökel C, Knappe A, Biesinger B, Meinl E, Fleischer B, Fleckenstein B, and Bröker BM (1997) Functional phenotype of transformed human alphabeta and gammadelta T cells determined by different subgroup C strains of herpesvirus Saimiri. *Journal of Virology 71*, 2252–2263

Fickenscher H, and Fleckenstein B (2001) Herpesvirus saimiri. *Philosophical Transactions of the Royal Society of London Series B Biological Sciences 356*, 545–567

Flint SJ, Racaniello VR, Rall GF, Skalka AM, and Enquist LW (2015) Principles of Virology. Fourth edition, ASM Press

Frolova-Jones EA, Ensser A, Stevenson AJ, Kinsey SE, and Meredith DM (2000) Stable marker gene transfer into human bone marrow stromal cells and their progenitors using novel herpesvirus saimiri-based vectors. *Journal of Hematotherapy & Stem Cell Research 9,* 573–581

Full F, Reuter N, Zielke K, Stamminger T, and Ensser A (2012) Herpesvirus saimiri antagonizes nuclear domain 10-instituted intrinsic immunity via an ORF3-mediated selective degradation of cellular protein Sp100. *Journal of Virology 86,* 3541–3553

Full F, Hahn AS, Großkopf AK, & Ensser A (2017) Gammaherpesviral tegument proteins PML-nuclear bodies and the ubiquitin-proteasome system. *Viruses 9*, 1–11

Gallego MD, Santamaria M, Pena J, and Molina IJ (1997) Defective actin reorganization and polymerization of Wiskott-Aldrich T cells in response to CD3-mediated stimulation. *Blood 90,* 3089-3097

Geevarghese SK, Geller DA, De Haan HA, Hörer M, Knoll AE, Mescheder A, Nemunaitis J, Reid TR, Sze DY, Tanabe KK, and Tawfik H (2010) Phase I/II study of oncolytic herpes simplex virus NV1020 in patients with extensively pretreated refractory colorectal cancer metastatic to the liver. *Human Gene Therapy 21*, 1119–1128

Giles S, Smith PG, Coletta PL, Hall KT, and Whitehouse A (2003) The herpesvirus saimiri ORF 73 regulatory region provides long-term transgene expression in human carcinoma cell lines, *Cancer Gene Therapy 10*, 49-56

Gill MB, Murphy JE, and Fingeroth JD (2005) Functional divergence of Kaposi's sarcoma-associated herpesvirus and related gamma-2 herpesvirus thymidine kinases: novel cytoplasmic phosphoproteins that alter cellular morphology and disrupt adhesion. *Journal of Virology 79*, 14647–14659

Gillen J, Li W, Liang Q, Avey D, Wu J, Wu F, Myoung J, and Zhu F (2015) A survey of the interactome of Kaposi's sarcoma-associated herpesvirus ORF45 revealed its binding to viral ORF33 and cellular USP7 resulting in stabilization of ORF33 that is required for production of progeny viruses. *Journal of Virology 89*, 4918–4931

Glykofrydes D, Niphuis H, Kuhn EM, Rosenwirth B, Heeney JL, Bruder J, Niedobitek G, Müller-Fleckenstein I, Fleckenstein B, and Ensser A (2000) Herpesvirus saimiri vFLIP provides an antiapoptotic function but is not essential for viral replication transformation or pathogenicity. *Journal of Virology 74*, 11919–11927

González CM, Wong EL, Bowser BS, Hong GK, Kenney S, Damania B, Hill C, and Carolina N (2006) Identification and characterization of the Orf49 protein of Kaposi's sarcoma-associated herpesvirus. *Journal of Virology 80*, 3062–3070

Grassmann R, and Fleckenstein B (1989) Selectable recombinant herpesvirus saimiri is capable of persisting in a human T-cell line. *Journal of Virology 63*, 1818–1821

Grassmann R, Dengler C, Müller-Fleckenstein I, Fleckenstein B, McGuire K, Dokhelar MC, Sodroski JG, and Haseltine WA (1989) Transformation to continuous growth of primary human T lymphocytes by human T-cell leukemia virus type I X-region genes transduced by a Herpesvirus saimiri vector. *Proceedings of the National Academy of Sciences of the United States of America 86,* 3351–3355

Hacein-Bey-Abina S, von Kalle C, Schmidt M, McCormack MP, Wulffraat N, Leboulch P, Lim A, Osborne CS, Pawliuk R, Morillon E, Sorensen R, Forster A, Fraser P, Cohen JI, de Saint Basile G, Alexander I, Wintergerst U, Frebourg T, Aurias A, Stoppa-Lyonnet D, Romana S, Radford-Weiss I, Gross F, Valensi F, Delabesse E, Macintyre E, Sigaux F, Soulier J, Leiva LE, Wissler M, Prinz C, Rabbitts TH, Le Deist F, Fischer A, and Cavazzana-Calvo M (2003) LMO2-associated clonal T cell proliferation in two patients after gene therapy for SCID-X1. *Science 302,* 415-419

Hacein-Bey-Abina S, von Kalle C, Schmidt M, Le Deist F, Wulffraat N, McIntyre E, Radford I, Villeval J, Fraser CC, Cavazzano-Calvo M, and Fischer A (2013) A serious adverse event after successful gene therapy for X-linked severe combined immunodeficiency. *New England Journal of Medicine 348,* 255-256

Hall KT, Giles MS, Goodwin DJ, Calderwood MA, Carr IM, Stevenson AJ, Markham AF, and Whitehouse A (2000) Analysis of gene expression in a human cell line stably transduced with herpesvirus saimiri. *Journal of Virology 74*, 7331–7337

Heyn I (2015) Self-repairing seamless rhadinovirus vector for antigen redirection of T cells. *Master thesis*, Christian-Albrechts-Universität, Kiel

Hiller C, Wittmann S, Slavin S, and Fickenscher H (2000a) Functional long-term thymidine kinase suicide gene expression in human T cells using a herpesvirus saimiri vector. *Gene Therapy 7,* 664–674

Hiller C, Tamgüney G, Stolte N, Mätz-Rensing K, Lorenzen D, Hör S, Thurau M, Wittmann S, Slavin S, and Fickenscher H (2000b) Herpesvirus saimiri pathogenicity enhanced by thymidine kinase of herpes simplex virus. *Virology 278*, 445–455

Hintz M, Reichenberg A, Altincicek B, Bahr U, Gschwind RM, Kollas AK, Beck E, Wiesner J, Eberl M, and Jomaa H (2001) Identification of (E)-4-hydroxy-3-methyl-but-2-enyl pyrophosphate as a major activator for human γδ T cells in Escherichia coli. *FEBS Letters 509,* 317–322

Honess RW, O'Hare P, and Young D (1982) Comparison of thymidine kinase activities induced in cells productively infected with herpesvirus saimiri and herpes simplex virus. *Journal of General Virology 58,* 237–249

Holländer GA, Barthlott T, Keller MP, Krenger W, and Piali L (2006) T-Zell-System. In: Immunologie - Grundlagen für Klinik und Praxis, Holländer GA (editor), Elsevier-Urban and Fischer

Hunt RD and Meléndez LV (1969) Herpesvirus infections of non-human primates: a review. *Laboratory Animal Care 19,* 221-34

Hüske L (2010) Regulierte Fremdgenexpression durch rhadinovirale Vektoren. *Dissertation* Christian-Albrecht University, Kiel

Jung JU, Choi J, Ensser A, and Biesinger B (1999) Herpesvirus saimiri as a model for gammaherpesvirus oncogenesis. *Seminars in Cancer Biology 9*, 231–239

Kabelitz D, Pechhold K, Bender A, Wesselborg S, Wesch D, Friese K, and Janssen O (1991) Activation and activation-driven death of human gamma/delta T cells. *Immunological Reviews 120,* 71–88

Kabelitz D, Wesch D, Pitters E, and Zöller M (2004) Characterization of tumor reactivity of human Vy9Vd2 yd T cells in vitro and in SCID mice in vivo. *Journal of Immunology 173,* 6767–6776

Khalil AM (2021) Apoptosis guardian of the genome. *World Journal of Biology Pharmacy and Health Sciences 5*, 37–54

Knappe A, Hiller C, Thurau M, Wittmann S, Hofmann H, Fleckenstein B, and Fickenscher H (1997) The superantigen-homologous viral immediate-early gene ie14/vsag in herpesvirus saimiri-transformed human T cells. *Journal of Virology 71*, 9124–9133

Knappe A, Hiller C, Niphuis H, Fossiez F, Thurau M, Wittmann S, Kuhn EM, Lebecque S, Banchereau J, Rosenwirth B, Fleckenstein B, Heeney J, and Fickenscher H (1998a) The interleukin-17 gene of herpesvirus saimiri. *Journal of Virology 72*, 5797–5801

Knappe A, Thurau M, Niphuis H, Hiller C, Wittmann S, Kuhn EM, Rosenwirth B, Fleckenstein B, Heeney J, and Fickenscher H (1998b) T-cell lymphoma caused by herpesvirus saimiri C488 independently of ie14/vsag a viral gene with superantigen homology. *Journal of Virology 72*, 3469–3471

Knappe A, Feldmann G, Dittmer U, Meinl E, Nisslein T, Wittmann S, Mätz-Rensing K, Kirchner T, Bodemer W, and Fickenscher H (2000) Herpesvirus saimiri-transformed macaque T cells are tolerated and do not cause lymphoma after autologous reinfusion. *Blood 95*, 3256–3261

Kraft MS, Henning G, Fickenscher H, Lengenfelder D, Tschopp J, Fleckenstein B, and Meinl E (1998) Herpesvirus saimiri transforms human T-cell clones to stable growth without inducing resistance to apoptosis. *Journal of Virology 72*, 3138–3145

Laggner U, Di Meglio P, Perera GK, Hundhausen C, Lacy KE, Ali N, Smith CH, Hayday AC, Nickoloff BJ, and Nestle FO (2011) Identification of a novel proinflammatory human skin-homing Vγ9Vδ2 T cell subset with a potential role in psoriasis. *The Journal of Immunology 187*, 2783–2793

Larralde O, Smith RWP, Wilkie GS, Malik P, Gray NK, and Clements JB (2006) Direct stimulation of translation by the multifunctional herpesvirus ICP27 protein. *Journal of Virology 80,* 1588–1591

Laufs S, Nagy KZ, Giordano FA, Hotz-Wagenblatt A, Zeller WJ, and Fruehauf S (2004) Insertion of retroviral vectors in NOD/SCID repopulating human peripheral blood progenitor cells occurs preferentially in the vicinity of transcription start regions and in introns, *Molecular Therapy 10,* 874-881

Lefkowitz EJ, Dempsey DM, Hendrickson RC, Orton RJ, Siddell SG, and Smith DB (2017) Virus taxonomy: the database of the International Committee on Taxonomy of Viruses (ICTV), *Nucleic Acids Research 46*, D708-D717

Liu Z, Guo BL, Gehrs BC, Nan L, and Lopez RD (2005) Ex vivo expanded human Vγ9Vδ2 γδ+ T cells mediate innate antitumor activity against human prostate cancer cells in vitro. *Journal of Urology 173,* 1552–1556

Lo Presti E, Dieli F, and Meraviglia S (2014). Tumor-infiltrating γδ T lymphocytes: pathogenic role clinical significance and differential programing in the tumor microenvironment. *Frontiers in Immunology 5,* 1–8

Lubinski J, Nagashunmugam T, and Friedman HM (1998) Viral interference with antibody and complement. *Viral Interference with Antibody and Complement 9*, 329–337

Lundstrom K (2018) Viral vectors in gene therapy. *Diseases 6*, 42, 1-20

Lussignol M and Esclatine A (2017) Herpesvirus and autophagy: “All right everybody be cool this is a robbery!” *Viruses 9*, 1-21

Majerciak V and Zheng ZM (2015) KSHV ORF57 a protein of many faces. *Viruses 7,* 604–633

Markert JM, Medlock MD, Rabkin SD, Gillespie GY, Todo T, Hunter WD, Palmer CA, Feigenbaum F, Tornatore C, Tufaro F, and Martuza RL (2000) Conditionally replicating herpes simplex virus mutant G207 for the treatment of malignant glioma: results of a phase I trial. *Gene Therapy 7*, 867–874

McGeoch DJ and Cook S (1994) Molecular phylogeny of the alphaherpesvirinae subfamily and a proposed evolutionary timescale. *Journal of Molecular Biology 238,* 9-22

Medveczky P, Szomolanyi E, Desrosiers RC, and Mulder C (1984) Classification of herpesvirus saimiri into three groups based on extreme variation in a DNA region required for oncogenicity. *Journal of Virology 52,* 938-944

Medveczky MM, Geck P, Vassallo R, and Medveczky PG (1993) Expression of the collagen-like putative oncoprotein of*Herpesvirus saimiri* in transformed T cells. *Virus Genes 7,* 349–365

Medveczky MM, Szomolanyi E, Hesselton R, DeGrand D, Geck P, and Medveczky PG (1989) Herpesvirus saimiri strains from three DNA subgroups have different oncogenic potentials in New Zealand white rabbits. *Journal of Virology 63*, 3601–3611

Meinl E and Hohlfeld R (2000) T cell transformation with Herpesvirus saimiri: a tool for neuroimmunological research. *Journal of Neuroimmunology 103*(1), 1–7

Meléndez LV, Hunt RD, Daniel MD, García FG, and Fraser CE (1969) Herpesvirus saimiri. II. Experimentally induced malignant lymphoma in primates. *Laboratory Animal Care 19,* 378-86

Meléndez LV, Hunt RD, Daniel MD, Blake BJ, and Garcia FG (1971) Acute lymphocytic leukemia in owl monkeys inoculated with herpesvirus saimiri. *Science 171*, 1161-1163

Messerle M, Crnkovic I, Hammerschmidt W, Ziegler H, and Koszinowski UH (1997) Cloning and mutagenesis of a herpesvirus genome as an infectious bacterial artificial chromosome. *Proceedings of the National Academy of Sciences of the United States of America 94*, 14759–14763

Mittrücker HW, Müller-Fleckenstein I, Fleckenstein B, and Fleischer B (1993) Herpes virus saimiri-transformed human T lymphocytes: normal functional phenotype and preserved T cell receptor signalling. *International Immunology 5*, 985–990

Murphy K and Weaver C (2018) Antigenerkennung durch B- Zell und T- Zell- Rezeptoren. In: Janeway Immunologie. 9. Auflage, 197-220, Springer Spektrum Verlag Heidelberg

Nava VE, Cheng EH, Veliuona M, Zou S, Clem RJ, Mayer ML, and Hardwick JM (1997) Herpesvirus saimiri encodes a functional homolog of the human bcl-2 oncogene. *Journal of Virology 71*, 4118–4122

Nicholas J, Smith EP, Coles L, and Honess R (1990) Gene expression in cells infected with gammaherpesvirus saimiri: properties of transcripts from two immediate-early genes. *Virology 179*, 189–200

O'Brien RL and Born WK (2015) Dermal γδ T cells – what have we learned? *Cellular Immunology 296*, 62–69

Panina Y, Germond A, Masui S, and Watanabe TM (2018). Validation of common housekeeping genes as reference for qPCR gene expression analysis during iPS reprogramming process. *Scientific Reports 8*, 1–8

Parham P (2009) The Immune System. Third Edition, Garland Science

Propp S (2015) Untersuchung der Funktion eines viralen NOD-like-Rezeptor-Homologs bei der Replikation eines Rhadinovirus mit Recombineering-Mutagenese. *Master thesis* Christian-Albrechts-University, Kiel

Schäfer A, Lengenfelder D, Grillhösl C, Wieser C, Fleckenstein B, and Ensser A (2003) The latency-associated nuclear antigen homolog of herpesvirus saimiri inhibits lytic virus replication. *Journal of Virology 77*, 5911–5925

Searles RP, Bergquam EP, Axthelm MK, and Wong SW (1999) Sequence and genomic analysis of a rhesus macaque rhadinovirus with similarity to Kaposi's sarcoma-associated herpesvirus/human herpesvirus 8. *Journal of Virology 73*, 3040–3053

Senzer NN, Kaufman HL, Amatruda T, Nemunaitis M, Reid T, Daniels G, Gonzalez R, Glaspy J, Whitman E, Harrington K, Goldsweig H, Marshall T, Love C, Coffin R, and Nemunaitis JJ (2009) Phase II clinical trial of a granulocyte-macrophage colony-stimulating factor-encoding second-generation oncolytic herpesvirus in patients with unresectable metastatic melanoma. *Journal of Clinical Oncology 27*, 5763–5771

Shiromizu CM and Jancic CC (2018) γδ T lymphocytes: An effector cell in autoimmunity and infection. *Frontiers in Immunology 9*, 1–8

Shizuya H, Birren B, Kim UJ, Mancino V, Slepak T, Tachiiri Y, and Simon M (1992) Cloning and stable maintenance of 300-kilobase-pair fragments of human DNA in Escherichia coli using an F-factor-based vector. *Proceedings of the National Academy of Sciences USA 89,* 8794- 8797

Silva-Santos B, Serre K, and Norell H (2015) γδ T cells in cancer. *Nature Reviews Immunology 15,* 1–9

Simmer B, Alt M, Buckreus I, Berthold S, Fleckenstein B, Platzer E, and Grassmann R (1991) Persistence of selectable herpesvirus saimiri in various human haematopoietic and epithelial cell lines. *Journal of General Virology 72,* 1953–1958

Smith PG, Oakley F, Fernandez M, Mann DA, Lemoine NR, and Whitehouse A (2005) Herpesvirus saimiri-based vector biodistribution using noninvasive optical imaging. *Gene Therapy 12,* 1465–1476

Stevenson AJ, Cooper M, Griffiths JC, Gibson PC, Whitehouse A, Jones EF, Markham AF, Kinsey SE, and Meredith DM (1999) Assessment of herpesvirus saimiri as a potential human gene therapy vector. *Journal of Medical Virology 57,* 269–277

Stevenson AJ, Frolova-Jones E, Hall KT, Kinsey SE, Markham AF, Whitehouse A, and Meredith DM (2000) A herpesvirus saimiri-based gene therapy vector with potential for use in cancer immunotherapy. *Cancer Gene Therapy 7*, 1077–1085

Szomolanyi E, Medveczky P, and Mulder C (1987) In vitro immortalization of marmoset cells with three subgroups of herpesvirus saimiri. *Journal of Virology 61*, 3485–3490

Tamgüney G, Van Snick J, and Fickenscher H (2004) Autocrine stimulation of rhadinovirus-transformed T cells by the chemokine CCL1/I-309. *Oncogene 23*, 8475–8485

Tanaka Y, Morita CT, Tanaka Y, Nieves E, Brenner MB, and Bloom BR (1995) Natural and synthetic non-peptide antigens recognized by human γδ T cells. *Nature 75,* 155–158

Tavalai N and Stamminger T (2009) Interplay between herpesvirus infection and host defense by PML nuclear bodies. *Viruses 1,* 1240–1264

Thies S (2016) Recombineering mutagenesis and regulated expression of a putatively essential NOD-like receptor homolog of the rhadinovirus herpesvirus saimiri and its effect on viral replication. *Master thesis,* Christian-Albrecht University, Kiel

Thurau M, Whitehouse A, Wittmann S, Meredith D, and Fickenscher H (2000) Distinct transcriptional and functional properties of the R transactivator gene orf50 of the transforming herpesvirus saimiri strain C488. *Virology 268*, 167–177

Tischer BK, Von Einem J, Kaufer B, and Osterrieder N (2006) Two-step Red-mediated recombination for versatile high-efficiency markerless DNA manipulation in Escherichia coli. *BioTechniques 40*, 191–197

Tischer BK and Kaufer BB (2012) Viral bacterial artificial chromosomes: Generation mutagenesis and removal of mini-F sequences. *Journal of Biomedicine and Biotechnology 2012,* 472537

Toptan T (2010) Rhadinovirus vector-mediated transgene expression and regulation. *Dissertation,* Christian-Albrecht University, Kiel

Townsend MH, Felsted AM, Ence ZE, Piccolo SR, Robison RA, and O'Neill KL (2019) Falling from grace: HPRT is not suitable as an endogenous control for cancer-related studies. *Molecular and Cellular Oncology 6*, 1–10

Tsai K, Messick TE, and Lieberman PM (2015) Disruption of host antiviral resistances by gammaherpesvirus tegument proteins with homology to the FGARAT purine biosynthesis enzyme. *Current opinion in Virology 14*, 30-40

Turrell SJ, Macnab SA, Rose A, Melcher AA, and Whitehouse A (2012) A Herpesvirus saimiri-based vector expressing TRAIL induces cell death in human carcinoma cell lines and multicellular spheroid cultures. *International Journal of Oncology 40,* 2081–2089

Verma SC and Robertson ES (2003) ORF73 of herpesvirus saimiri strain C488 tethers the viral genome to metaphase chromosomes and binds to cis-acting DNA sequences in the terminal repeats. *Journal of Virology 77*, 12494–12506

Wade-Martins R, White RE, Kimura H, Cook PR, and James MR (2000) Stable correction of a genetic deficiency in human cells by an episome carrying a 115 kb genomic transgene. *Nature Biotechnology 18,* 1311–1314

Weber F, Meinl E, Drexler K, Czlonkowska A, Huber S, Fickenscher H, Müller-Fleckenstein I, Fleckenstein B, Wekerle H, and Hohlfeld R (1993) Transformation of human T-cell clones by herpesvirus saimiri: intact antigen recognition by autonomously growing myelin basic protein-specific T cells. *Proceedings of the National Academy of Sciences USA 90.* 11049–11053

Werny L (2017) En Passant-Mutagenese der Genregion für das NOD-LIKE-Rezeptor-Homolog von Herpesvirus saimiri und ihre Rolle für die Virusreplikation. *Master thesis,* Christian-Albrechts-University, Kiel

White RE, Calderwood MA, and Whitehouse A (2003) Generation and precise modification of a herpesvirus saimiri bacterial artificial chromosome demonstrates that the terminal repeats are required for both virus production and episomal persistence. *Journal of General Virology 84*, 3393–3403

Whitehouse A, Carr IM, Griffiths JC, and Meredith DM (1997) The herpesvirus saimiri ORF50 gene encoding a transcriptional activator homologous to the Epstein-Barr virus R protein is transcribed from two distinct promoters of different temporal phases. *American Society for Microbiology 71*, 2550–2554

Wieser C (2004) Herpesvirus saimiri basierte Vektoren für die somatische Gentherapie der Rheumatoiden Arthritis. *Dissertation Chemie und Pharmazie,* Universität Regensburg

Woodson EN, Anderson MS, Loftus MS, and Kedes DH (2014) Progressive accumulation of activated ERK2 within highly stable ORF45-containing nuclear complexes promotes lytic gammaherpesvirus infection. *PLoS Pathogens 10*, 1-15

Wussow F, Spieckermann T, Brunnemann A, Hüske L, Toptan T, and Fickenscher H (2011) Bacterial genetics of large mammalian DNA viruses: bacterial artificial chromosomes as a prerequisite for efficiently studying viral DNA replication and functions. In: DNA Replication-Current Advances, Seligmann H (editor), Intech, Rijeka

Xie Y, Wu L, Wang M, Cheng A, Yang Q, Wu Y, Jia R, Zhu D, Zhao X, Chen S, Liu M, Zhang S, Wang Y, Xu Z, Chen Z, Zhu L, Luo Q, Liu Y, Yu Y, Zhang L, and Chen X (2019) Alpha-herpesvirus thymidine kinase genes mediate viral virulence and are potential therapeutic targets. *Frontiers in Microbiology 10,* (article 949) 1–17

Zingler P (2015) Deletion of antiapoptotic genes by multi-step homologous recombination and its effect on the replication of self-repairing rhadinovirus vectors. *Master thesis,* Christian-Albrechts-University, Kiel

Acknowledgements

First of all, I would like to thank Prof. Dr. Helmut Fickenscher for the opportunity to deepen my understanding of viruses, especially herpesvirus saimiri. Working on this project made me fall in love with virology all over again, new methods I had to research led to new insights and thus to rekindled curiosity to the secrets nature still holds. On the other hand, this project also helped me to develop the skill set to deal with setbacks and disappointments.

Furthermore I want to thank my dear colleagues, past and present, for their kindness, their encouragement, their support and open ears in both, times of trouble and when celebrations were in order. Gerrit Andresen, Anne-Kathrin Brunnemann, Linda Bremer, Andrea Hölzgen, Michael Mannbar, Gregor Maschkowitz, and Janine Römpke, thank you for every advice given and for the time you invested. Thank you to my master students, Sarah Thies, Ludwig Werny, and Philipp Zingler who made me realise my strength and weaknesses as a teacher and consequently helped me improve and grow.

For his unceasing emotional support, patience, and encouragement I would like to say thank you to Simon Nordstad. Similarly I would like to express my gratitude to my family and friends who were always there when I needed someone to talk to, offered advice and solace but also shared my joy over small successes along the way.

Erklärung

Hiermit erkläre ich, daß die Abhandlung der vorliegenden Dissertation, abgesehen von der Beratung durch meinen Betreuer Prof. Dr. Helmut Fikentscher, nach Inhalt und Form meine eigene Arbeit ist und nur mit den angegebenen Quellen und Hilfsmitteln verfasst wurde. Stellen, die wörtlich oder sinngemäß aus veröffentlichten oder noch nicht veröffentlichten Quellen entnommen sind, sind als solche kenntlich gemacht. Teile dieser Arbeit wurden bereits in Form meiner eigenen oder von mir betreuten Masterarbeiten veröffentlicht, weiterhin baut diese Arbeit zum Teil auf Ergebnissen meiner Vorgängerin Linda Bremer, geb. Hüske auf. Weitere Teile dieser Arbeit sind zur Veröffentlichung in einem Fachjournal eingereicht. Nicht von mir erstellte Ergebnisse sind als solche ausgewiesen ebenso wie von anderen Personen generierte Daten. Weiterhin entstand die vorliegende Arbeit unter Einhaltung der Regeln guter wissenschaftlicher Praxis der Deutschen Forschungsgemeinschaft. Zu guter Letzt erkläre ich, dass ich noch keinen Promotionsversuch unternommen habe und dass mir kein akademischer Grad entzogen wurde.

Kiel, den 30. Mai 2022

Ines Heyn